

Strategies to Improve Luminescence Efficiency of Metal-Halide Perovskites and Light-Emitting Diodes

Young-Hoon Kim, Joo Sung Kim, and Tae-Woo Lee*

Metal-halide perovskites (MHPs) are well suited to be vivid natural color emitters due to their superior optical and electrical properties, such as narrow emission linewidths, easily and widely tunable emission wavelengths, low material cost, and high charge carrier mobility. Since the first development of MHP light-emitting diodes (PeLEDs) in 2014, many researchers have tried to understand the properties of MHP emitters and the limitations to luminescence efficiency (LE) of PeLEDs, and have devoted efforts to increase the LE of MHP emitters and PeLEDs. Within three and half years, PeLEDs have shown rapidly increased LE from external quantum efficiency $\approx 0.1\%$ to $\approx 14.36\%$. Herein, the factors that limit the LE of PeLEDs are reviewed; the factors are characterized into the following groups: i) photophysical properties of MHP crystals, ii) morphological factors of MHP layers, and iii) problems caused by device architectures. Then, the strategies to overcome those luminescence-limiting factors in MHP emitters and PeLEDs are critically evaluated. Finally, research directions to further increase the LE of MHP emitters and the potential of MHPs as a core component in next-generation displays and solid-state lightings are suggested.

emitters (FWHM ≈ 30 nm; color gamut $\approx 100\%$ in NTSC standard and $<90\%$ in Rec. 2020 standard).^[11–15]

MHPs are composed of three atoms or molecules in simple crystal structures, ABX_3 or A_2BX_4 , where A is an organic ammonium (OA, e.g., methylammonium (MA; $CH_3NH_3^+$) and formamidinium (FA; $CH(NH_2)_2^+$) or an alkali metal cation (e.g., Cs^+), B is a transition metal cation (e.g., Au^{2+} , Sn^{2+} , Mn^{2+} , and Pb^{2+}), and X is a halide anion (I^- , Br^- , and Cl^-). In 3D ABX_3 cubic crystal structure, one B cation is coordinated to the six halide anions in a corner of BX_6 octahedral configuration and A is located in the octahedral voids. Although bandgap formation mechanism of MHP crystals is still under debate, electronic structure of MHP crystals is mainly contributed by the inorganic BX_6 octahedra rather than by the A cations;^[16–18] these studies indicate that emission wavelength λ of MHP emitters can easily be tuned ($380 \leq \lambda \leq 1000$ nm)

1. Introduction


Metal-halide perovskites (MHPs) have superior electrical and optical properties, which give them great potential for use in light-emitting diodes (LEDs).^[1–4] Especially, their narrow emission linewidths (full width at half-maximum (FWHM) ≤ 20 nm) can achieve ultrahigh color purity (color gamut $\geq 140\%$ in National Television Standards Committee (NTSC) TV color standard^[1,5] and $>95\%$ in International Telecommunication Union Recommendation BT 2020 (Rec. 2020) standard^[6]); these are superior to the properties of organic emitters (FWHM > 40 nm; color gamut $< 100\%$ in NTSC standard and $<90\%$ in Rec. 2020 standard)^[7–10] and inorganic quantum dot (QD)

by totally or partially replacing B cations or X anions. Perovskite crystal structure is also affected by A-site cations due to hydrogen bonding and vibrational coupling between BX_3^- and A^+ , so bandgap and concomitant λ of MHPs can be controlled by tuning the A-site cations.^[19,20] These emission spectra with high color purity and wide λ tunability do not depend on the size of grains or crystals of MHP emitters when their dimension is larger than exciton Bohr diameter D_B ;^[21,22] this size-independent high color purity of MHPs is particularly suited as a vivid natural color emitter in future display technology.

Because of their unique crystal structure (e.g., ionic bonding) and bandgap formation mechanism, MHPs have balanced and high charge carrier mobility (e.g., both electron and hole mobility ≈ 1000 cm^2 (V s)⁻¹ in $CsPbBr_3$ single crystals^[23]) and have comparable energy level to those of organic semiconductors.^[24] Furthermore, MHP emitters have low material cost and good compatibility with diverse solution processes to synthesize MHP crystals; these are great advantages of MHPs to mass production and commercialization.

In the early 1990s, several researchers tried to fabricate the MHP light-emitting diodes (PeLEDs) by using layered MHP emitters as an emitting layer (EML).^[25,26] However, MHPs showed low photoluminescence quantum efficiency (PLQE), and yielded bright electroluminescence (EL) only at cryogenic temperature, which may be ascribed to immature MHP crystallization processes, ineffective confinement of electrons and holes,

Dr. Y.-H. Kim, J. S. Kim, Prof. T.-W. Lee
 Department of Materials Science and Engineering
 Institute of Engineering Research
 Research Institute of Advanced Materials
 Nano Systems Institute (NSI)
 BK21 PLUS SNU Materials Division for Educating Creative Global Leaders
 Seoul National University
 1 Gwanak-ro, Gwanak-gu, Seoul 08826, Republic of Korea
 E-mail: twlees@snu.ac.kr, taewlees@gmail.com

 The ORCID identification number(s) for the author(s) of this article can be found under <https://doi.org/10.1002/adma.201804595>.

DOI: 10.1002/adma.201804595

and suboptimal device structures.^[25,26] Although LEDs using a perovskite-structured material with an organic emitting dye in A cation sites showed an external quantum efficiency (EQE) $\approx 0.11\%$ at room temperature in 1999, their color purity was very poor (FWHM > 100 nm) because the emission comes from an organic emitting dye in A cation sites not from BX₆ octahedra.^[27] Therefore, this LED does not follow the emission mechanism of MHP emitters but that of organic emitters. Because of those MHP's physical properties that are favorable for charge separation and transport but unfavorable for radiative emission, MHPs have been developed preferentially as light absorbers in photovoltaics rather than as light emitters in LEDs.^[28,29]

Instead, organic emitters and QD emitters have been mainly developed as EML in self-emissive LEDs over decades. Organic LEDs achieved EQE $\approx 30\%$,^[10,30] and QD LEDs achieved EQE $\approx 20\%$.^[14,31,32] Many efforts to demonstrate bright MHPs at room temperature were tried, such as coating of MAPbBr₃ precursor solution onto porous alumina^[33] or synthesizing MAPbBr₃ nanoparticles in warm solutions.^[34,35] The desire to achieve bright room-temperature EL in PeLEDs was fulfilled in 2014 by using the device structure of high-efficiency OLEDs and QD LEDs: bright green-emitting PeLEDs (EQE $\approx 0.1\%$, current efficiency (CE) ≈ 0.3 cd A⁻¹, and luminance $L \approx 364$ cd m⁻²) were fabricated in conventional structure (indium tin oxide (ITO)/poly(3,4-ethylenedioxythiophene):poly(styrenesulfonate) (PEDOT:PSS)/MAPbBr₃/poly(9,9-dioctyl-fluorene) (F8)/Ca/Ag); efficient near-infrared (NIR)-emitting PeLEDs (EQE $\approx 0.76\%$ and radiance ≈ 13.2 W sr⁻¹ m⁻²) were demonstrated in inverted structure (ITO/TiO₂/MAPbI_{3-x}Cl_x/F8/MoO₃/Ag).^[2] Kim et al. reported PeLEDs (ITO/buffer hole injection layer (Buf-HIL)/MAPbBr₃/2,2',2''-(1,3,5-benzinetriyl)-tris(1-phenyl-1-H-benzimidazole) (TPBI)/LiF/Al) with improved brightness (EQE $\approx 0.125\%$, CE ≈ 0.577 cd A⁻¹ and $L \approx 417$ cd m⁻²) by applying the device structures of OLEDs in which Buf-HIL can efficiently prevent quenching of electron-hole pairs at the interface between PEDOT:PSS and EML and facilitate hole injection from electrode to EML.^[3] However, these efficiencies are still far below those of state-of-the-art OLEDs and commercially required levels. Therefore, these reports also indicate that the PeLEDs still have fundamental limitations to achieve high luminescence efficiency (LE) at room temperatures. Therefore, fundamental breakthroughs are required to make MHP films favorable for radiative decay of electron-hole pairs. The EL efficiency similar to the level of phosphorescent OLEDs can be achieved when the intrinsic issues of perovskite polycrystalline films were solved: the perovskite films were prepared to have small grains (<100 nm), fine stoichiometry control was done to avoid uncoordinated Pb species, and the grain boundaries were healed by an electron-transporting organic additive.^[4,36]

Since those pioneering achievements, many researchers have tried to understand the properties of MHP materials and the limitations to LE of PeLEDs, and have devoted effort to increase the LE of MHP materials and PeLEDs. Within three and half years, PeLEDs have shown rapidly increased LE (from EQE $\approx 0.1\%$ to $\approx 14.36\%$ in green-emitting PeLEDs,^[37] and from EQE $\approx 0.76\%$ to $\approx 11.7\%$ in NIR-emitting PeLEDs^[38]). MHPs in different crystal forms have also shown dramatically improved LE (EQE $\approx 13.4\%$ in green-emitting colloidal nanocrystals (NCs),^[39] EQE $\approx 6.3\%$ in red-emitting colloidal NCs,^[40] and EQE



Young-Hoon Kim received his M.S. degree (2014) in Division of Environmental Science and Engineering and Ph.D. degree (2016) in material science and engineering from Pohang University of Science and Technology (POSTECH), Korea. He is currently working in Materials Science and Engineering at Seoul National University, Korea, as a postdoctoral researcher (2016–2018). His research focuses on solution-processed electronics based on organic and organic–inorganic hybrid materials for flexible displays and solid-state lightings.



Joo Sung Kim received his B.S. degree in materials science and engineering from Pohang University of Science and Technology (POSTECH) in 2016. He is currently pursuing his integrated Ph.D. degree in materials science and engineering at Seoul National University (SNU). His research interests include organic–inorganic hybrid optoelectronics, organic light emitting diodes, and spectroscopy.



Tae-Woo Lee is an associate professor in materials science and engineering at Seoul National University, Korea. He received his Ph.D. degree in chemical engineering from KAIST, Korea, in 2002. He joined Bell Laboratories, USA, as a postdoctoral researcher and worked in Samsung Advanced Institute of Technology as a member of research staff (2003–2008). He was an associate professor in materials science and engineering at Pohang University of Science and Technology (POSTECH), Korea, until Aug 2016. His research focuses on printed electronics based on organic and organic–inorganic hybrid materials for flexible displays, solid-state lightings, and solar-energy-conversion devices.

≈ 0.1 – 0.2% in single crystals).^[41] Compared with green-, red- and NIR-emitting PeLEDs, blue-emitting PeLEDs have not shown dramatic improvement in LE yet (EQE $\approx 0.004\%$ for deep blue ($\lambda \approx 432$ nm),^[42] EQE $\approx 0.024\%$ for blue (456 nm),^[42] and EQE $\approx 1.9\%$ for sky-blue ($\lambda \approx 490$ nm)^[43])

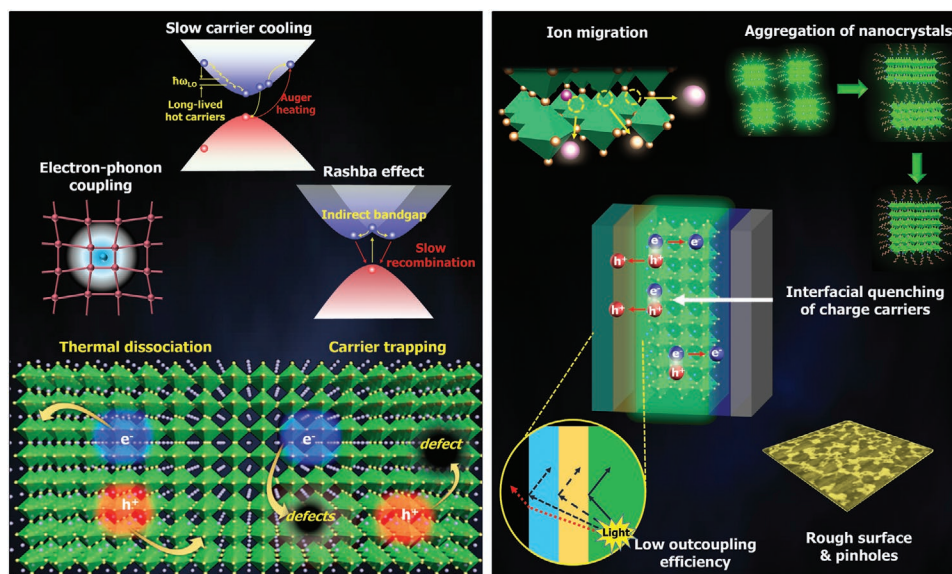


Figure 1. Schematic illustration describing the limitations to luminescence efficiency of MHPs (left) and LEDs (right).

due to low PLQE^[44] arising from high defect density related to wide band-gap,^[45] long lifetime, and diffusion length of charge carriers in the case of chloride-doped perovskite crystals,^[46] and inefficient hole injection arising from deep valence band maximum (VBM).^[47] These LEs are still too low to be commercialized in displays and solid-state lightings, but considering their rapid increase over time, we believe that EL efficiency will merit commercialization in the near future.

Here, we review the factors that limit the LE of PeLEDs; we categorize the factors into i) photophysical properties of MHP crystals (charge carrier recombination, charge carrier–ionic lattice coupling, defect states and PLQE), ii) factors that affect morphology of MHP EML (crystallization mechanisms, and aggregation and insulating problems of colloidal NCs), and iii) problems caused by device architectures (electrical and optical losses at the interfaces, and operating instability) (Figure 1). Then we provide recently reported suggestions to overcome those LE-limiting factors in MHP emitters and PeLEDs. We also suggest research directions to further increase the LE of MHP emitters. We ultimately highlight the potential of MHPs as a core component in displays and solid-state lightings.

2. Limitations to Luminescence Efficiency of MHPs and LEDs

2.1. Limitations to Luminescence Efficiency of MHP Materials

2.1.1. Charge Carrier Recombination and Photoluminescence Quantum Efficiency

The most important phenomena that determine EL efficiency of PeLEDs are charge carrier recombination processes and concomitant PLQE of MHP emitters. Charge carrier recombination in MHP emitters occurs in several steps (Figure 2A):

1) photoillumination excites the electrons from VBM into conduction band minimum (CBM) where they induce formation of electron–hole pairs; 2.1) some of these pairs recombine with each other and emit light (radiative recombination of electron–hole pairs; excitonic recombination) or 2.2) other pairs separate into free charge carriers. The ratio of the radiative recombination to separation into free charge carriers of electron–hole pairs R_{REC} is mainly determined by exciton binding energy

$$E_b = R_H \frac{\mu}{m_0 \epsilon_r^2} \quad (1)$$

where $R_H = 13.6$ eV is the binding energy of electron in H atom, $m_0 = 9.11 \times 10^{-31}$ kg is the mass of a free electron, $\mu = \left(\frac{1}{m_e} + \frac{1}{m_h} \right)^{-1}$ is the reduced mass of charge carriers in semiconducting MHPs, where m_e is the effective mass of an electron and m_h is the effective mass of a hole, and ϵ_r is the relative dielectric constant (relative permittivity) of MHPs.

MHPs have low and similar effective mass ($m_e \approx 0.15m_0$; $m_h \approx 0.14m_0$) and are ion-bonded, so electrons and holes can freely move, rotate, and oscillate in the MHP crystals. However, heavy-metal atoms (e.g., Pb) and orientational motion of organic cations^[48] in MHPs prevent the movement of charge carriers and induce largely screened Coulomb interaction, large polarization, and large ϵ_r . Therefore, as a result, MHPs have low E_b ($\approx 30 - 50$ meV in MAPbI₃^[49,50] and ≈ 76 meV in MAPbBr₃^[49]) which is similar to the thermal energy at room temperature (≈ 25 meV); these values have been confirmed by various measurement methods such as magneto-optical absorption spectroscopy,^[49,51] optical absorption,^[52] and temperature-dependent PL.^[53] In MHPs, R_{REC} can be estimated by using the Saha–Langmuir equation:^[54] 3D MHPs with small E_b ($\approx 30 - 76$ meV)^[49,50] have dominant free charge carriers at room temperature; if E_b increases and temperature decreases, R_{REC} gradually increases (Figure 2B). This direct dissociation of electron–hole pairs into free charge carriers and concomitantly

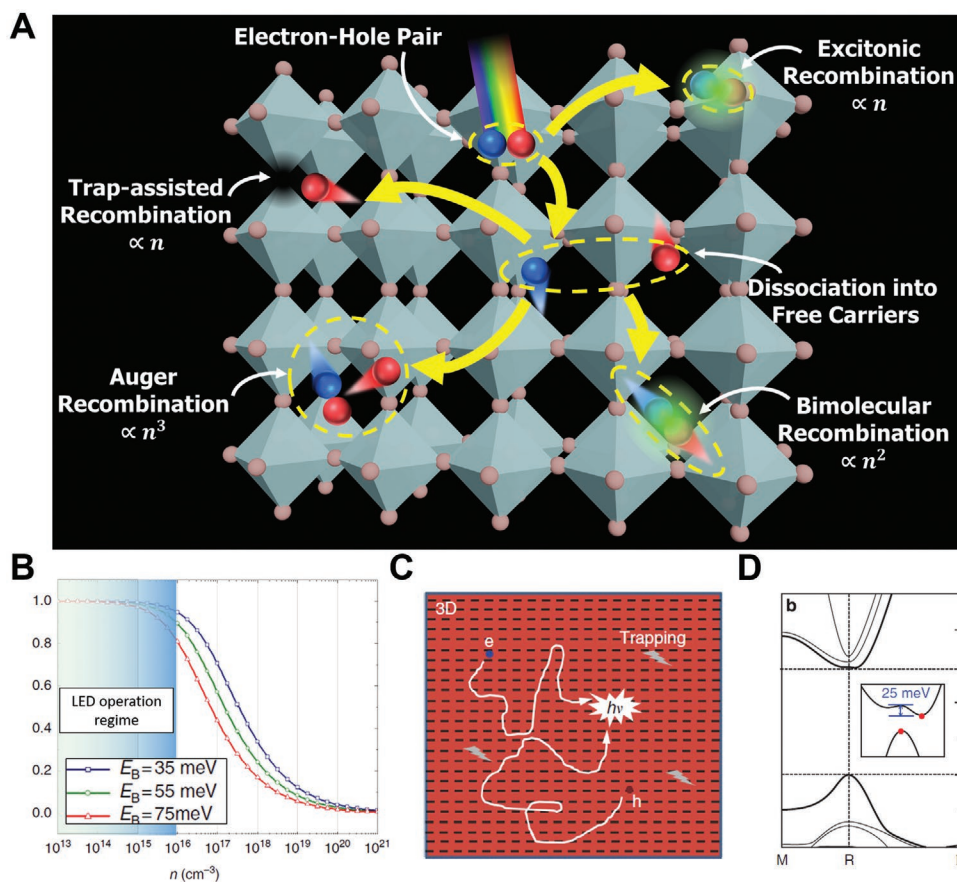


Figure 2. A) Schematic illustration describing the recombination pathways of charge carriers in MHPs, B) excitation density (n) versus fraction of free charge carriers over the total excited charge carriers with different exciton binding energy. Reproduced with permission.^[54] Copyright 2014, Nature Publishing Group. C) Recombination pathways of excited charge carriers in 3D bulk MHPs (dissociated into free charge carriers and then trapped in defect states or recombined to emit light). Reproduced with permission.^[55] Copyright 2017, Nature Publishing Group. D) Band structure of indirect bandgap in MHPs induced by orientation of MA. Reproduced with permission.^[20] Copyright 2015, Nature Publishing Group.

dominant free charge carriers has stimulated research into MHP solar cells, but has impeded the development of MHP LEDs because efficient light emission in PeLEDs requires strongly bound electron–hole pairs.

Photoexcited charge carriers that separate into free charge carriers (process 2.2) can then (process 2.2.1) undergo radiative recombination, or (process 2.2.2) be trapped into defect states (Shockley–Read–Hall (SRH) recombination) or (process 2.2.3) recombine by multiparticle interaction (three-body Auger recombination). The recombination kinetics of charge carriers in MHPs can be described as^[55]

$$\frac{\partial n(t)}{\partial t} = -k_1 n - k_2 n^2 - k_3 n^3 \quad (2)$$

where $n(t)$ is the charge carrier density at time t , k_1 is excitonic recombination rate $k_{1,\text{exciton}}$ or defect-mediated recombination rate $k_{1,\text{defects}}$, k_2 is the bimolecular recombination rate of free charge carriers, and k_3 is the trimolecular Auger recombination rate. Recombination rates of MHPs can be attained by fitting the transient absorption kinetics (exciton bleach kinetics) according to the different pump fluences; 3D MAPbBr₃ films showed $k_1 \approx 27.2 \mu\text{s}^{-1}$, $k_2 \approx 4.9 \times 10^{-10} \text{ cm}^3 \text{ s}^{-1}$, and

$k_3 \approx 13.5 \times 10^{-28} \text{ cm}^6 \text{ s}^{-1}$; 3D MAPbI₃ films showed $k_1 \approx 72.7 \mu\text{s}^{-1}$, $k_2 \approx 1.5 \times 10^{-10} \text{ cm}^3 \text{ s}^{-1}$, and $k_3 \approx 3.4 \times 10^{-28} \text{ cm}^6 \text{ s}^{-1}$.^[56] In MHPs, k_2 and k_3 are inherent values, whereas k_1 can be affected by the degree of charge carrier confinement and by defect density; these characteristics indicate that specific recombination pathways in conventional 3D MHPs can be controlled by tuning the defect density, crystallinity, and dimensionality or dimension of MHP crystals.^[55] In conventional 3D MHPs, E_b is small, so at room temperature most electron–hole pairs dissociate directly into free charge carriers, and defect-mediated recombination and Auger recombination occur mainly by nonradiative recombination; these observations suggest that bimolecular recombination of free charge carriers is the main radiative mechanism in conventional 3D MHPs at room temperature (Figure 2C).

Therefore, in MHPs, PLQE can be represented as^[55]

$$\text{PLQE} = \frac{k_{1,\text{exciton}} + k_2 n}{k_{1,\text{exciton}} + k_{1,\text{defect}} + k_2 n + k_3 n^2} \quad (3)$$

In 3D MHP films, defect-mediated recombination of charge carriers dominates other recombination mechanisms (e.g., radiative recombination of excitons (Coulombically bound electron–hole pairs); radiative recombination of free charge

carriers) in low excitation fluences (in LED operating condition; charge carrier density $< 10^{15} \text{ cm}^{-3}$) due to fast $k_{1,\text{exciton}}$, slow k_2 , and moderate defect densities ($10^{14} - 10^{17} \text{ cm}^{-3}$ in thin films and $10^9 - 10^{10} \text{ cm}^{-3}$ in single crystals).^[48] In high excitation fluences, multicharge carrier interactions such as Auger recombination and biexciton recombination can occur as nonradiative recombination channels.^[55] Therefore, PLQE of MHP emitters and resultant EQE of PeLEDs are limited.

Indirect bandgap in MHPs also slows down the recombination rate of charge carriers and limits the PLQE of MHPs (Figure 2D).^[56,57] Heavy center metals (e.g., Pb) induce strong spin-orbit coupling, and thus conduction band and valence band are spin polarized and split in momentum space; these changes (Rashba splitting) induce indirect bandgap in MHPs.^[57,58] The orientation of organic A cations can also induce the indirect bandgap of MHPs.^[20,59] This indirect bandgap is measured to be $\approx 25 - 75 \text{ meV}$ below the direct bandgap in MAPbI₃; this result has been confirmed by numerical simulation,^[20] temperature-dependent PL,^[59] temperature-dependent transient absorption,^[58] and magneto dielectric studies.^[60]

2.1.2. Coupling between Charge Carriers and Ionic Lattices: Polaron Formation and Hot-Phonon Bottleneck

Long-lived hot carriers can also limit the LE of MHPs because i) radiative recombination is slower in hot carriers than in charge carriers at the band edge, ii) energy of hot carriers can be reabsorbed in the crystals,^[61] and iii) hot carriers with long lifetime can also be easily trapped by defect states and undergo nonradiative recombination. Slow cooling of long-lived hot carriers in MHPs can be attributed to two mechanisms: (1) formation of large polarons at low excitation densities ($< 10^{18} \text{ cm}^{-3}$) due to i) vibrational coupling between BX_3^- and A^+ ,^[61,62] and ii) soft, polarized and flexible PbBr_6^{4-} frameworks;^[63-66] (2) a hot-phonon bottleneck under high excitation densities ($> 10^{18} \text{ cm}^{-3}$).^[67-69]

Photoexcitation in MHPs (MAPbBr₃, FAPbBr₃, and CsPbBr₃) with higher energy than their bandgap at low exciton densities ($\approx 7 \times 10^{16} \text{ cm}^{-3}$) induces formation of charge carriers at the bandgap edge and also of hot carriers. Anisotropic local-reorientation motion of organic A cations in organic-inorganic hybrid MHPs (e.g., MAPbBr₃ and FAPbBr₃) induces strong vibrational coupling between BX_3^- and A^+ ; it screens scattering of hot carriers with longitudinal optical (LO) phonons that is caused by Coulomb interaction, prevents the energetic hot carriers from cooling down, and thus forms hot carriers of which $\approx 24\%$ of the PL population was long-lived ($\approx 0.5 \text{ ns}$) (Figure 3).^[61] Recently, all-inorganic MHPs (e.g., CsPbBr₃) were also reported to have polarons due to soft, polarized and flexible PbBr_6^{4-} frameworks which can easily couple with charge carriers.^[63-66] In addition, these large polarons, which are formed by vibronic coupling between charge carriers (excess electrons or holes) and highly ionized crystalline lattices, are widely delocalized in crystals (over several unit cells), and can screen the scattering of hot carriers with LO phonons, and thus dramatically reduce the cooling rate of hot carriers.^[61] Furthermore, polarons themselves recombine much more slowly than do charge carriers,^[63,66] i.e., vibrational coupling between BX_3^- and

A^+ , coupling between PbBr_6^{4-} frameworks and charge carriers, and concomitant polaron formations can reduce the recombination rate of charge carriers and thus limit the LE of MHPs. This screening effect of large polarons on scattering between hot carriers and LO phonons can be confirmed by the decrease in long-lived excess electronic energy as excitation density increases; as excitation intensity increases until $< 10^{18} \text{ cm}^{-3}$ and the resultant density of large polaron increases, large polarons become destabilized due to repulsive interaction among them. Then their screening effect on the interaction between hot carriers and LO phonons decreases, so the cooling rate of hot carriers increased.^[61]

Under high excitation densities ($> 10^{18} \text{ cm}^{-3}$), an excess of hot phonons was generated, so phonon reabsorption can occur.^[69] This process slowed down the cooling of hot carriers; this mechanism is called hot-phonon bottleneck effect. Hot phonons can reheat the charge carriers and thus reduce the cooling rate of charge carriers.^[63] Directly after photoexcitation by energy larger than the bandgap of MHPs, transient absorption (TA) spectra showed high-energy tails (at $\approx 1.58 \text{ eV}$ in MAPbI₃) and broadened spectra due to distribution and reabsorption of hot carriers over the bandgap as a result of reheating by the phonon bottleneck, which increased the lifetime of hot

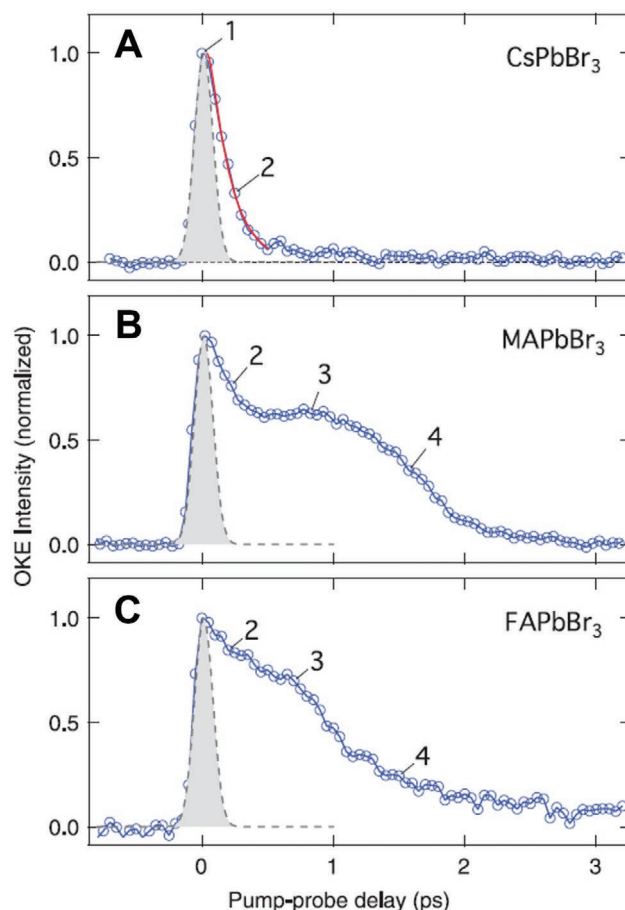


Figure 3. Time-resolved optical Kerr effect transients of single-crystal A) CsPbBr₃, B) MAPbBr₃, and C) FAPbBr₃. Reproduced with permission.^[61] Copyright 2016, The American Association for the Advancement of Science.

carriers.^[68] In MAPbI₃, the lifetime of hot carriers gradually increases as excitation densities increase under high excitation densities ($>10^{18}$ cm⁻³); this trend confirms that long-lived hot carriers are formed by the hot phonon-bottleneck effect rather than by the polaron effect.^[68]

These charge carrier–ionic lattice interactions can be intensified in low-dimensional (e.g., 2D, 0D) perovskites in which self-assembled quantum wells (in 2D crystals) or NCs (in colloidal 0D crystals) are bound by a weak van der Waals interaction.^[55] Many dangling bonds such as out-of-plane self-terminations of PbX₆ octahedra (in 2D crystals) and NC surfaces (in 0D crystals), and excess charge carriers due to efficient spatial confinement perturb the lattices and cause large charge carrier–ionic lattice interaction.^[55] 2D MHPs ((C₁₀H₇CH₂NH₃)₂PbI₄) show much larger exciton–LO phonon coupling strength (≈ 260 meV)^[55] than do 3D MHPs (≈ 40 meV in FAPbI₃, ≈ 61 meV in FAPbBr₃, ≈ 40 meV in MAPbI₃, ≈ 58 meV in MAPbBr₃,^[70] ≈ 92.1 meV in MAPbI_{3-x}Cl_x^[53]).

2.1.3. Defect States

In MHPs, k_2 and k_3 are inherent values and k_1 is strongly affected by $k_{1,\text{defects}}$ according to the charge carrier recombination kinetic mechanisms.^[55] Therefore, recombination pathways of charge carriers are dominantly affected by the defect density. Furthermore, PLQE of MHPs also depends strongly on the defect density because defect-mediated recombination occurs mostly by non-radiative recombination and is much faster than other recombination pathways ($k_{1,\text{defect}} > k_{1,\text{exciton}}$ or k_2) (Figure 4A).^[16,71]

Therefore, defect formation mechanisms may explain the low PLQE in MHPs.

Because MHP crystals are formed at relatively low temperature (room temperature (≈ 25 °C) for colloidal NCs synthesized by recrystallization methods;^[72] <100 °C for MHP polycrystalline bulk films;^[4] <200 °C for MHP NCs synthesized by hot-injection methods^[5]) and are held together by brittle ionic bonding, they naturally incorporate various defect states such as Schottky defects which are neutral vacancy defects (e.g., PbX₂ vacancy; MAX vacancy), Frenkel defects which induce the charge difference in crystals (e.g., elemental defects of Pb²⁺, I⁻ and MA⁺; unintentional doping) and structural defects (e.g., lattice distortion by accumulated charges and impurities; grain boundaries). Formation of defect states at surfaces is accelerated because perovskite crystals are susceptible to deformation at the surface (in MAPbI₃ thin films; bulk trap density $\approx 5 \times 10^{16}$ cm⁻³, surface trap density $\approx 1.6 \times 10^{17}$ cm⁻³).^[73] These defect states can also be formed by electron–phonon

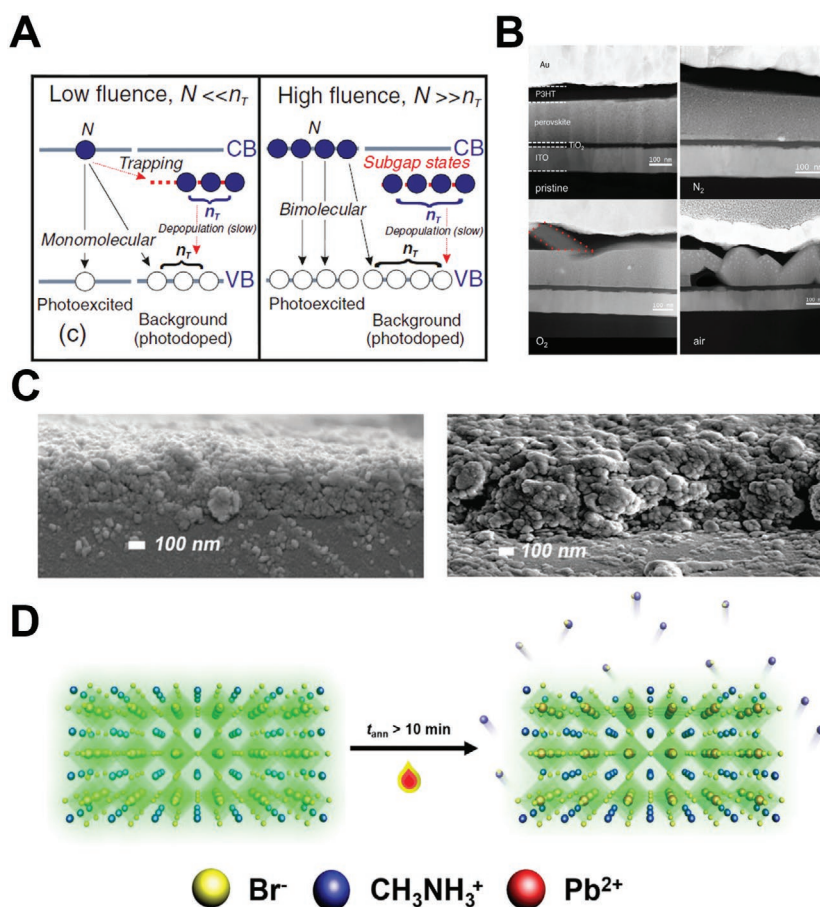


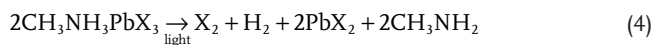
Figure 4. A) Schematic illustration describing the recombination mechanism of charge carriers in MHP under the low and high excitation fluences. Reproduced with permission.^[88] Copyright 2014, American Physical Society. B) Transmission electron microscopy images of MHP devices based MHP layers without annealing and with annealing in different atmosphere conditions. Reproduced with permission.^[119] Copyright 2015, Wiley-VCH. C) Scanning electron microscope images of MAPbI₃ films stored in dark (left) and light (right) under humidity conditions. Reproduced with permission.^[87] Copyright 2016, Royal Society of Chemistry. D) Schematic illustration of sublimation or decomposition of MABr, MA⁺, and Br⁻ from MAPbBr₃ films under long thermal annealing. Reproduced with permission.^[110] Copyright 2016, Elsevier B.V.

coupling and ion migration.^[74–76] Easily decomposed lattices of MHP crystals show low formation energy of defects (e.g., 27 – 73 meV for Schottky defects).^[16,77,78] These defect sites have energy levels located 100 – 400 meV below the bandgap in the MHPs,^[78] and therefore can trap the charge carriers and limit the LE. Here, we categorize the reasons for defect formations in MHP crystals into i) flaws during crystal formation and ii) effects of external factors.

Defect states can easily be formed as the perovskite crystallizes. Representatively, MHPs are crystallized by one-step solution process to fabricate polycrystalline bulk films. During solvent evaporation and crystallization, MHP films develop defects due to solubility difference between each precursors (e.g., MAX, PbX₂) in solvents,^[79] loss of ions,^[4] and incomplete reaction between each precursors.^[4] These phenomena yield nonstoichiometric crystal structures, so the MHP films include metallic Pb that can quench the PL.^[4] Fast and direct crystallization during solution process can also induce unreacted

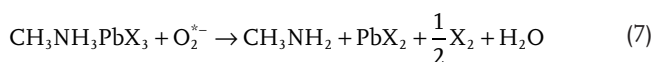
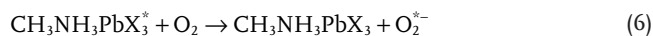
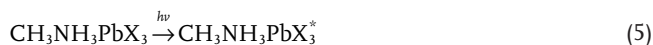
intermediate products,^[80,81] and byproducts from solvent–precursor reactions (e.g., MA vacancy ((CH₃NH₂)_xHPbI₃), iodide vacancy ((CH₃NH₂)_xH_yPbI_{2+y} ($x > 0$, $y < 1$)),^[80] Insufficient conversion of precursors to perovskite crystals, and precursor residues on perovskite crystals can occur during other crystallization processes such as two-step solution,^[82] vacuum evaporation,^[83] or chemical vapor deposition.^[84] In the case of excess MABr vapor concentration in the vapor-assisted solution process, redissolution of solid perovskite crystals or precursors into vapor states can occur,^[85] and then induce defect states.

Although perfect perovskite crystals without any defect states can be formed using well-controlled crystallization methods, perovskite crystals can degrade and develop defect states during exposure to light, moisture, air or other environmental factors.^[86,87] Light exposure causes significant and complex effects on the perovskite crystals; examples include change of defect density and shape of crystal structure. Light excitation on MHPs at moderate intensity can increase the LE by reducing the defect-mediated recombination pathway^[55,88] and inducing halide redistribution,^[89] but light exposure can also induce defect states.^[90,91] The positive effect of light exposure on MHP crystals is a result of defect passivation, whereas the negative effect is a result of decomposition of perovskite crystals as^[90]



in the presence of the halogen gas (X₂), decomposition of perovskite crystals has negative Gibbs free energy,^[92,93] this means that degradation and defect formation in MHPs become spontaneous and further accelerated.^[94] Light excitation can also reduce the LE of MHP crystals by inducing ion segregation,^[95] transformation of crystal structures,^[96] metastable states,^[97] and ion migration,^[98] and decomposition of PbX₂ to Pb metal and X₂.^[91]

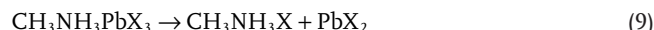
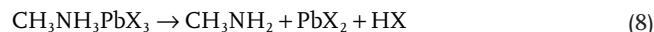
Oxygen also has mixed effects on the LE of MHP crystals. The positive effect is that the unpaired electron in oxygen passivates the trap states (uncoordinated Pb²⁺ or MA⁺)^[99] in a manner that is similar to passivation by Lewis bases.^[100] The negative effect is that oxygen can induce hydrolysis of perovskite crystals (Figure 4B).^[93] Simultaneous exposure to light and oxygen causes formation of superoxide (O₂⁻) in MHP crystals, and further accelerates the decomposition and defect formation in MHP crystals as^[101,102]



Moisture can react with MHPs to generate hydrated species similar to ((CH₃NH₃)₄PbX₆ · 2H₂O) which weaken the hydrogen bonding between organic cations and inorganic PbX₆ octahedra, and thereby change the crystal structure (Figure 4C).^[103] These hydrated species consist of isolated PbX₆⁴⁻ octahedra and (CH₃NH₃ ··· H₂O ··· H₃NH₃C)⁴⁺ dimers;^[104] 0D PbX₆⁴⁻ octahedra are nonemissive^[105] or emit at

low efficiency,^[106] so their presence can reduce LE. The degree of moisture effects on LE of different MHP crystals can vary; MAPbI₃ have unstable tetragonal structure, whereas MAPbBr₃ has relatively stable cubic structure due to radii of halogen anions (Cl⁻: 167 pm; Br⁻: 182 pm; I⁻: 206 pm).^[107] Therefore, moisture can more easily penetrate into the MAPbI₃ crystal structure than into MAPbBr₃ crystal structure. MAPbI₃ began to decompose and to change color from dark brown to yellow at humidity >55%, however, MAPb(Br_xI_{1-x})₃ maintained crystal structure under the same conditions.^[108] MAPbBr₃ polycrystalline films with cubic structure showed stable PL efficiency, PL spectrum and crystallinity in ambient air for >1 h.^[3] Short exposure of FAPbI₃ crystals to 55% moisture increase their LE,^[109] therefore, further studies of the effects of moisture exposure on MHP crystals should be conducted.

Heat can also induce formation of defect states in MHP crystals and reduce LE of PeLEDs because MHPs are very vulnerable to heat treatment (Figure 4D). One factor is thermal annealing, which is necessary to fabricate highly crystalline MHP^[110] and to achieve uniform MHP films for high-efficiency PeLEDs.^[111] Joule heating^[112] during device operation can also cause damage. The optimal annealing temperature T_{ANN} of MHPs is 60 ≤ T_{ANN} ≤ 100 °C considering their decomposition temperatures (≈125 °C for MAPbI₂Br;^[113] ≈150 °C for MAPbI₃;^[114] ≈220 °C for MAPbBr₃^[115]), but optimal annealing time varies with T_{ANN}.^[110,116] If T_{ANN} is too low, the residual solvents are not fully evaporated, and the perovskite precursors^[117] or intermediate species^[80] are not completely converted to perovskite crystals. If T_{ANN} is too high, the MHP crystals can decompose as^[117]



these reactions can severely reduce the LE of MHPs.

Growth of PbX₂ in the grain boundary can passivate the grain boundary^[116] and increase the LE of MHPs,^[4] but the insulating properties of PbX₂ limit the EL efficiency of PeLEDs.^[4] Annealing time can also affect the LE of MHPs and PeLEDs.^[110] Damage to MHPs by thermal annealing can be accelerated in the presence of O₂,^[115] light,^[118] or moisture;^[119,120] these factors can even induce recrystallization, segregation and delamination of perovskite crystals from underlayers.^[119,120] These defects induce gap states within the bandgap of MHP crystals^[78] which trap the charge carriers and limit the LE of MHPs and PeLEDs.

2.2. Limitations in Luminescence Efficiency of PeLED Devices

When electrical bias is applied to PeLEDs that have multilayered structure (e.g., anode/hole injection layer (HIL)/MHP EML/electron transport layer (ETL)/cathode), holes are injected into anode and electrons are injected into cathode. Then holes move to the VBM of the MHPs through the highest occupied molecular orbital of the HIL, and electrons move to the CBM of the MHPs through the lowest unoccupied molecular orbital of the ETL. These charge carriers recombine in the MHP EML

and generate light that has similar energy to the bandgap of the MHPs. These lights are emitted through transparent electrodes. Here, the EL efficiency (EQE) of PeLEDs is mainly calculated as^[121]

$$\text{EQE} = \chi\gamma\beta\phi_L \quad (10)$$

where χ is the outcoupling factor, γ is the charge-balance factor, β is the probability of production of emissive species, and ϕ_L is the quantum efficiency of luminescence. Therefore, in addition to the inherently low PLQE in MHP crystals due to low radiative recombination rate of charge carriers, charge carrier–ionic lattice coupling and defect states as mentioned in the previous Section 2.1 (related to the ϕ_L in Equation (10)), poor outcoupling efficiency of light (optical losses at interfaces; related to the χ in Equation (10)) and low charge balances in devices (electrical losses at interfaces; related to the γ in Equation (10)) severely limit the EL efficiency of PeLEDs. Furthermore, rough MHP film morphology, aggregation of colloidal MHP NCs during film formation, operational instability, and diffusion of metallic quenchers from electrode into MHP EML can reduce the EL efficiency of PeLEDs.

2.2.1. Rough Film Morphology

The simplest and best-known method to fabricate the MHP films is a one-step solution process in which perovskite precursors are dissolved in polar solvents, then perovskite crystals are produced by evaporating the solvents during spin-coating or other film-formation methods.^[3] However, MHP crystals formed by this process have very large cuboid structure >1 μm and numerous voids in films which severely reduce the EL efficiency by inducing leakage current in devices.^[4] Fast crystallization^[122] and large colloidal lead polyhalides ($\text{PbX}_2 + \text{CH}_3\text{NH}_3\text{X} \rightarrow \text{PbX}_3^- \cdot x\text{DMF} + \text{CH}_3\text{NH}_3^+$)^[80,123] in solution induced by solubility difference between each precursors in polar solvents (e.g., *N,N*-dimethylformamide (DMF)) are the main causes of nonuniform MHP films with large cuboid structures, numerous voids and low crystal density (Figure 5A). Various pathways of perovskite crystal growth (solution growth and colloidal growth) can also induce rough film morphology.^[123]

Two-step solution process and vacuum-deposition process can minutely control the crystallization process and fabricate high-quality MHP films. However, in these processes, incomplete conversion of BX_2 films to ABX_3 crystals or excess AX residues,^[82] redissolution of perovskite crystals into ions,^[85] and inaccurate deposition rate of each perovskite precursors^[124] can also induce rough MHP films and limit the EL efficiency of PeLEDs.

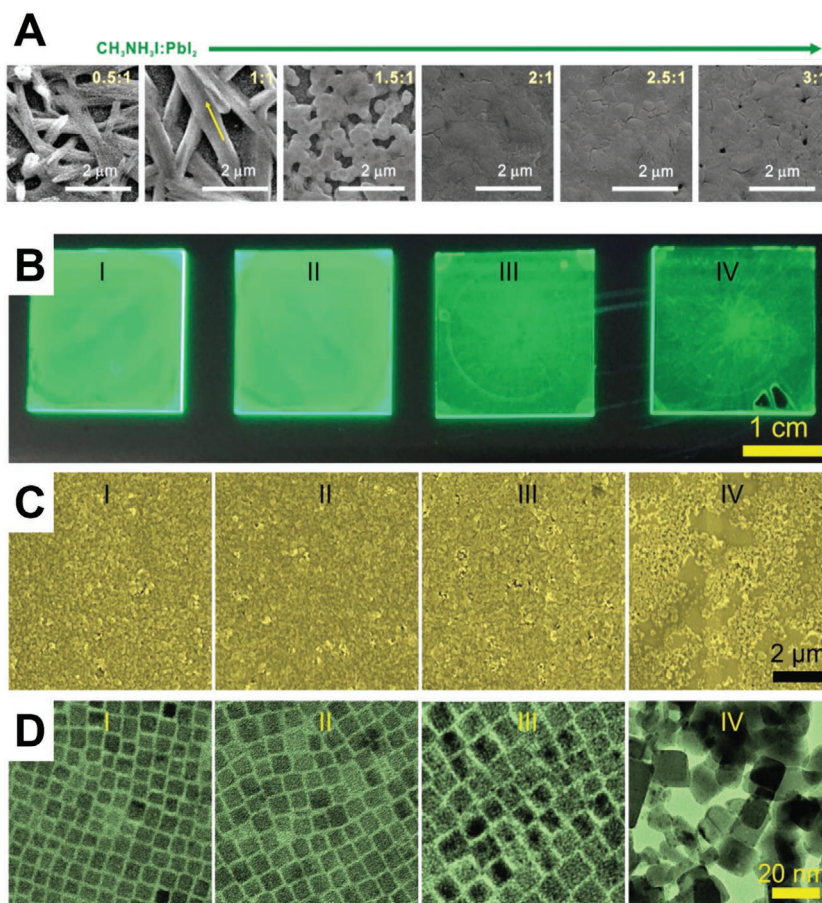


Figure 5. A) Scanning electron microscope images of MAPbI_3 films with different MAI:PbI₂ ratio. Reproduced with permission.^[123] Copyright 2015, American Chemical Society. B) Photographs, C) scanning electron microscope images, and D) transmission electron microscopy images of NC films after different number of purification cycles ((1)–(4)). Reproduced with permission.^[130] Copyright 2017, Wiley-VCH.

2.2.2. Aggregation and Insulating Ligands of Colloidal MHP NCs

Colloidal MHP NC is a promising MHP crystal form to achieve highly efficient PeLEDs. Colloidal MHP NCs have much higher PLQE (>90% in solution at both low and high excitation intensities)^[5] than do other crystal forms ($\approx 36\%$ in polycrystalline forms),^[4] but achieve similar EL efficiency in PeLEDs (EQE $\approx 13.4\%$ in green emission^[39]) compared to that in PeLEDs based on PC films (EQE $\approx 14.36\%$ in green emission,^[37] EQE $\approx 11.7\%$ in NIR emission^[38]). The main reasons for limited EL efficiency in PeLEDs based on colloidal MHP NCs despite high PLQE are that they aggregate readily in highly concentrated solution^[125] or during film formation,^[6] that fabrication of thick and uniform films is difficult,^[125] and that insulating organic ligands surround NC surfaces.^[21,43,126]

Colloidal MHP NCs with initial dimension ≈ 10 nm synthesized by various methods (e.g., hot-injection methods,^[40,127] reprecipitation methods^[6]) can easily form agglomerations with diameter >100 nm during film formation; they yield a rough film with many pinholes.^[128] Large grains decrease the electron–hole wavefunction overlaps and consequently reduce PLQE (from $\approx 80\%$ in solution states to $\approx 10\%$ in film states,

in CsPbBr₃ NCs),^[129] and rough film limits the EL efficiency in PeLEDs by inducing severe leakage current.^[128] Agglomeration can also complicate fabrication of thick and uniform NC films.^[21]

Organic ligands are necessary for synthesis of stable colloidal MHP NCs, but these organic ligands consist of long alkyl chains, which can impede charge transport in film states and limit the EL efficiency of PeLEDs. Therefore, many researchers have tried to remove organic ligands by washing,^[130] by replacing long ligands with short ligands^[43] or by controlling ligand density and length during synthesis.^[21,22] However, inadequate or excess ligand post-treatments can induce further aggregation of NCs and reduce their PLQE (Figure 5B–D).^[43,130] Furthermore, functional groups in organic ligands such as amine (NH³⁺) and carboxyl (COO⁻) are unstable on the NC surface, and can react with each other; these processes can also induce aggregation and limit the LE of NCs and PeLEDs.^[43,126] Randomly deposited NCs in films also prevent the formation of densely packed uniform film and thus limit the EL efficiency of PeLEDs.^[131]

2.2.3. Electrical and Optical Losses at the Interfaces

Interfaces between MHP EML and HIL or ETL have a strong influence on the EL efficiency of PeLEDs because MHPs have different optical^[132,133] and electrical^[24] properties with conventional organic^[3] or inorganic^[134,135] interlayers. MHPs have a much deeper VBM (≈ 5.6 eV in MAPbI₃, and ≈ 5.9 eV in MAPbBr₃)^[24] than the workfunction (WF) of conventional transparent conductive oxide (TCO) electrodes (≈ 4.8 eV in ITO, ≈ 5.0 eV in fluorine-doped tin oxide (FTO),^[136] ≈ 5.0 eV in indium zinc oxide (IZO)^[137]) and than that of hole injection materials (≈ 4.8 eV in PEDOT:PSS,^[3] ≈ 5.3 – 5.4 eV in NiO_x^[134]). MHP also has a CBM (≈ 3.6 eV in MAPbI₃, ≈ 3.6 eV in MAPbBr₃)^[24] that is shallower than the WF of conventional metal-oxide electron transport materials (≈ 4.2 eV^[135] or ≈ 3.7 eV^[138] in ZnO). These energy-level offsets induce large hole/electron injection barriers and reduce the EL efficiency by impeding the electron–hole charge injection balance (reducing γ in Equation (10)) in PeLEDs.

MHPs have refractive indices $n > 2.2$ in solution-processed thin films,^[132,139] and ≈ 2.5 in single crystals^[132] which are higher than those of typical organic layers ($n \approx 1.8$) and transparent electrode ($n \approx 1.8$ in ITO).^[140] When generated light passes from an MHP with higher n to adjacent organic interlayers with lower n , a large amount of light is reflected at the interfaces and trapped inside the MHP layer; this process is called waveguide mode and is explained by Snell's law.^[140] Light that is generated by MHP EMLs can also be trapped at the transparent electrode/air interfaces ("substrate mode") and at the MHP/nontransparent electrode interfaces ("surface plasmon mode") as also occur in OLEDs and QD LEDs.^[140] These

effects can reduce χ in Equation (10) and thereby reduce the EL efficiency of PeLEDs.

The recombination mechanism and PLQE of MHPs are also strongly affected by interlayers. Because of unprecedentedly long charge carrier-diffusion length of MHPs (e.g., ≈ 100 nm in CH₃NH₃PbI₃,^[46,141] > 1 μm in CH₃NH₃PbI_{3-x}Cl_x^[46]), charge carriers can easily be quenched by the PEDOT:PSS interfaces^[3] or the ZnO interfaces.^[142,143] Metallic species that migrate from electrodes into inner layers in PeLEDs (e.g., Au diffusion from Au cathode during annealing at moderate $T_{\text{ANN}} \approx 70$ °C,^[144] etched In and Sn from ITO anode by overcoating acidic PEDOT:PSS layer as^[145,146])



also severely quench the radiative recombination and limit the LE of MHPs (Figure 6A).

Adsorption of polystyrene sulfonate (PSS⁻) ligands in PEDOT:PSS to a protonated ITO surface can weaken the In–O and Sn–O bond strengths and detach PSS–In and PSS–Sn complexes from the ITO surface.^[147,148] Direct contact between metal electrodes (e.g., Al) and MHPs induces redox reactions that convert Pb²⁺ to Pb⁰ and MAPbI₃ to MA₄PbI₆·2H₂O; these species reduce both the stability and PLQE of MHPs.^[149] Even in the presence of interlayers, moisture exposure facilitates ion diffusion that causes the redox reaction, and acts as a decomposition reagent (Figure 6B).^[149] Moreover, MHPs reacted with Ag electrodes and severely degraded by a change of silver (Ag⁰) to silver iodide (Ag⁺I⁻);^[150] these reactions severely reduce the LE of MHPs and PeLEDs.

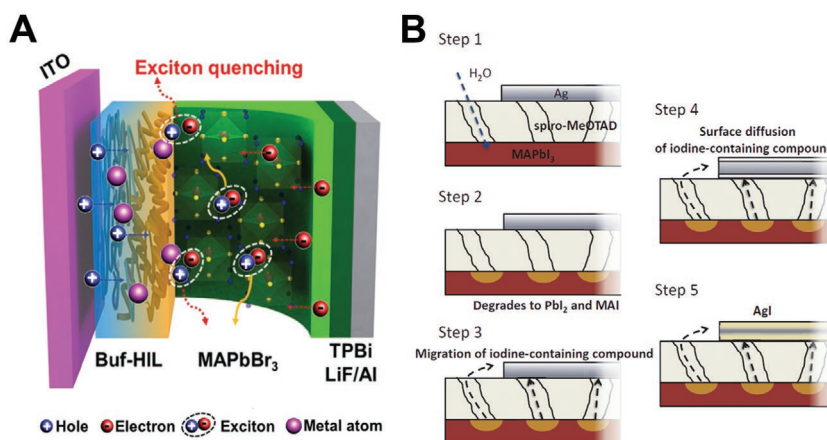


Figure 6. A) Schematic illustration describing the diffusion of metallic species from ITO electrode into MHP EML and exciton quenching induced by them in PeLEDs. Reproduced with permission.^[145] Copyright 2017, Wiley-VCH. B) Schematic illustration of degradation mechanism of Ag electrode induced by H₂O penetration. Reproduced with permission.^[150] Copyright 2015, Wiley-VCH.

2.2.4. Operating Instabilities

Electrical stresses during device operation can passivate the defect states and increase the EL efficiency; these changes temporarily increase the luminance and device efficiencies of PeLEDs under increasing applied current density (or bias)^[4] or under multiple electrical scans.^[151] However, electrical stresses can also induce migration of charged defects (e.g., MA vacancies, Pb vacancies, and X defects)^[152] or ions^[151] in MHP crystals, and these processes generate defect states by inducing accumulation or deficiency of ions in crystal structures, and result in reversible conversion from perovskite (MAPbX₃) to lead halide (PbX₂); these processes limit the EL efficiency of PeLEDs.^[153]

The crystal structure of MHPs formed by ionic bonding results in low activation energy for ion-migration (0.08^[152] or 0.33 eV^[154] for I⁻; 0.23 – 0.25^[155] or 0.09 eV^[152,156] for Br⁻; 0.8 eV for Pb²⁺;^[152] 0.36^[157] or 0.46^[152] or 0.55 eV^[154] for MA⁺) and low formation energy of charged defects (0.23 – 0.83 eV for I⁻; 0.2 – 0.93 eV for MA⁺).^[78] Owing to these low energies, ions can move in MHP crystals under small electric fields of 0.3 – 1 V μm⁻¹^[157,158] in MAPbI₃ films and 0.5 V μm⁻¹ in MAPbBr₃ films.^[98] Ions can migrate through various diffusion channels such as grain boundaries, Schottky defects, Frenkel defects, and lattice distortions caused by electric fields, accumulated charges or impurities.^[76]

Ion migration can also have both beneficial and harmful effects on device operation and EL efficiency in PeLEDs. MA⁺ cations and X⁻ anions that accumulate on the cathode and anode side induce p-doping and n-doping (p–i–n structure, also called poling) in MHP layers; these induce a sharp tunneling barrier and facilitate injections of electrons and holes from the each electrodes into the EML.^[157,159] Furthermore, short-distance migration of local excess ions can passivate defect states and increase the EL efficiency.^[89,151] However, ion migration can easily generate defect states by back-diffusion of ions or migration of nonexcess ions which were located in the perovskite crystal structure.^[89,151] Furthermore, charge imbalance in PeLEDs which can arise by ion-migration can induce luminescence quenching by annihilation of electron–hole pairs that in turn reduces the EL efficiency in PeLEDs.^[160]

Electrical fields also induce color instability in PeLEDs based on mixed-halide MHPs. PeLEDs based on mixed-halide MHPs (e.g., CsPbCl_xBr_yI_{3-x-y}, MAPbCl_xBr_yI_{3-x-y}) show driving-voltage or operating-time dependent variable emission spectrum due to halide separation and phase segregation in MHP emission layer.^[161,162] These color instability of mixed-halide based PeLEDs can be further analyzed by molecular dynamics simulation and cathodoluminescence imaging.^[163]

3. Strategies to Improve Luminescence Efficiency of MHP Materials and PeLEDs

Many research groups have tried to overcome the limitations to LE and to increase the EL efficiency of PeLEDs.^[3,138,145] Methods include fabrication of uniform MHP EML,^[4,164,165] crystal engineering,^[166] dimension and dimensionality control of MHP crystals or grains,^[4,167,168] synthesis and ligand

engineering of MHP colloidal NCs or QDs,^[21,22,43,130,169] defect passivation,^[100,170] and optimization of device architecture. Especially, researchers have mainly tried to i) reduce the grain size^[4] or dimensionality^[167] of MHPs, which are necessary to improve the LE of MHPs by confining the electron–hole pairs, ii) heal the surface defects in the grain boundary by organic additives,^[36] Lewis bases,^[100,171] and amine-based molecules,^[170] iii) reduce the ligand concentration and length in NC films,^[21,22] and iv) decrease the luminescence quenching sites in device architecture.^[4,145] In this section, we provide various recently reported strategies to improve the LE of MHPs and PeLEDs (Figure 7). We also summarize the improvement of EL efficiencies in PeLEDs by categorizing these strategies (Tables 1 and 2).

3.1. Dimensionality and Dimension Control

Decreasing the dimension from micrometer scale to nanometer scale,^[4,36] and dimensionality from 3D to 2D or 0D^[167] are the most effective ways to increase the LE of PeLEDs because they can increase LE of MHPs by confining the charge carriers and improving the possibility of radiative recombination of electron–hole pairs (excitons).

Dimension of MHPs can easily be reduced by nanocrystal pinning (NCP) in which dripping volatile solvents on the perovskite quasifilms during spin coating wash out the remaining solvents (e.g., dimethyl sulfoxide (DMSO), DMF), quench the growth of perovskite crystals and thus induce the reduced grain size (Figure 8A).^[4,36,134] NCP also effectively smoothens the surface morphology (Figure 8B,C). Grain size and film morphology can be controlled by choosing the dripping solvents^[172,173] and perovskite precursors.^[174] The grain size-reduction effect by NCP is maximized by adding organic semiconductors (TPBI), which can act as impurities that impede grain growth, into volatile solvents; small grain size of 50 – 200 nm (average grain size ≈ 87 nm) in MAPbBr₃ films was achieved (Figure 8D).^[4,36] TPBI also improved the charge balance in MAPbBr₃ EMLs and healed the defect states in the grain boundaries (Figure 8E,F); these methods yielded PeLEDs that had high EL efficiencies (EQE ≈ 8.79%).^[36]

2D MHPs, in which a PbX₆ octahedra is sandwiched between long or large OA, showed more strongly confined electron–hole pairs in PbX₆ inorganic layers and much lower trap density than 3D MHPs (MAPbI₃); these causes k_1 to be related to $k_{1,\text{exciton}}$ rather than to $k_{1,\text{defects}}$ and increases PLQE.^[55,175] However, in 2D MHP polycrystalline bulk films and PeLEDs based on them, long and huge insulating OA groups inhibit charge transport and thereby limit EL efficiency in PeLEDs.^[167] To achieve moderate charge transport characteristics while maintaining efficient confinement of electron–hole pairs, quasi-2D structures, called Ruddlesden–Popper (RP) phase, were incorporated by mixing 3D perovskites with 2D perovskites. The average number of layers (dimensionality) of PbX₆ octahedral planes (m in (large OA)₂(MA or FA)_{*m*-1}Pb_{*m*}X_{3*m*-1}, m = from 1 (2D structure) to ∞ (3D structure)) can be tailored by controlling the mixing ratio between 2D perovskite precursors and 3D perovskite precursors.^[167] The large OA cations intercalate between separated 3D perovskites by relatively weak van der Waals

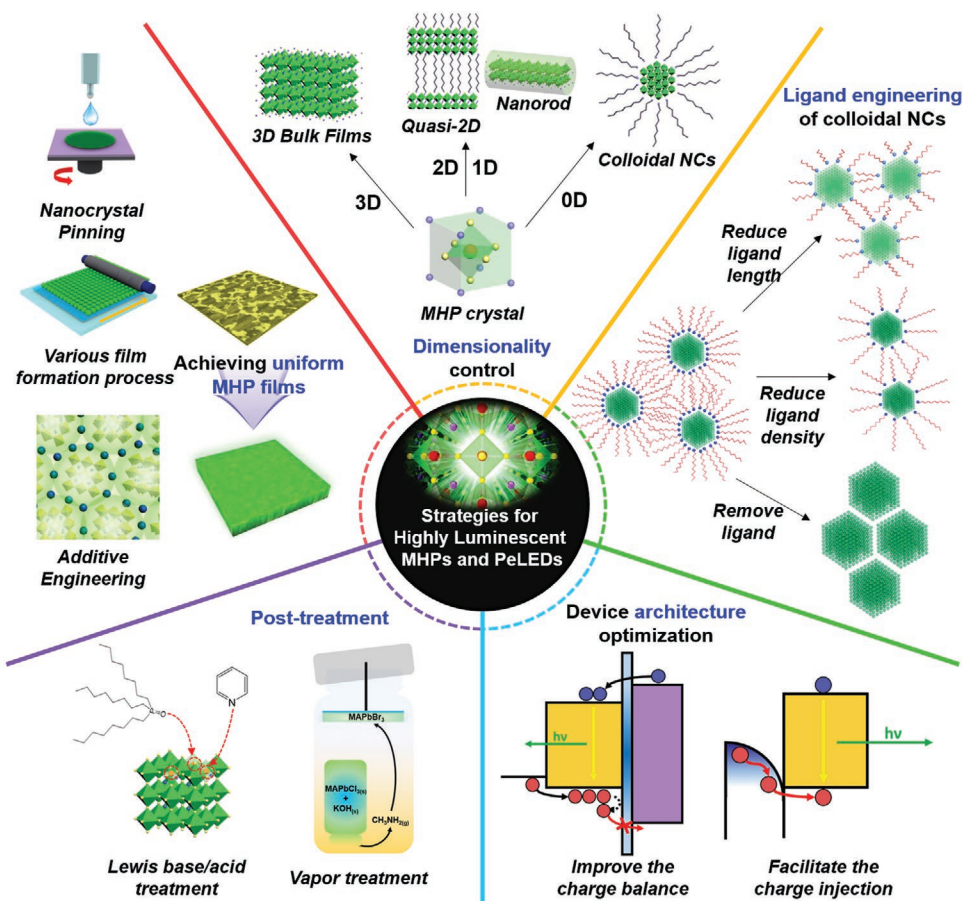


Figure 7. Schematic illustration of various strategies to improve the LE of MHPs and PeLEDs.

interactions,^[55] in this way they confine the electron–hole pairs inside the 3D MHP crystals and thereby prevent the dissociation of electron–hole pairs into free charge carriers. As a result, radiative recombination of electron–hole pairs is increased; this effect can be confirmed by much shorter PL lifetime of quasi-2D MHPs (≈ 20 ns) than that of 3D MHPs (≈ 1200 ns) and the linear dependence of PL intensity on injected carrier density.^[55] Quasi-2D MHPs also showed higher E_b (>200 meV for $(\text{PEA})_2(\text{MA})_{m-1}\text{Pb}_m\text{I}_{3m-1}$ (PEA: phenylethylene ammonium) than did 3D MHPs (≈ 20 meV for MAPbI_3).^[168] However, in 2D and quasi-2D MHP polycrystalline bulk films, large exciton–LO phonon coupling caused by many dangling bonds (e.g., out-of-plane self-terminations of PbX_6 octahedra) and excess excitons due to efficient spatial confinement can also limit LE as described in Section 2.1.2.^[55] Therefore, optimum MHP crystal structures which have efficient exciton confinement, moderate charge transport, and low exciton–LO phonon coupling should be developed to maximize the LE in PeLEDs.

Quasi-2D MHPs are composed of various perovskite structures that have different dimensionalities; this arrangement induces energy transfer from crystals with large bandgap (small m) to crystals with low bandgap (large m) because crystals with different dimensionality were located near each other (Figure 9A). This energy transfer induced a higher concentration of electron–hole pairs (excitons) on crystals that had relatively smaller bandgaps, and achieved high PLQE under

low excitation density because only defect states in crystals with relatively smaller bandgaps need to be passivated.^[168]

The dimensionality (bandgap) distribution in MHP crystals can be controlled by changing the compositions, and by solvent engineering; when quasi-2D MHPs have large-bandgap crystals as major components and a relatively graded dimensionality distribution, energy transfer was boosted, so PLQE and EL efficiency in PeLEDs can be increased (PLQE $\approx 12\%$, EQE $\approx 5\%$ in pristine quasi-2D films; PLQE $\approx 60\%$, EQE $\approx 7.4\%$ in optimized quasi-2D films) (Figure 9B,C).^[176]

Quasi-2D MHP films also showed reduced trap density and reduced number of nonradiative recombination channels compared to the 3D MHP films, because large OA can passivate the surface defects in 3D MHP films;^[177] this effect can be confirmed by measuring the trap density of states (tDOS) in PeLEDs,^[167] and by increase of PLQE (from 1 to 2% for MAPbBr_3 to 34% for $(\text{PEA})_2(\text{MA})_{m-1}\text{Pb}_m\text{Br}_{3m-1}$,^[167] from 0.2% for MAPbI_3 to 10.6% for $(\text{PEA})_2(\text{MA})_{m-1}\text{Pb}_m\text{I}_{3m-1}$ ^[168]). Quasi-2D MHPs also showed much faster recombination rates ($k_1 \approx 5 \times 10^7 \text{ s}^{-1}$, $k_2 \approx 2 \times 10^{-9} \text{ cm}^3 \text{ s}^{-1}$, $k_3 \approx 2 \times 10^{-26} \text{ cm}^6 \text{ s}^{-1}$) than did 3D MHPs ($k_1 \approx 9 \times 10^5 \text{ s}^{-1}$, $k_2 \approx 7 \times 10^{-10} \text{ cm}^3 \text{ s}^{-1}$, $k_3 \approx 3 \times 10^{-28} \text{ cm}^6 \text{ s}^{-1}$).^[55] These indicate that quasi-2D MHPs can have much higher PLQE in LED operating conditions (charge carrier density $< 10^{15} \text{ cm}^{-3}$) than do 3D MHPs.

Incorporating large or long OA into perovskite precursors can also yield small grain size in uniform MHP films.

Table 1. Reported EL efficiencies and strategies in PeLEDs based on MHP polycrystalline bulk films.

Publication date ^[ref.]	Strategies	Emission layer (emission color, wavelength)	Device structure	EL efficiencies
2014/04 ^[2]	Confine the charge carriers in thin MHP PC films	MAPbBr ₃ (green, 517 nm) MAPbI _{3-x} Cl _x (NIR, 773 nm)	ITO/PEDOT:PSS/MAPbBr ₃ /F8/Ca/Ag ITO/TiO ₂ /MAPbI _{3-x} Cl _x /F8/MoO ₃ /Ag	EQE ≈ 0.1%, CE ≈ 0.3 cd A ⁻¹ , L ≈ 364 cd m ⁻² EQE ≈ 0.76 %, radiance ≈ 13.2 W sr ⁻¹ m ⁻²
2014/11 ^[3]	Prevent exciton quenching and improve hole injection at the interface (Buf-HIL)	MAPbBr ₃ (green, 543 nm)	ITO/buffer-HIL/MAPbBr ₃ /TPBI/LiF/Al	EQE ≈ 0.125%, CE ≈ 0.577 cd A ⁻¹ , L ≈ 417 cd m ⁻²
2015/02 ^[202]	Prevent the crystal growth by adding PIP additive	MAPbBr ₃ :PIP (green, ≈540 nm)	ITO/PEDOT:PSS/MAPbBr ₃ :PIP/F8/ Ca/Ag	EQE ≈ 1.2%, L ≈ 2800 cd m ⁻²
2015/02 ^[138]	Improve the film morphology and reduce electron injection barrier by adding PEI interlayer	MAPbI _{3-x} Cl _x (NIR, 768 nm) MAPbBr ₃ (green, 532 nm)	ITO/ZnO/PEI/MAPbI _{3-x} Cl _x /LiF/Al ITO/ZnO/PEI/MAPbBr ₃ /LiF/Al	EQE ≈ 3.5%, radiance ≈ 28 W sr ⁻¹ m ⁻² EQE ≈ 0.8%, PE ≈ 4 lm W ⁻¹ L > 20 000 cd m ⁻²
2015/08 ^[165]	Prevent the crystal growth by adding PEO additive	MAPbBr ₃ :PEO (green, 532 nm)	ITO/MAPbBr ₃ :PEO/In/Ga	EQE ≈ 0.165%, CE ≈ 0.74 cd A ⁻¹ , L ≈ 4064 cd m ⁻²
2015/09 ^[217]	Fabricate the uniform and bright EML by using coevaporation	MAPb(I _{0.6} Br _{0.4}) ₃ (NIR, ≈680 nm)	ITO/PEDOT:PSS/MAPb(I _{0.6} Br _{0.4}) ₃ / PCBM ³ /Ba/Ag	EQE ≈ 0.06%
2015/11 ^[164]	Retarding the crystallization by adding HBr additive	MAPbBr ₃ (green, 540 nm)	ITO/PEDOT:PSS/MAPbBr ₃ /SPB-02T ^b / LiF/Ag	EQE ≈ 0.1%, CE = 0.43 cd A ⁻¹ , L ≈ 3490 cd m ⁻²
2015/12 ^[4]	Improve the film morphology and reduce grain size by NCP and prevent metallic Pb by adding excess MABr additive	MAPbBr ₃ (green, ≈545 nm)	Polymeric anode/MAPbBr ₃ /TPBI/LiF/Al	EQE ≈ 8.52%, CE ≈ 42.9 cd A ⁻¹
2015/12 ^[216]	Fabricate the uniform EML by adding PEO additive in blade-coating process	MAPbBr ₃ :PEO (green)	ITO/MAPbBr ₃ :PEO/Ag nanowires	EQE ≈ 1.1%, CE = 4.91 cd A ⁻¹ , L ≈ 21 014 cd m ⁻²
2016/06 ^[167]	Improve the film morphology, reduce defect states, induce energy funneling by controlling MA:PEA ratio	PEA ₂ (MA) _{n-1} Pb _n Br _{3n+1} (green, 510 – 520 nm)	ITO/buffer-HIL/PEA ₂ (MA) _{n-1} Pb _n Br _{3n+1} / TPBI/LiF/Al	CE = 4.9 cd A ⁻¹ , L ≈ 2935 cd m ⁻²
2016/06 ^[168]	Improve the film morphology, reduce defect states, induce energy funneling by controlling MA:PEA ratio	PEA ₂ (MA) _{n-1} Pb _n I _{3n+1} (NIR, ≈760 nm)	ITO/TiO ₂ /PEA ₂ (MA) _{n-1} Pb _n I _{3n+1} /F8/ MoO ₃ /Au	EQE ≈ 8.8%, R = 80 W sr ⁻¹ m ⁻²
2016/08 ^[199]	Prevent the crystal growth by adding PEO additive	CsPbBr ₃ :PEO (green, 521 nm)	ITO/PEDOT:PSS/CsPbBr ₃ :PEO /TPBI/ LiF/Al	EQE ≈ 4.26%, CE ≈ 15.67 cd A ⁻¹ , L ≈ 53 525 cd m ⁻²
2016/08 ^[134]	Improve the film morphology by using NiO _x interlayer and MA gas treatment	MAPbBr ₃ (green, 540 nm)	ITO/NiO _x /MAPbBr ₃ /TPBI/LiF/Al	CE ≈ 15.9 cd A ⁻¹ , L ≈ 70 000 cd m ⁻²
2016/09 ^[38]	Improve the film morphology, reduce defect states, induce energy funneling by controlling FA:NMA ratio	NMA ₂ (FAPbI ₃) _{n-1} PbI ₄ (NIR, 786 nm)	ITO/ZnO/PEIE/NMA ₂ (FAPbI ₃) _{n-1} PbI ₄ / TFB ^d /MoO ₃ /Au	EQE ≈ 11.7%, R ≈ 82 W sr ⁻¹ m ⁻²
2016/09 ^[159]	Prevent the crystal growth by adding PEO and PVP additives	CsPbBr ₃ :PEO:PVP (green, 522 nm)	ITO/CsPbBr ₃ :PEO:PVP/In/Ga	EQE ≈ 5.7 %, PE ≈ 14.1 lm W ⁻¹ , L ≈ 593 178 cd m ⁻²
2016/10 ^[206]	Improve the film morphology by adding excess MABr additive	MAPbBr ₃ (green, 531 nm)	ITO/PEDOT:PSS/MAPbBr ₃ /TmPyPB ^d / LiF/Al	EQE ≈ 3.38 %, CE ≈ 15.26 cd A ⁻¹ , L ≈ 6124 cd m ⁻²
2016/11 ^[135]	Fabricate the uniform EML by using two-step solution process	FAPbBr ₃ (green, 540 nm)	ITO/ZnO/FAPbBr ₃ /poly-TPD/MoO ₃ /Al	EQE ≈ 1.16%, CE ≈ 2.65 cd A ⁻¹ , L ≈ 13 062 cd m ⁻²
2016/12 ^[212]	Fabricate the uniform EML by optimizing solution concentration in two-step solution process	MAPbBr ₃ (green, 539 nm)	ITO/ZnO/PEIE ^e /MAPbBr ₃ /PCDTBT ^f / MoO ₃ /Au	EQE ≈ 0.023%, CE ≈ 0.1 cd A ⁻¹
2016/12 ^[177]	Improve the film morphology by controlling MA:POEA ^g ratio	POEA ₂ (MA) _{n-1} Pb _n Br _{3n+1} (green, 520 nm)	ITO/PEDOT:PSS/ POEA ₂ (MA) _{n-1} Pb _n Br _{3n+1} /TPBI/LiF/Al	EQE ≈ 2.82%, CE ≈ 8.2 cd A ⁻¹
2016/12 ^[205]	Modify the crystal growth by adding excess CsBr additive	CsPbBr ₃ (green, 524 nm)	ITO/PEDOT:PSS/CsPbBr ₃ / B3PYMPM ^h /Cs ₂ CO ₃ /Al	EQE ≈ 0.15 %, CE ≈ 0.57 cd A ⁻¹ , L ≈ 7276 cd m ⁻²

Table 1. Continued.

Publication date ^[ref.]	Strategies	Emission layer (emission color, wavelength)	Device structure	EL efficiencies
2017/01 ^[178]	Improve the film morphology and reduce grain size by controlling MA:BA ratio	BA _{0.17} MA _{0.83} PbBr ₃ (green, 513 nm) BA _{0.2857} MA _{0.7143} PbI ₃ (NIR, 748 nm)	ITO/PVK/BA _{0.17} MA _{0.83} PbBr ₃ /TPBI/LiF/Al ITO/poly-TPD/BA _{0.2857} MA _{0.7143} PbI ₃ /TPBI/LiF/Al	EQE ≈ 9.3%, 17.1 cd A ⁻¹ EQE ≈ 10.4%,
2017/01 ^[172]	Improve the film morphology and reduce grain size by NCP	MAPbBr ₃ (green, ≈545 nm)	ITO/PEDOT:PSS/ MAPbBr ₃ /TPBI/LiF/Ag	EQE ≈ 0.71%, CE ≈ 3.31 cd A ⁻¹ , L ≈ 14 460 cd m ⁻²
2017/03 ^[215]	Improve the film morphology, by multicoating the MHP solution	MAPb _{1-x} Br _x (green, 540 nm yellow, 580 nm red, 635 nm)	ITO/PEDOT:PSS/ MAPb _{1-x} Br _x /Ca:ZnO/Ca/Al	green: EQE ≈ 6.2%, CE ≈ 21 cd A ⁻¹ , L ≈ 16 060 cd m ⁻² yellow: EQE ≈ 4.2%, CE ≈ 16 cd A ⁻¹ , L ≈ 4200 cd m ⁻² red: EQE ≈ 5.8%, CE ≈ 19 cd A ⁻¹ , L ≈ 10 100 cd m ⁻²
2017/04 ^[204]	Prevent the crystal growth by adding PVK and TPBI additives	MAPbBr ₃ :PVK:TPBI (green, 534 nm)	ITO/PEDOT:PSS/ MAPbBr ₃ :PVK:TPBI/Cs ₂ CO ₃ /Al	EQE ≈ 2.28 %, CE ≈ 9.45 cd A ⁻¹ , L ≈ 7263 cd m ⁻²
2017/05 ^[200]	Prevent the crystal growth by adding PEO additive and CF vapor treatment	CsPbBr ₃ :PEO (green, 525 nm)	ITO/PEDOT:PSS/CsPbBr ₃ :PEO/TPBI/LiF/Al	EQE ≈ 4.76%, CE ≈ 21.38 cd A ⁻¹ , L ≈ 51 890 cd m ⁻²
2017/05 ^[201]	Prevent the crystal growth by adding PVP additive	MAPbBr ₃ :PVP (green, 516 nm)	ITO/PVK:TPD/ MAPbBr ₃ :PVP/TPBI/Ba/Al	EQE ≈ 1.88 %, CE ≈ 6.5 cd A ⁻¹ , L ≈ 1427 cd m ⁻²
2017/05 ^[176]	Maximize the energy funneling by tailoring the composition of quasi-2D structure	PEA ₂ (MA) _{n-1} Pb _n Br _{3n+1} (green, 526 nm)	ITO/PEDOT:PSS/ PEA ₂ (MA) _{n-1} Pb _n Br _{3n+1} /TPBI/LiF/Al	EQE ≈ 7.4%, L = 8400 cd m ⁻²
2017/06 ^[143]	Improve the film morphology by using PVP interlayer and MABr additive	Cs _{0.87} MA _{0.13} PbBr ₃ (green, 520 nm)	ITO/ZnO/PVP/Cs _{0.87} MA _{0.13} PbBr ₃ /CBP ^{l)} /MoO ₃ /Al	EQE ≈ 10.43%, CE ≈ 33.9 cd A ⁻¹ , L ≈ 91 000 cd m ⁻²
2017/06 ^[156]	Improve the film morphology by adding excess CsBr additive and using Buf-HIL interlayer	CsPbBr ₃ (green, 522 nm)	ITO/Buf-HIL/CsPbBr ₃ /TPBI/LiF/Al	CE ≈ 5.39 cd A ⁻¹ , L ≈ 13 752 cd m ⁻²
2017/06 ^[84]	Improve the film morphology, by controlling substrate temperature and film thickness in chemical vapor deposition	MAPbBr ₃ (green, 510 nm)	ITO/PFN-OX ^{l)} /MAPbBr ₃ /TAPC/MoO ₃ /Au	EQE ≈ 0.02%, CE ≈ 0.06 cd A ⁻¹ , L ≈ 900 cd m ⁻²
2017/08 ^[203]	Prevent the crystal growth by adding PEG additive	CsPbBr ₃ :PEG (green, 522 nm)	ITO/PEDOT:PSS/ MAPbBr ₃ :PEG/TPBI/LiF/Al	EQE ≈ 5.34 %, CE ≈ 19 cd A ⁻¹ , L ≈ 36 600 cd m ⁻²
2017/10 ^[179]	Improve the film morphology, reduce defect states, induce energy funneling by controlling the Cs:PBA ^{k)} ratio	PBA ₂ (CsPbBr ₃) _{n-1} Pb _n Br ₄ (green, 514 nm) PBA ₂ (CsPbI ₃) _{n-1} Pb _n I ₄ (NIR, 683 nm)	ITO/NiO/TFB/PVK/ PBA ₂ (CsPbBr ₃) _{n-1} Pb _n Br ₄ /TPBI/LiF/Al ITO/NiO/TFB/PVK/ PBA ₂ (CsPbI ₃) _{n-1} Pb _n I ₄ /TPBI/LiF/Al	EQE ≈ 10.4% EQE ≈ 7.3%
2017/10 ^[132]	Fabricate the uniform and bright EML with low n by controlling MABr and PEABr ratio in vacuum deposition	PEA ₂ (MA) _{n-1} Pb _n Br _{3n+1} (green, 531 nm)	ITO/PEDOT:PSS/ PEA ₂ (MA) _{n-1} Pb _n Br _{3n+1} /TPBI/Liq/Al	EQE ≈ 0.36%, CE ≈ 1.36 cd A ⁻¹ , L ≈ 6200 cd m ⁻²
2017/11 ^[85]	Improve the film morphology, by controlling the evaporation time of MABr powder in vapor-assisted solution process	MAPbBr ₃ (green, 532 nm)	ITO/P-NiO/ MAPbBr ₃ /TPBI/LiF/Al	EQE ≈ 4.36%, CE ≈ 8.16 cd A ⁻¹ , L ≈ 6530 cd m ⁻²
2017/12 ^[36]	Improve the film morphology, passivate the defect and n-dope the EML by A-NCP	MAPbBr ₃ (green, 541 nm)	Polymeric anode/ MAPbBr ₃ /TPBI/LiF/Al	EQE ≈ 8.79%
2018/02 ^[37]	Confine the charge carriers in quasi-2D structure and passivate the defects by TOPO post-treatment	PEA ₂ (FAPbBr ₃) _{n-1} Pb _n Br ₄ (green, 532 nm)	ITO/m-PEDOT:PSS/ PEA ₂ (FAPbBr ₃) _{n-1} Pb _n Br ₄ /TOPO/TPBI/LiF/Al	EQE ≈ 14.36%, CE ≈ 62.4 cd A ⁻¹

^{a)}PCBM: [6,6]-phenyl-C₆₁-butyric acid methyl ester. ^{b)}SPB-02T: polymer blue (Merck). ^{c)}TFB: Poly[(9,9-dioctylfluorenyl-2,7-diyl)-co-(4,4'-(N-(4-sec-butylphenyl)diphenylamine))]. ^{d)}TmPyPB: 1,3,5-Tris(3-pyridyl-3-phenyl)benzene. ^{e)}PEIE: polyethylenimine ethoxylated. ^{f)}PCDTBT: poly[N-9'-heptadecanyl-2,7-carbazole-alt-5,5'-(4,7-di-2-thienyl-2',1',3'-benzothiadiazole)]. ^{g)}POEA: 2'phenoxyethylamine. ^{h)}B3PYMPM: 4,6-Bis(3,5-di(pyridin-3-yl)phenyl)-2-methylpyrimidine. ⁱ⁾CBP: 4,4'-Bis(N-carbazolyl)-1,1'-biphenyl. ^{j)}PFN-OX: 6,6'-(9',9'-Bis((3-ethoxyhexan-3-yl)methoxy)hexyl)-7,7'-diphenyl-9H,9'H-2,2'-bifluorene-9,9-diy]bis(N,N-diethylhexan-1-amine). ^{k)}PBA: phenylbutylammonium.

Table 2. Reported EL efficiencies and strategies in PeLEDs based on MHP NC films.

Publication date ^[ref.]	Strategies	Emission layer (emission color, wavelength)	Device structure	EL efficiencies
2015/10 ^[169]	High PLQE in colloidal MHP NCs	CsPbX ₃ (blue, 455 nm, green, 516 nm, orange, 531 nm)	ITO/PEDOT:PSS/PVK/CsPbX ₃ /TPBi/LiF/Al	Blue: EQE ≈ 0.07%, CE ≈ 0.14 cd A ⁻¹ L ≈ 742 cd m ⁻² green: EQE ≈ 0.12%, CE ≈ 0.43 cd A ⁻¹ , L ≈ 946 cd m ⁻² orange: EQE ≈ 0.09%, CE ≈ 0.08 cd A ⁻¹ , L ≈ 528 cd m ⁻²
2015/11 ^[128]	Improve the film morphology by overcoating PVK:PBD on NC films	MAPbBr ₃ (green, 530 nm)	ITO/PEDOT:PSS/MAPbX ₃ /PVK:PBD/BCP ³ /LiF/Al	EQE ≈ 0.48%, PE ≈ 1 lm W ⁻¹ , L ≈ 10 590 cd m ⁻²
2016/03 ^[44]	Improve the film morphology, passivate the surface defects and facilitate the charge carrier transport by TMA crosslinking method on NC films	CsPbX ₃ (blue, 480 nm, green, 523 nm, orange, 619 nm, red, 698 nm)	ITO/ZnO/CsPbX ₃ /TFB/MoO ₃ /Ag	Blue: EQE ≈ 0.0074%, L ≈ 8.7 cd m ⁻² green: EQE ≈ 0.19%, L ≈ 2335 cd m ⁻² orange: EQE ≈ 1.4%, L ≈ 1559 cd m ⁻² red: EQE ≈ 5.7%, L ≈ 206 cd m ⁻²
2016/05 ^[125]	Fabricate the uniform NC films by dip-coating method	MAPbX ₃ (blue, 445 nm, blue-green, 495 nm, green, 525 nm, orange, 595 nm, red, 640 nm)	ITO/PEDOT:PSS/PVK/MAPbX ₃ /TPBi/LiF/Al	Blue: EQE ≈ 1.38%, CE ≈ 4.01 cd A ⁻¹ L ≈ 2673 cd m ⁻² blue-green: EQE ≈ 1.13%, CE ≈ 3.87 cd A ⁻¹ L ≈ 2452 cd m ⁻² green: EQE ≈ 1.06%, CE ≈ 3.72 cd A ⁻¹ , L ≈ 2398 cd m ⁻² orange: EQE ≈ 0.98%, CE ≈ 2.02 cd A ⁻¹ , L ≈ 1053 cd m ⁻² red: EQE ≈ 0.53%, CE ≈ 1.52 cd A ⁻¹ , L ≈ 986 cd m ⁻²
2016/06 ^[45]	Convert as-deposited PC films to 2D nanoplates by solvent vapor annealing	(PEA) ₂ PbBr ₄ (blue, 410 nm)	ITO/PEDOT:PSS/(PEA) ₂ PbBr ₄ /TPBi/Ca/Al	EQE ≈ 0.038%
2016/08 ^[43]	Facilitate the charge carrier injection by replacing long ligands with short ligands	CsPbBr ₃ Cl _{3-x} (blue, 490 nm, green, 515 nm)	ITO/PEDOT:PSS/PVK/CsPbBr ₃ Cl _{3-x} /TPBi/LiF/Al	Blue: EQE ≈ 1.9%, L ≈ 35 cd m ⁻² green: EQE ≈ 3%, L ≈ 330 cd m ⁻²
2016/09 ^[42]	Boost the exciton binding energy by inducing dielectric confinement effect in 2D structure	MAPbBr ₃ :CBP (deep blue, 432 nm, blue, 456 nm, sky blue, 492 nm, green, 520 nm)	ITO/PEDOT:PSS/PVK/MAPbBr ₃ :CBP/TPBi/LiF/Al	Deep blue: EQE ≈ 0.004% blue: EQE ≈ 0.024% sky blue: EQE ≈ 0.23% green: EQE ≈ 2.31%, CE ≈ 8.1 cd A ⁻¹
2016/09 ^[40]	Improve the film morphology, and PLQE by adding PEI interlayer	CsPbBr ₃ _{1-3-x} (green, 516 nm, red, 688 nm)	ITO/ZnO/PEI/CsPbBr ₃ _{1-3-x} /CBP/TCTA/MoO ₃ /Au	Green: EQE ≈ 0.4%, CE ≈ 1.32 cd A ⁻¹ , L ≈ 3019 cd m ⁻² red: EQE ≈ 7.25%, CE ≈ 0.49 cd A ⁻¹ , L ≈ 435 cd m ⁻²
2016/11 ^[130]	Facilitate the charge carrier injection by washing the surface ligands	CsPbBr ₃ (green, 512 nm)	ITO/PEDOT:PSS/poly-TPD/CsPbBr ₃ /TPBi/LiF/Al	EQE ≈ 6.27%, CE ≈ 13.3 cd A ⁻¹ , L ≈ 15 185 cd m ⁻²
2017/03 ^[174]	In situ form MHP NC films without ligand and aggregation	MAPbBr ₃ :PEABr (green, ≈524 nm) MAPbI ₃ :FPMAl (NIR, 749 nm)	ITO/PEDOT:PSS/poly-TPD/MAPbBr ₃ :PEABr/TPBi/LiF/Al ITO/PEDOT:PSS/PVK/MAPbI ₃ :FPMAl/TPBi/LiF/Al	MAPbBr ₃ : EQE ≈ 7% MAPbI ₃ : EQE ≈ 7.9%
2017/03 ^[222]	In situ form MHP NC films without ligand and aggregation	MAPbBr ₃ :MABr (green, ≈527 nm)	ITO/PEDOT:PSS/MAPbBr ₃ :MABr/TPBi/LiF/Al	EQE ≈ 8.21%, CE ≈ 34.46 cd A ⁻¹
2017/03 ^[223]	Improve the crystallinity, PLQE and hole injection capability by controlling FA:Cs ratio	FA _{1-x} Cs _x PbBr ₃ (green, ≈526 nm)	ITO/PEDOT:PSS/TFB/FA _{1-x} Cs _x PbBr ₃ /TPBi/LiF/Al	EQE ≈ 2.8%, CE ≈ 10.09 cd A ⁻¹ , L ≈ 55 005 cd m ⁻²
2017/05 ^[126]	Both ligand exchange and wash the surface ligand	CsPbBr ₃ (green, 512 nm)	ITO/modified PEDOT:PSS/poly-TPD/CsPbBr ₃ /TPBi/LiF/Al	EQE of 8.73%, CE of 18.8 cd A ⁻¹
2017/06 ^[21]	Reduce ligand density during NC synthesis	MAPbBr ₃ (green, ≈515 nm)	ITO/Buffer-HIL/MAPbBr ₃ /TPBi/LiF/Al	EQE ≈ 5.09%, CE ≈ 15.5 cd A ⁻¹
2017/07 ^[218]	Improve the film morphology, conductivity, and PLQE by radical-based crosslinking	MAPbBr ₃ (green, 528 nm)	ITO/TiO ₂ /Al ₂ O ₃ /MAPbBr ₃ /F8/MoO ₃ /Ag	EQE ≈ 0.58%, CE ≈ 2.47 cd A ⁻¹ , L > 7000 cd m ⁻²

Table 2. Continued.

Publication date ^[ref.]	Strategies	Emission layer (emission color, wavelength)	Device structure	EL efficiencies
2017/07 ^[226]	Stabilize CsPbBr ₃ NCs by Mn ²⁺ doping	Mn ²⁺ doped CsPbBr ₃ (green, 512–515 nm)	ITO/PEDOT:PSS/poly-TPD/Mn ²⁺ doped CsPbBr ₃ /TPBI/LiF/Al	EQE ≈ 1.49%, CE ≈ 3.71 cd A ⁻¹ , L ≈ 9971 cd m ⁻²
2017/08 ^[6]	Boost the dielectric confinement effect by dispersing 2D MHP NCs in low <i>n</i> -PMMA matrix	FAPbBr ₃ :PMMA (green, 529 nm)	ITO/PEDOT:PSS/poly-TPD/FAPbX ₃ :PMMA/3TPYMB ^{m)} /LiF/Al	EQE ≈ 3.04%, CE ≈ 13.02 cd A ⁻¹ , PE ≈ 13.36 lm W ⁻¹ , L ≈ 2939 cd m ⁻²
2017/08 ^[131]	Fabricate the uniform NC films with preferred orientation	CsPbBr ₃ (green, 515 nm)	ITO/PEDOT:PSS/NPB/CsPbBr ₃ /BCP/LiF/Al	CE ≈ 0.09 cd A ⁻¹ , L ≈ 23 cd m ⁻²
2017/08 ^[22]	Reduce ligand length during NC synthesis	FAPbBr ₃ (green)	ITO/Buffer-HIL/FAPbBr ₃ /TPBI/LiF/Al	CE ≈ 9.16 cd A ⁻¹
2017/10 ^[221]	Fabricate the uniform NC films by centrifugal coating	CsPb ₂ Br ₅ (green, 520 nm)	ITO/PEDOT:PSS/CsPb ₂ Br ₅ /TPBI/LiF/Al	EQE ≈ 1.1%, CE ≈ 1.32 cd A ⁻¹ , L ≈ 7317 cd m ⁻²
2018/01 ^[228]	Synthesize stable NCs with octylphosphonic acid ligands	CsPbBr ₃ (green, 516 nm)	ITO/PEDOT:PSS/poly-TPD/CsPbBr ₃ /TPBI/LiF/Al	EQE ≈ 6.5%, CE ≈ 18.13 cd A ⁻¹ , L ≈ 7085 cd m ⁻²
2018/03 ^[39]	Induce energy cascade by controlling the FA:OAm ratio	(OAm) ₂ (FA) _{n-1} Pb _n Br _{3n+1} (green, 528–532 nm)	ITO/PEODT:PSS/(OAm) ₂ (FA) _{n-1} Pb _n Br _{3n+1} /PO-T2T ⁿ⁾ /Ca/Al	EQE ≈ 13.4%, CE ≈ 57.6 cd A ⁻¹ , L ≈ 34 480 cd m ⁻²

^{l)}BCP: bathocuproine; ^{m)}3TPYMB: Tris[2,4,6-trimethyl-3-(pyridine-3-yl)phenyl]borane; ⁿ⁾PO-T2T: 2,4,6-Tris[3-(diphenylphosphinyl)phenyl]-1,3,5-triazine.

The reason is that large or long OA effectively impedes the growth of 3D perovskite grains.^[167] Quasi-2D MHP films showed much decreased roughness ($\gamma_{\text{rms}} \approx 0.6$ nm in butylammonium (BA)_{0.2857}MA_{0.7143}PbI₃ films, $\gamma_{\text{rms}} \approx 1$ nm in BA_{0.2857}MA_{0.7143}PbBr₃ films) than did 3D MHP films ($\gamma_{\text{rms}} \approx 4.9$ nm in MAPbI₃ films, $\gamma_{\text{rms}} \approx 3.4$ nm in MAPbBr₃

films).^[178] With these advantages, PeLEDs based on quasi-2D MHP achieved high EL efficiencies (CE ≈ 4.9 cd A⁻¹^[167] or EQE ≈ 7.4%^[176] for (PEA)₂(MA)_{m-1}Pb_mBr_{3m-1}; EQE ≈ 2.82% and CE ≈ 8.23 cd A⁻¹ for (C₆H₅OCH₂CH₂NH₂)₂(MA)_{m-1}Pb_mBr_{3m-1},^[177] EQE ≈ 10.4% for (C₆H₅C₄H₈NH₃)₂(CsPbBr₃)_{m-1}PbBr₄ and EQE ≈ 7.3% for (C₆H₅C₄H₈NH₃)₂(CsPbI₃)_{m-1}PbI₄,^[179] EQE ≈ 8.8% and radiance ≈ 80 W sr⁻¹ m⁻² for (PEA)₂(MA)_{m-1}Pb_mI_{3m-1},^[168] EQE ≈ 9.3% for BA_{0.17}MA_{0.83}PbI₃ and EQE ≈ 10.4% for BA_{0.17}MA_{0.83}PbBr₃,^[178] EQE ≈ 11.7% and radiance ≈ 82 W sr⁻¹ m⁻² for (C₁₀H₇CH₂NH₂)₂(FAPbI₃)_{n-1}PbI₄,^[38] EQE ≈ 14.36% and CE ≈ 62.4 cd A⁻¹ for PEA₂(FAPbBr₃)_{n-1}PbBr₄ with TOPO treatments (EL data was measured by silicon photodiode and EQE was calculated by assuming Lambertian emission profile)^[37] (Figure 9D,E)). These LEs of PeLEDs based on quasi-2D MHPs are the highest values among PeLEDs so far, thus further optimization of large or long OA and their processing should be intensively conducted.

Mixing various small OA cations can also yield uniform MHP films with smaller grains, and yield efficient PeLEDs. Partially incorporating inorganic cation (Cs⁺) into FA-based MHPs increased the crystallinity, phase-stability, and stability during excitation by light, humidity heat.^[180–182] Furthermore, 10% doping of Cs on FAPbBr₃ films reduced grain size from ≈325 nm to ≈199 nm and reduced trap density while maintaining a single phase, so PLQE (≈28.3%) and EL efficiencies in PeLEDs (EQE ≈ 3.1%, CE ≈ 14.5 cd A⁻¹) were increased.^[183] Mixing a small amount of organic cations (MA⁺) into

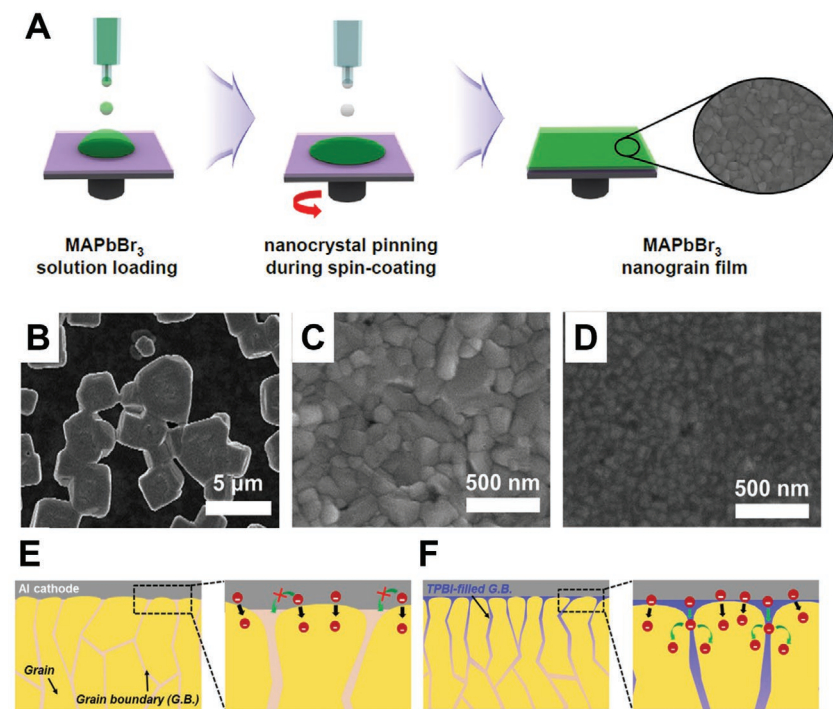


Figure 8. A) Schematic illustration describing the NCP. Scanning electron microscope images of MAPbBr₃ polycrystalline films B) without NCP, C) with NCP, and D) with TPBi based NCP. Reproduced with permission.^[4] Copyright 2015, The American Association for the Advancement of Science. E,F) Schematic illustration of trap-filling and electron injection improvement effect by A-NCP. Reproduced with permission.^[36] Copyright 2017, Elsevier Ltd.

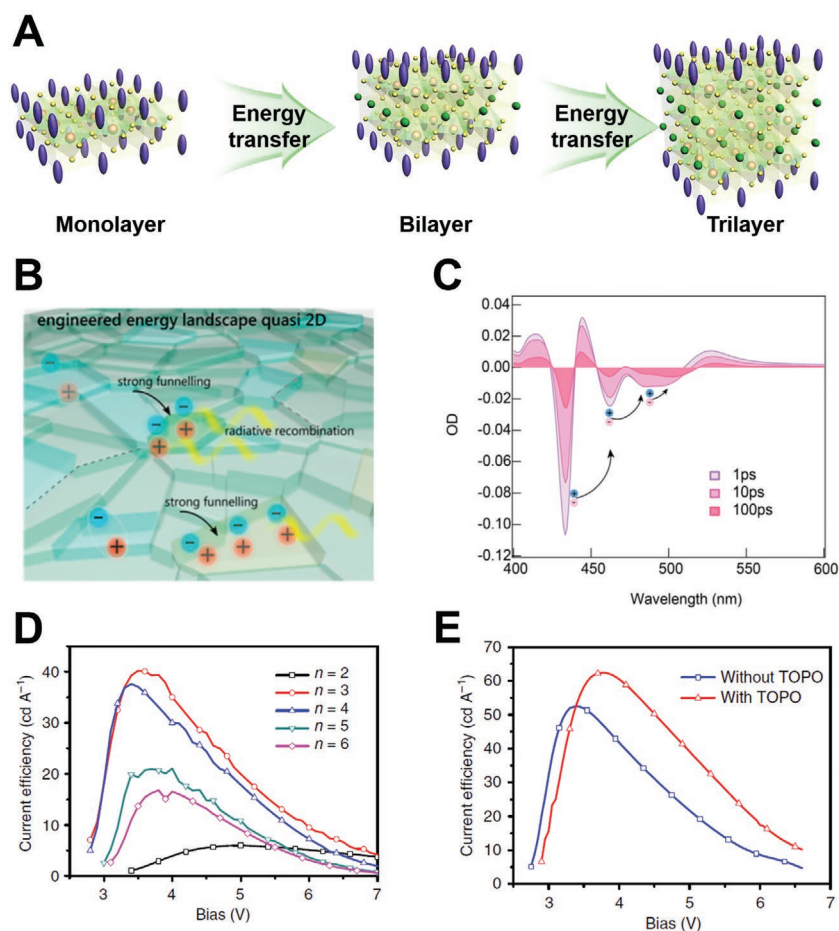


Figure 9. A) Schematic illustration describing the energy transfer in quasi-2D MHPs. B) Schematic illustration of enhanced energy transfer and C) transient absorption spectra of engineered quasi-2D MHPs. Reproduced with permission.^[176] Copyright 2015, American Chemical Society. D) Current efficiency of PeLEDs based on quasi-2D MHP EMLs with different average number of layers (dimensionality) and E) current efficiency of PeLEDs based on quasi-2D MHP EMLs with TOPO post-treatments. Reproduced with permission.^[37] Copyright 2018, Nature Publishing Group.

Cs-based MHPs (CsPbBr_3) also controlled the crystallization kinetics, and thereby smoothed the surface and helped to achieve high EL efficiency ($\text{EQE} \approx 10.43\%$, $\text{CE} \approx 33.9 \text{ cd A}^{-1}$).^[143] Mixing large or long OA into these MHPs based on various small A site cations can be more effective to enhance the LE of PeLEDs. Mixed cations (e.g., Cs/MA and Cs/MA/BA) can also improve the color-stability of PeLEDs based on mixed-halide MHPs by preventing the phase separation.^[184]

Colloidal MHP NCs and QDs are also a promising emitter form for high-efficiency PeLEDs.^[11] Colloidal MHP NCs constitute a small grain or particle size ($\approx 10 \text{ nm}$) and MHP QDs have a smaller grain or particle size than D_B ($< 10 \text{ nm}$) (quantum size regime),^[21] in which electron and hole wavefunctions easily overlap, and surface organic ligands that passivate the surface defect states.^[5,72] Furthermore, organic ligands with low dielectric constant induce dielectric confinement of electron-hole pairs (excitons) inside NCs and QDs and weak van der Waals coupling between NCs and QDs.^[55] Therefore, MHP NCs and QDs undergo radiative recombination by exciton, and have

high PLQE ($> 90\%$) under both low and high excitation density.^[5,72] Overall crystal shapes and dimensionality of MHP NCs can be tuned by controlling the ligands,^[185,186] synthesis conditions,^[187] compositions,^[42] and post-treatments such as light excitation^[188] and electron beams.^[189] MHP NCs and QDs have also various advantages for use in efficient PeLEDs; examples include simple and diverse synthesis processes,^[5,72,190,191] easy scale-up^[192] and postsynthesis color tunability by exchange of compositions.^[193]

3.2. Fabrication of Uniform MHP Films

Fabricating uniform MHP films is also very important to achieve high EL efficiency in PeLEDs. To avoid development of rough film morphology and large pinholes in MHP EML by fast and abrupt crystallization during one-step solution process, uniform MHP films can be achieved by i) retarding the crystallization rate, ii) preventing the growth of crystals or iii) increasing the number of nucleation sites.

Small amounts of acid additives such as HBr^[122,164] and HI^[194] increase the viscosity and supersaturation concentration of solutions, and also increase the solubility of inorganic compounds in perovskite solutions. Acid additives can also induce an intermediate step in crystallization and thus retard the crystallization. Organic or inorganic additives with low vapor pressure (e.g., 1,8-dioctane (DIO),^[195] *N*-cyclohexyl-2-pyrrolidone (CHP)^[196] and NH_4Cl ^[197]) delay the evaporation of solvents (e.g., DMF). These additive methods prevent abrupt crystallization of perovskite precursors, and achieve uniform MHP films with high crystal density

by slowing the crystallization rate (Figure 10A). MHP films fabricated by adding 6 vol% HBr showed well-connected crystalline structure with decreased grain size ($\approx 500 \text{ nm}$) and green EL emission with full coverage over the pixel area.^[164] The PbBr_2 peak disappeared from XRD patterns by adding HBr additives;^[164] this change confirms that HBr additives increase the solubility of inorganic compounds (PbBr_2) and prevent the formation of luminescence quenching sites (e.g., metallic Pb^{4+}). Despite improved film morphology, PeLEDs still had low EL efficiency ($\text{EQE} \approx 0.1\%$, $\text{CE} \approx 0.43 \text{ cd A}^{-1}$, and $L \approx 3490 \text{ cd m}^{-2}$);^[164] this failure to improve the LE of PeLEDs indicates that the EL efficiency of PeLEDs is limited by dissociation of most Coulombically bound electron-hole pairs into free charge carriers in their large grain size due to small E_b ,^[4] and their nonradiative recombination.^[55]

Organic additives such as polymers and small molecules can inhibit the growth of perovskite crystals and thus induce formation of uniform MHP films. These impurity effects can be explained by the Kossel-Stranski terrace-step-kink model;^[198]

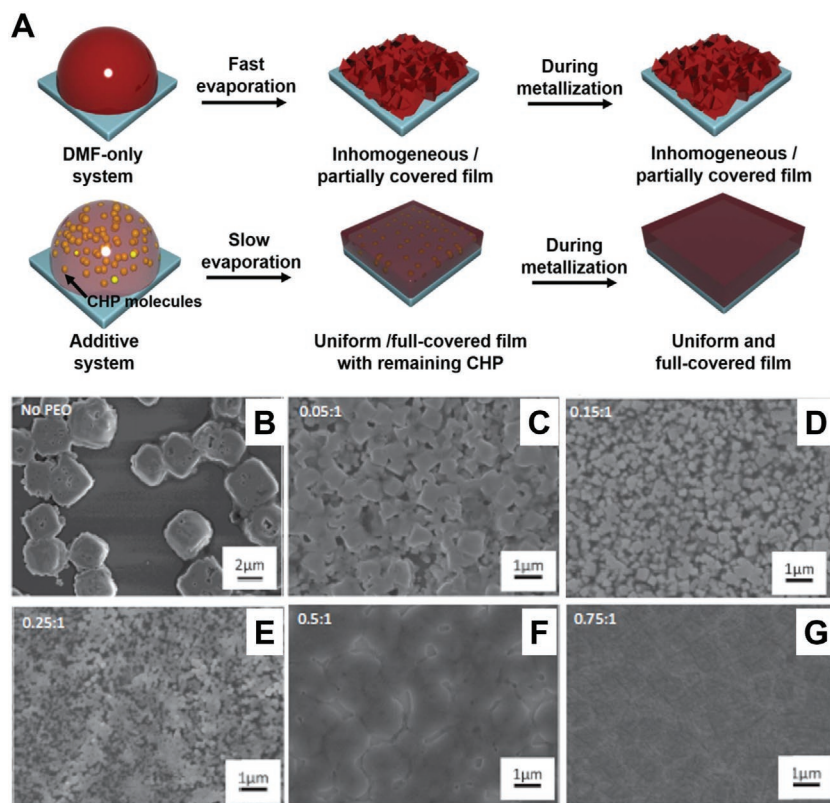


Figure 10. A) Schematic illustration of MHP film formation without and with organic additive (CHP) with low vapor pressure. Reproduced with permission.^[196] Copyright 2014, Nature Publishing Group. Scanning electron microscope images of PEO:MAPbBr₃ polycrystalline films with different PEO:MAPbBr₃ ratio of B) pure MAPbBr₃, C) 0.05:1, D) 0.15:1, E) 0.25:1, F) 0.5:1, and G) 0.75:1. Reproduced with permission.^[165] Copyright 2015, Wiley-VCH.

crystallization rate decreases exponentially as impurity concentration increases. Adding polyethylene oxide (PEO) to perovskite precursors (e.g., MAPbBr₃,^[165] CsPbBr₃^[199]) limited their diffusion and yielded small crystal grains with uniform and full-covered films (root-mean-squared roughness $\gamma_{rms} \approx 9$ nm in PEO:CsPbBr₃ (0.086:1 in molar ratio) films,^[199] ≈ 100 nm grain size with >95% film coverage in PEO:MAPbBr₃ (0.25:1 in molar ratio) films^[165]) (Figure 10B–G). PEO additives also improved the uniformity of current distribution in films; this uniformity can prevent leakage current in PeLEDs.^[199] The ion-conducting property of PEO facilitated the migration of ions in composite films and thus induced formation of p–i–n junctions under the external electric fields; these junctions diminished the charge injection barriers at the electrode/MHP EML interfaces and enabled fabrication of single-layered PeLEDs (ITO/PEO:MAPbBr₃/In-Ga or Au) with high device yield of 95%. These electrical poling effects are similar to those of light-emitting electrochemical cells (LECs), but further studies should be conducted to elucidate the device operating mechanism. PEO can also suppress nonradiative recombination by passivating surface defect states and thus improve PLQE ($\approx 60\%$)^[199] and E_b (≈ 128.4 meV after CF treatments)^[200] in PEO:CsPbBr₃ films. PeLEDs based on PEO showed high EL efficiencies (EQE $\approx 4.26\%$ and CE ≈ 15.67 cd A⁻¹^[199] or EQE $\approx 4.76\%$ and CE ≈ 21.38 cd A⁻¹^[200] for PeLEDs based on PEO:CsPbBr₃; CE ≈ 0.74 cd A⁻¹ for PeLEDs

based on PEO:MAPbBr₃^[165]). PEO:CsPbBr₃ film morphology and EL efficiency of PeLEDs based on PEO:CsPbBr₃ films (EQE $\approx 5.7\%$, PE ≈ 14.1 lm W⁻¹) can be further improved by adding poly(vinylpyrrolidone) (PVP) into PEO:CsPbBr₃ solutions because polar pyrrolidone group in PVP facilitates the dispersion of perovskite precursors in the polymer matrix.^[159] Incorporating poly(9-vinylcarbazole) (PVK),^[201] polyimide precursor dielectric (PIP),^[202] polyethylene glycol (PEG)^[203] and PVK with TPBI^[204] into perovskite precursors also help to achieve uniform MHP films and high EL efficiencies.

Excess OA cations^[80,123] or inorganic cations^[205] can reduce colloidal and grain size by increasing the coordination number of lead polyhalide complexes in solutions; MHP films with excess MABr (MABr:PbBr₂ (2.2:1)) showed reduced surface roughness with decreased grain size and thus had enhanced EL efficiencies (EQE $\approx 3.38\%$, CE ≈ 15.26 cd A⁻¹) compared to those with equimolar precursor ratio (EQE $\approx 0.004\%$, CE ≈ 0.02 cd A⁻¹).^[206] Large or long OA can also hinder the crystal growth and thus help to achieve uniform MHP films (Section 3.1).

Increasing the number of nucleation sites is also a good strategy to achieve uniform MHP films with small grain size.^[207] The activation energy of heterogeneous nucleation is much lower than that of homogeneous nucleation,^[208] so nucleation can be facilitated by improving the wettability of perovskite solutions on the underlayer. Polyethylene imine (PEI) interlayer^[138] or self-assembly monolayer^[209] or PVP interlayer^[143] on ZnO, and NiO_x interlayer^[134] increase the wettability of perovskite solutions and heterogeneous nucleation of perovskite crystals, and thus fabricate uniform MHP films. PeLEDs based on ZnO/PVP/Cs_{0.87}MA_{0.13}PbBr₃ layers achieved EQE $\approx 10.43\%$ and CE ≈ 33.9 cd A⁻¹.^[143] Increasing substrate temperature during the spin coating of perovskite solution also facilitates the nucleation of perovskite crystals and yields dense and uniform MHP films.^[111] Intermixing between perovskite (CsPbBr₃) solution and PFI underlayers also facilitates heterogeneous nucleation, increases the number of nucleation sites, and thus induces uniform CsPbBr₃ film morphology with full coverage, because PFI molecules have many branches.^[156]

Two-step solution process can also achieve uniform MHP films, because in this process nucleation is the main crystallization mechanism rather than growth of crystals.^[210,211] FAPbBr₃ films coated using the two-step solution process showed uniform films with $\gamma_{rms} < 20$ nm and small grain size (100 – 200 nm) and achieved moderate EL efficiency in PeLEDs (EQE $\approx 1.16\%$, CE ≈ 2.65 cd A⁻¹).^[135] The film morphology and grain size can be controlled by modifying solution concentration,^[212] loading time of the second solution,^[82] reaction temperature,^[210] and solvents.^[213,214] Other methods such as multicoating,^[215] roll-to-roll process,^[216] thermal evaporation,^[132,217] vapor-assisted

solution process,^[85] chemical vapor deposition^[84] have been also tested to fabricate the uniform MHP films and efficient PeLEDs.

3.3. Ligand Engineering of Colloidal MHP NCs and QDs

Although colloidal MHP NCs and QDs have high PLQE in solution states, the first reported PeLEDs based on MHP QDs showed very low EL efficiencies (EQE \approx 0.07%, CE \approx 0.14 cd A⁻¹, power efficiency (PE) \approx 0.07 lm W⁻¹ for blue emission, EQE \approx 0.12%, CE \approx 0.43 cd A⁻¹, PE \approx 0.18 lm W⁻¹ for green emission, EQE \approx 0.09%, CE \approx 0.08 cd A⁻¹, PE \approx 0.06 lm W⁻¹ for orange emission)^[169] for two main reasons: i) NCs and QDs easily agglomerate in highly concentrated solutions (>0.5 mg mL⁻¹)^[125] or during film formation process^[21] so fabrication of uniform and thick NC and QD films is very difficult; ii) insulating organic ligands (e.g., oleylamine, oleic acid), which are necessary to stabilize NCs and QDs in solutions, severely prevent charge injection and transport in NC films.^[21,22] Furthermore, decreased PLQE of MHP NCs and QDs, especially CsPbBr₃ QDs,^[129] in film states limits EL efficiency.

Many research groups have tried various strategies to fabricate uniform and thick NC films and to fabricate highly efficient PeLEDs based on them. The surface coverage can be improved by overcoating the bipolar organic host semiconductors (PVK):2-(4-biphenyl)-5-phenyl-1,3,4-oxadiazole (PBD) on predeposited NC films,^[128] or by mixing NCs with poly(methyl methacrylate) (PMMA).^[6,127] Especially, PMMA matrix, which has low dielectric constant, increased the E_b (\approx 161.6 meV) and PLQE (\approx 92%) of NC films by inducing the dielectric confinement effect, and thereby achieved high EL efficiency (EQE \approx 3.04%, CE \approx 13.02 cd A⁻¹) in PeLEDs.^[6]

Treatments that use trimethylaluminium (TMA) vapor on coated MHP NC films can crosslink the NCs; this process makes NC films insoluble during washing and while overcoating upper layers; these induce uniform NC films with full coverage. TMA treatments also dramatically increase PLQE of NC films from \approx 25 to \approx 85% by passivating the surface defects, and achieve high EL efficiencies in PeLEDs (EQE \approx 5.7% in red emission).^[44] Crosslinking the organic ligands by using initiators or heat treatment is also an effective method; MHP NCs capped with 4-vinylbenzyl-dimethyloctadecylammonium chloride can easily be crosslinked by initiator (azobisisobutyronitrile); crosslinked NC films had homogenous film morphology and high PLQE (\approx 56%) and achieved moderate EL efficiencies (EQE \approx 0.58% and CE \approx 2.47 cd A⁻¹).^[218] Crosslinking by X-ray irradiation^[219] can also increase the density of NC films and facilitate the charge transport.

Control of underlayers such as PEI^[40] or PFI-enriched surface^[21] can also improve the surface morphology and device efficiencies (EQE \approx 6.3%, CE \approx 3.4 cd A⁻¹ for red-emitting PeLEDs based on PEI interlayer;^[40] EQE \approx 5.09%, CE \approx 15.5 cd A⁻¹ for green-emitting PeLEDs based on PFI-enriched surface (BuF-HIL)^[21]). Various coating methods such as dip-coating,^[125] ink-jet printing^[220] and centrifugal coating^[221] have also been tried to fabricate uniform MHP NC or QD films and efficient PeLEDs. Preferred orientation of QDs (well-aligned QDs)

also results in densely packed QD films and increased EL efficiencies.^[131]

Even though uniform MHP NC and QD films were fabricated and high PLQE was achieved in NC and QD films, their EL efficiencies were not still higher than those of MHP bulk films, because insulating organic ligands hindered efficient charge injection or transport from the electrodes or within the NC and QD films. Postligand engineering is an effective method to reduce the ligand length and density. Replacing long ligands (oleic acid and oleylamine) with didodecyl dimethyl ammonium bromide greatly increased the charge transport characteristics, and increased EQE from \approx 0.1% to \approx 3% in PeLEDs (Figure 11A).^[43] Washing synthesized QDs with hexane/ethyl acetate cosolvents in which ethyl acetate is a solvent with moderate polarity (\approx 4.3) can effectively reduce the surface ligand density (Figure 11B). Washing \leq 3 times can effectively reduce the surface ligand density, improve the charge transport characteristics while maintaining high PLQE of QDs, and can achieve high EL efficiencies in PeLEDs (EQE \approx 6.27%, CE \approx 13.3 cd A⁻¹).^[130] Conducting both ligand-exchange and washing process is more effective to improve the EL efficiencies (EQE \approx 6.25%, CE \approx 18.8 cd A⁻¹ and PE \approx 18.9 lm W⁻¹)^[126] than doing either process individually.

In situ methods can be used to control ligand length and density on the surface of MHP NCs (Figure 11C,D).^[21,22] When NCs were synthesized using recrystallization methods, reduction in the density^[21] or length^[22] of ligands caused increase in NC size in the regime beyond the quantum size effect. In these NCs, luminescent quenching at the surface defects was suppressed, so the NCs showed size-independent high color purity and PLQE. Furthermore, these NC films had reduced length and density of ligands, and therefore showed increased charge transport characteristics. With these methods, highly efficient PeLEDs based on MAPbBr₃ NCs (EQE \approx 5.09%, CE \approx 15.5 cd A⁻¹)^[21] and FAPbBr₃ NCs (EQE \approx 2.05%, CE \approx 9.16 cd A⁻¹)^[22] were achieved.

NCs that had been formed in situ were also effective to fabricate highly efficient PeLEDs because these NCs do not have organic ligand and do not aggregate with each other.^[174,222] Small NCs can be fabricated in situ by performing NCP on perovskite quasifilms that incorporate suitable amount of excess OA halides (MABr)^[222] or bulky OA halides (e.g., phenethylammonium bromide (PEABr), 4-fluorophenylmethylammonium iodide (FPMAI))^[174] which can prevent the growth of 3D MHP crystals (e.g., MAPbBr₃, MAPbI₃). Surfaces of NCs were capped by bulky OA rather than by organic long ligands; bulky OA passivates the surface defects and induces efficient dielectric confinement of excitons in NCs. With these strategies, high PLQE and high EL efficiencies in PeLEDs based on NC films that had been formed in situ were achieved (PLQE \approx 4.4%, EQE \approx 7.9%, radiance \approx 72 W sr⁻¹ m⁻² for (FPMAI)_{0.2}MAPbI₃ based NCs; PLQE \approx 10.9%, EQE \approx 7% for (PEABr)_{0.2}MAPbBr₃ based NCs;^[174] EQE \approx 8.21%, CE \approx 34.46 cd A⁻¹ for (MABr)₃MAPbBr₃ based NCs^[222]). Solvent-vapor annealing on preformed polycrystalline bulk films can also obtain ligand-free NCs by transforming the bulk films into NCs;^[45] these processes avoid the problems of organic ligands and aggregation, and therefore can yield efficient PeLEDs.

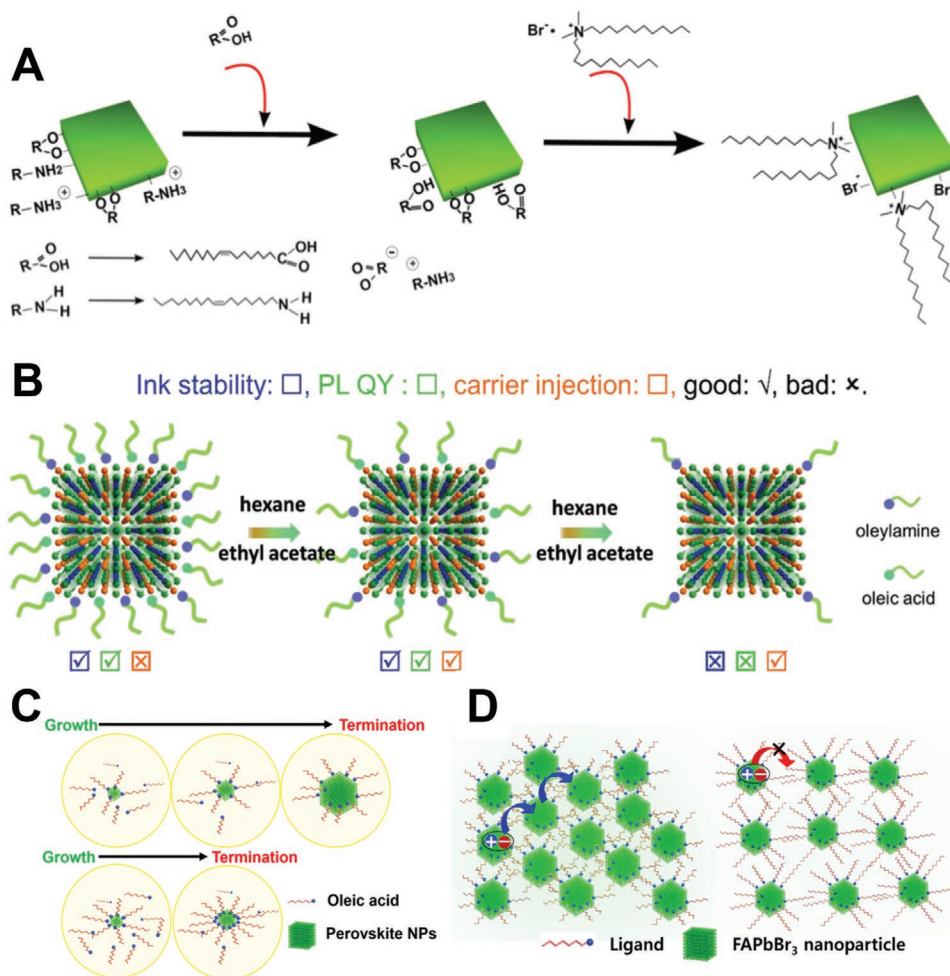


Figure 11. A) Schematic illustration describing the postligand exchange. Reproduced with permission.^[43] Copyright 2016, Wiley-VCH. B) Schematic illustration of postligand density control by purification. Reproduced with permission.^[130] Copyright 2016, Wiley-VCH. C) Schematic illustration describing the in situ control of ligand density during NC synthesis.^[21] Copyright 2017, American Chemical Society. D) Schematic illustration of charge transport in NC films with different ligand length (left: short; right: long). Reproduced with permission.^[22] Copyright 2016, Elsevier Ltd.

Similar to the bulk films (Section 3.1), partial substitution of Cs cations for FA cations in FAPbBr₃ NCs^[223] or for MA cations in MAPbBr₃ NCs^[224] can align energy levels and increase surface morphology, hole-injection capability and PLQE, and thereby increase device efficiencies. Recently, high EL efficiencies in PeLEDs based on NCs were achieved by incorporating some amount of octylammonium (OAm) into FAPbBr₃ crystals ((OAm)₂(FA)_{n-1}Pb_nBr_{3n+1}) (EQE ≈ 13.4%, CE ≈ 57.6 cd A⁻¹).^[39] CsPbBr₃-CsPb₂Br₅ dual phase,^[225] Mn²⁺ doping on CsPbBr₃,^[226] use of other ligands (e.g., polyhedral oligomeric silsesquioxane^[227] and octylphosphonic acid^[228]), and excess halide anions^[229] stabilize perovskite crystal structures and also increase the PLQE and EL efficiencies of MHP NCs or QDs. To further improve the EL efficiency of PeLEDs based on NC and QD films, comprehensive strategies considering all the luminescence-resulting factors (e.g., precursor components, type of ligands, doping and fabrication process) should be done. We also suggest that chemical fusion of organic ligands after formation of NC and QD films, in which all the organic ligands were removed, maintaining high PLQE can facilitate the charge

carrier transport and enhance the LE of PeLEDs based on NC and QD films.

3.4. Post-Treatments

Even if uniform MHP films are fabricated, they can retain residual solvents,^[110] unconverted precursors^[110] and trap sites.^[151,170,206,230,231] These unavoidable factors limit the EL efficiency of PeLEDs. Therefore, many researchers have tried to suppress these luminescence-quenching sites by various post-treatments such as i) overcoating of trap-passivation agents, ii) electrical, photo- or thermal annealing, and iii) control of environmental atmosphere.

Overcoating of Lewis bases (e.g., thiophene, pyridine)^[100,171] or amine-based molecules (e.g., PEI, ethylenediamine (EDA))^[170] on preformed MHP films can passivate the surface defects and achieve high EL efficiencies (EQE ≈ 6.19%, CE ≈ 28.9 cd A⁻¹ in PeLEDs based on EDA post-treatments)^[170] because they react with uncoordinated Pb. Overcoating of pure

chlorobenzene solvent^[232] and steaming chloroform solvent^[200] or MA vapor^[134] also smoothen the surface, reduce the numbers of pinholes and defects, suppress the non-radiative recombination, and achieve efficient PeLEDs (Figure 12). Overcoating of triethylphosphine oxide (TOPO) on quasi-2D MHPs ($\text{PEA}_2(\text{FAPbBr}_3)_{n-1}\text{PbBr}_4$) passivates trap states, reduces nonradiative recombination pathways, increases PLQE from 57.3 to 73.5% and PL lifetime from 0.17 to 0.36 μs , and achieves the highest EL efficiencies (EQE \approx 14.36%, CE \approx 62.4 cd A^{-1} ; EL data was measured by silicon photodiode and EQE was calculated by assuming Lambertian emission profile) yet reported.^[37] Overcoating of acid-based molecules can also be effective to passivate the surface defects because MHPs have various surface defect states,^[16,77,78] however, related research has not been intensively studied yet.

Although electrical stress, photoirradiation and thermal annealing can induce defect states in perovskite crystals (Section 2.1.3), moderate treatments with these factors can increase the PLQE and EL efficiencies in PeLEDs. Brief electrical scans induced local movement of excess ions (here, mobile I^-) in MHP films; these ions can fill local interstitial defects or vacancies, and thereby improve the radiative recombination and device efficiency (from EQE \approx 5.9% to \approx 7.4%) in PeLEDs based on MAPbI_3 films.^[151]

Photoirradiation excites the electrons and holes, which then become trapped in the iodine vacancies (i.e., uncoordinated Pb ions).^[89] These trap fillings create an electrical field, which induce local movement of excess I^- into vacancies and interstitials, and reduce the number of traps and the degree of nonradiative recombination of charge carriers. After photoexcitation of MAPbI_3 films for 862 s at 258 J cm^{-2} , trap density of MAPbI_3 films decreased from $\approx 1.7 \times 10^{17} \text{ cm}^{-3}$ to $\approx 2.5 \times 10^{16} \text{ cm}^{-3}$. Furthermore, this trap-filling effect by redistribution of excess ions can be superior in dark spots that have more nonradiative recombination centers than the bright spots; as a result, photoexcitation can improve the luminescence-uniformity in polycrystalline bulk films.^[89,231] Photoexcitation can also dope the EML and induce in situ p-i-n homojunctions by inducing ion migration, and thereby increase the LE of PeLEDs.^[89,233]

Thermal annealing under optimized conditions can improve the LE and crystallinity of MHP films by evaporating residual solvents,^[110,116] and also smoothen the films' surface morphology.^[117] Thermal annealing at moderate T_{ANN} (60 – 90 °C) for 2 h induced recrystallization and grain growth of MAPbBr_3

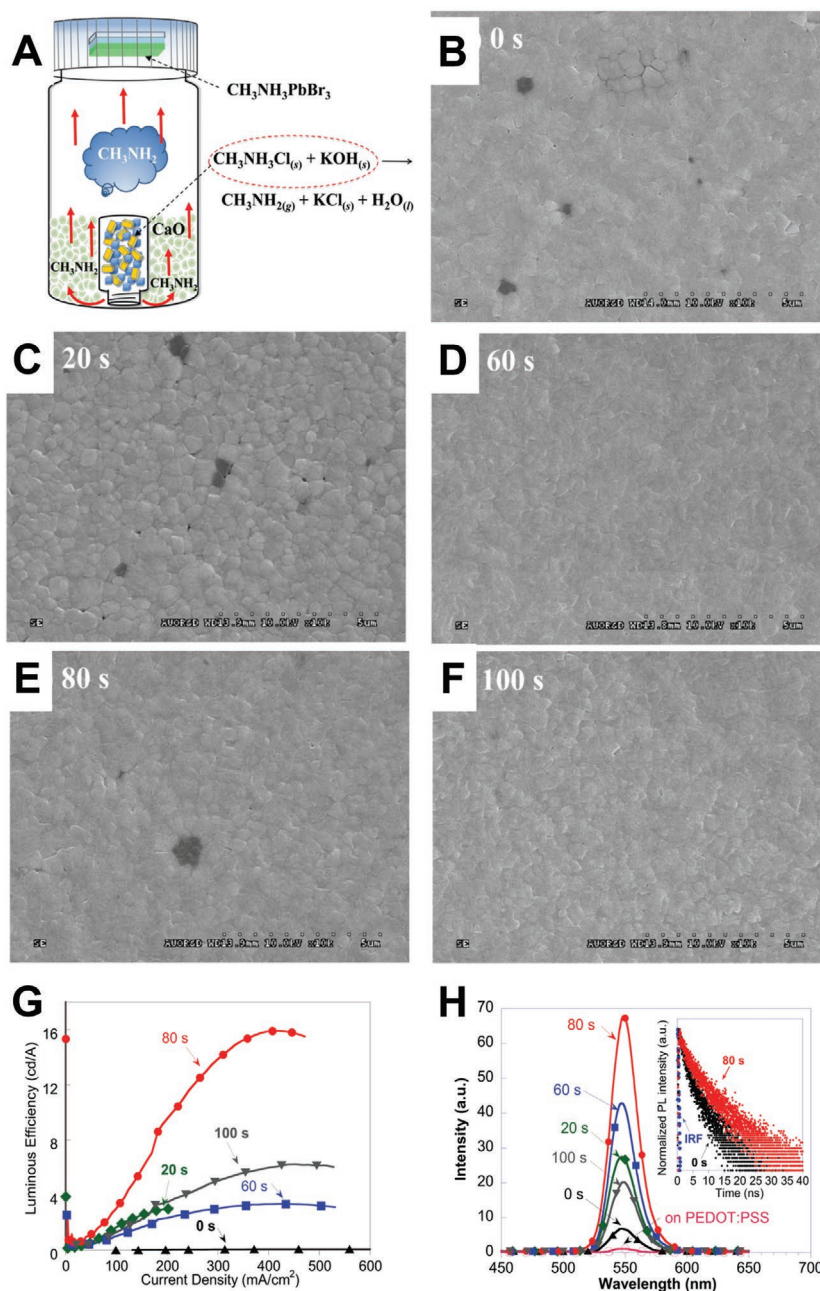


Figure 12. A) Schematic illustration describing the MA vapor post-treatment, scanning electron microscope images of MAPbBr_3 polycrystalline films after different MA vapor post-treatment duration of B) 0 s, C) 20 s, D) 60 s, E) 80 s, and F) 100 s, G) current efficiency of PeLEDs based on MAPbBr_3 EML after different MA vapor post-treatment duration, and H) PL spectrum and PL lifetime (inset) of MAPbBr_3 polycrystalline films after different MA vapor post-treatment duration. Reproduced with permission.^[134] Copyright 2016, Wiley-VCH.

crystallites and thereby achieved uniform and continuously linked MAPbBr_3 films with improved EL efficiencies in PeLEDs.^[230] However, thermal annealing at too high T_{ANN} (>100 °C) for 2 h melted the MAPbBr_3 crystallites and induced vertical cracks, possibly as a result of sublimation of MABr or decomposition of MABr to MA and HBr because of the relatively low decomposition temperature (≈ 100 °C) of perovskite crystals (MAPbX_3).^[113] Annealing at too low T_{ANN} cannot fully

evaporate residual solvents^[110,116] and can yield randomly oriented crystals^[234] which can reduce the LE of PeLEDs.

Although MHP crystals can be hydrolyzed^[93] or decomposed^[101,102] by exposure to moisture or oxygen (Section 2.1.3), in some cases H₂O or O₂ molecules can increase the LE by passivating the uncoordinated Pb atoms.^[99,235] Furthermore, exposure to moist atmosphere induces merging of perovskite grains due to the hygroscopic properties of MAX molecules;^[236] this process can reduce the number of pinholes in MHP films, and thereby suppress leakage current in PeLEDs.

3.5. Device Architecture Optimization

The EL efficiency (EQE) of PeLEDs is influenced by the outcoupling factor χ and the charge-balance factor γ (Equation (10)). These factors can be controlled by optimizing device architecture such as interlayers or interfacial treatments.

First, interlayers or interfacial treatments are very effective to facilitate charge injection into perovskite EML by reducing the charge injection barrier between electrode and MHP EML, and thereby enhance the charge balance in PeLEDs. Buf-HIL, which is composed of PEDOT:PSS and PFI,^[3] or PFI on PEDOT:PSS/poly(bis-4-butylphenyl-*N,N*-bisphenyl)benzidine (poly-TPD) underlayers^[237] reduced the hole-injection barrier into MHP EMLs, suppressed the luminescence quenching at the interfaces, and thus improved the EL efficiencies in PeLEDs (EQE \approx 0.125%, CE \approx 0.577 cd A⁻¹ for PeLEDs based on Buf-HIL) compared to those in PeLEDs based on PEDOT:PSS (EQE \approx 0.000393%, CE \approx 0.00165 cd A⁻¹ for PeLEDs based on PEDOT:PSS).^[3] Addition of interlayers (e.g., PEI,^[138] spatial atmospheric atomic layer-deposited (SAALD) Zn_{0.56}Mg_{0.44}O films^[238]) and interfacial solvent treatments (e.g., ethanolamine)^[239] on top of n-type inorganic metal oxide (e.g., TiO₂ and ZnO) layers also lowered the WF of underlayers, and thus reduced the electron injection barrier into MHP EMLs. Interlayers and interfacial treatments can also prevent luminescence quenching (Figure 13A,B)^[3,237,239] and modify the morphology of MHP films.^[40,143,227] Several combinations of these interlayers have been tested to maximize device efficiencies.^[6,199]

Interlayers can also effectively extract the light from EML to the outer surface; controlling the refractive index of charge injection/transport layers can increase the outcoupling efficiency in PeLEDs as do Buf-HIL in OLEDs.^[240] Gold nanoparticles^[241] dispersed in PEDOT:PSS, and silver nanorods^[242] dispersed in *N,N'*-bis(1-naphthalenyl)-*N,N'*-bis(phenylbenzidine) (NPB) interlayers caused a localized surface plasmon resonance effect, which increased light extraction. Although outcoupling efficiency is one of the most important factors resulting EL efficiency of PeLEDs, research about the degree of outcoupling efficiency and strategies to improve it has been seldom reported. We suggest that studies about outcoupling efficiency in PeLEDs should be conducted in parallel with research about modification of MHP EML and inner structure in PeLEDs.

To prevent luminescence quenching induced by diffused In and Sn impurities from TCO electrodes (Section 2.2.3), researchers have used TCO-free electrodes such as self-organized conducting polymer (SOCP) and graphene.^[4,145] These electrodes do not have any impurities that can diffuse into MHP

EML during the formation of upper layers (Figure 13C,D).^[145] PeLEDs with SOCP and graphene showed much higher EL efficiencies (EQE \approx 8.53% and CE \approx 42.9 cd A⁻¹ for PeLEDs using SOCP^[4] and CE \approx 18.0 cd A⁻¹ and EQE \approx 3.8% for PeLEDs using graphene^[145]) than those with the conventional ITO anode (CE \approx 10.6 cd A⁻¹ and EQE \approx 2.2%) (Figure 13E,F).^[145] TCO-free electrodes were also used to fabricate flexible PeLEDs,^[4,145] and PEDOT:PSS-PEO composite electrodes were used to fabricate stretchable PeLEDs.^[243]

4. Summary and Outlook

We have reviewed factors that limit the LE of PeLEDs. We have categorized these factors into i) inherent properties of MHP crystals (e.g., slow radiative recombination rate of free charge carriers, low E_b , coupling between charge carriers and ionic lattices, and easily formed defect states), ii) morphological properties of MHP EML (e.g., rough film, and aggregation and insulating organic ligands of MHP NCs), and iii) problems caused by device architectures (e.g., electrical and optical losses at the interfaces, diffusion of luminescence-quenching species from electrodes, and low operational stability). We explained these factors by coupling with equations that derive the PLQE of emitters and EQE of LEDs.

Then, we summarized recent progress in research on PeLEDs to overcome those limiting factors and improve their EL efficiency. Uniform MHP films are necessary to reduce leakage current in PeLEDs. Such films can be achieved by modifying the crystallization kinetics and film formation process. Reducing the dimensionality and dimension of grains, particles and crystals from the micrometer scale to the nanometer scale are very effective to increase radiative recombination of electron-hole pairs and to smoothen the film; RP phase, and colloidal NCs and NCP are representative methods that try this approach. In the presence of large or long OA (in the case of RP phase), organic ligands (in the case of colloidal NCs), and solvent-dripping process (in the case of NCP), crystal-growth processes are prevented, so relatively small grains, particles, or crystals are formed. This reduction in the size of grains, particles, or crystals of MHPs causes increase in the overlap of electron and hole wavefunctions, so the possibility of excitonic recombination and PLQE in emitters are increased.

Ligand engineering methods were developed to reduce the density and length of organic ligands and increase the charge transport characteristics in NC films. Several methods such as postligand exchange, postligand washing, in situ control, and in situ formation of ligand-free NCs were reviewed. Post-treatments of preformed MHP crystals were effective to passivate the surface defect states although the effects of moisture, oxygen, and photoexcitation on luminescence efficiencies are still being clarified. Device optimization strategies can also be used to maximize the charge balance and outcoupling efficiency in PeLEDs. These strategies have dramatically improved the EL efficiencies of MHPs from EQE \approx 0.1% for green emission and EQE \approx 0.76% for NIR emission^[2] to EQE \approx 14.36%^[37] in green-emitting PeLEDs within only three and a half-year. However, this efficiency is still lower than that of OLEDs^[7-10] and QD LEDs,^[11-15] therefore, LE of PeLEDs must be improved

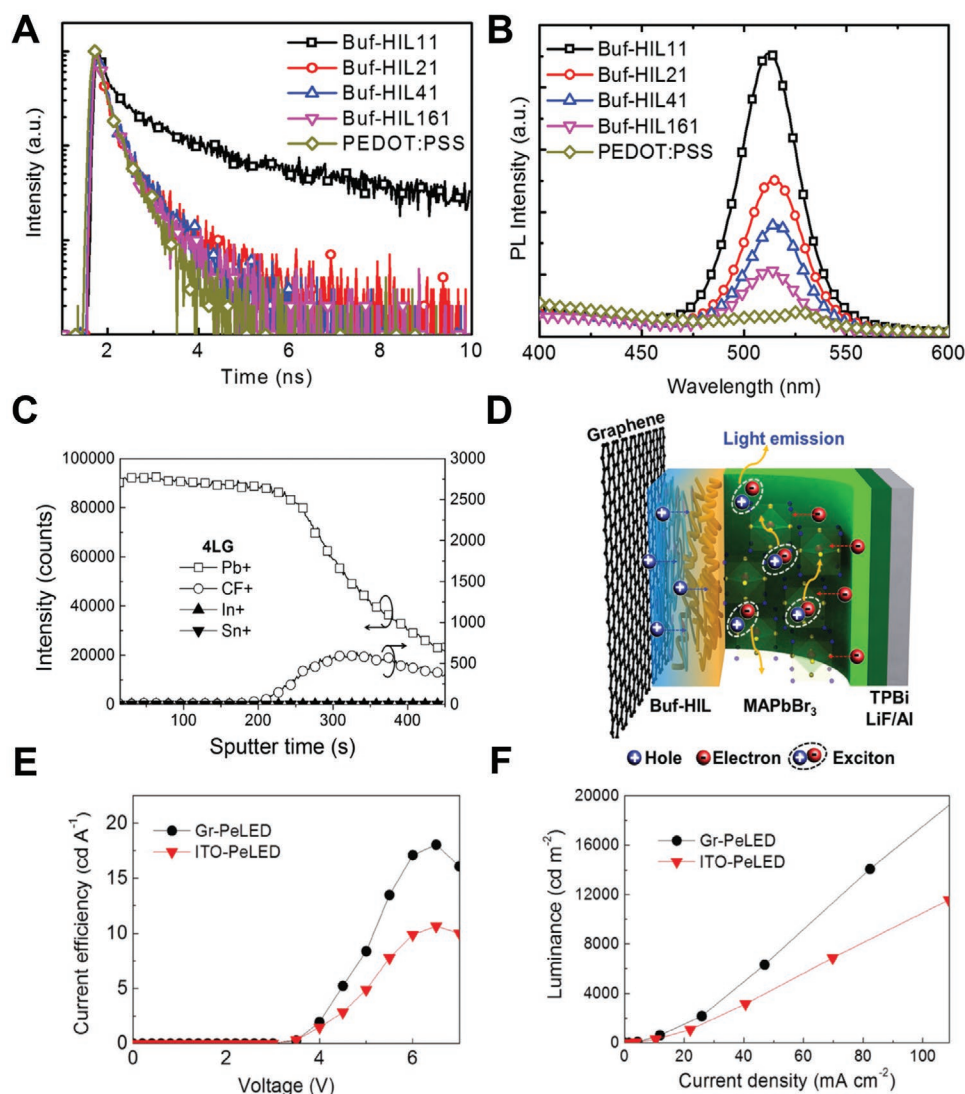


Figure 13. A) PL lifetime and B) PL intensity of MAPbBr₃ polycrystalline films on different underlayers (PEDOT:PSS and BuF-HIL with different PFI ratio). Reproduced with permission.^[3] Copyright 2015, Wiley-VCH. C) Time-of-flight secondary ion mass spectrometry (TOF-SIMS) depth profile of MAPbBr₃ polycrystalline films on graphene/BuF-HIL underlayers, D) schematic illustration describing the efficient radiative recombination in PeLEDs based on graphene electrodes, and E) current efficiency and F) luminance characteristics of PeLEDs based on graphene electrodes and ITO electrodes. Reproduced with permission.^[145] Copyright 2017, Wiley-VCH

further. Here, we suggest some future research directions to accomplish this goal.

Basically, LE of Pb-based MHPs is limited due to their inherently slow $k_2 \approx 10^{-10} \text{ cm}^3 \text{ s}^{-1}$.^[55] If we could increase k_2 to $>10^{-8} \text{ cm}^3 \text{ s}^{-1}$ while maintaining k_1 and k_3 , we could obtain highly luminescent MHP crystals. Although MHPs that have these recombination rates have not been reported yet, we expect that MHP crystals based on other central metals such as Mn^[226] and Bi^[244,245] or partial doping of them into Pb could be candidates.

LE of MHPs can be increased by facilitating the radiative decay of charge carriers by reducing the charge carrier–ionic lattice interactions such as polaron effect and hot-phonon bottleneck.^[69] Because hot-phonon bottleneck is boosted by the nonequilibrium LO-phonon population that can arise due to the mass difference between each ions,^[69] ions with similar

mass must be used in MHP crystals to prevent the hot-phonon bottleneck. The hot-phonon bottleneck can also result from ferroelectric characteristics of MHPs which arise from reorientation of OA (e.g., MA⁺) under the electric fields;^[69,246] therefore, MHPs which do not have hot-phonon bottleneck as well as polaron effect should be developed to further improve the EL efficiency in PeLEDs by facilitating the radiative recombination of electron–hole pairs.^[61] Multiple-quantum-well nanostructures increase the charge carrier–ionic lattice interactions (Section 2.1.2);^[67,69] therefore, other nanostructures that both effectively confine the electron–hole pairs and prevent the charge carrier–ionic lattice interactions should be designed.

Among many MHP crystal systems (e.g., 3D MHP bulk films, quasi-2D MHP bulk films, and colloidal NCs), quasi-2D MHP bulk films have shown the highest EL efficiency in

PeLEDs up to now.^[37,38,176–179] However, these PeLEDs used different large OAs, i.e., the best structure of OA has not been found. Thus, we suggest that some research should be devoted to finding the best OA with optimum size, length, alkyl group structure (e.g., aromatic, aliphatic or a combination), and functional groups (e.g., carboxylic acid, amine, phosphonic acid) to further improve the EL efficiency.

Study of the functional groups in organic ligands in NCs is imperative to increase the EL efficiency of PeLEDs based on MHP NCs. The most widely used organic ligands such as carboxylic acid ligands and amine ligands interact dynamically with each other although they adhere to the NC's surface; these reduce the stability and PLQE of NCs during purification.^[247] Recently, MHP NCs without amine ligands,^[248] with only alkyl ammonium ligands,^[218] and with only octylphosphonic acid ligands^[228] were synthesized and incorporated in PeLEDs, however, their stability and EL efficiencies were still low. Zwitterionic capping ligands^[249] that have both amine (NH_3^+) and acid (e.g., SO_3^- , COO^- , and PO_3^-) can stably adhere to the NC surface and can therefore endure the purification process; NCs with these ligands can achieve high EL efficiency in PeLEDs. We also suggest that synthesis of MHP NC–polymer composites,^[250] MHP NC–inorganic semiconductor heterostructure,^[251] or gradient-alloy or core–shell-type NCs (e.g., inorganic semiconductor or oxide^[252] shell) can be effective strategies to realize highly efficient and stable emitters and PeLEDs based on them.

Furthermore, inspired by the development of OLEDs, we suggest that organic host–MHP guest system in which energy is transferred from organic host into MHP emitters can be an effective method to concentrate the electron–hole pairs only in MHP emitters and reduce annihilation of bound electron–hole pairs. These new systems can be realized by i) mixing the organic semiconductors with MHP precursors^[165,199] or NCs^[6,127] in solution and ii) thermally depositing the organic semiconductors with MHP precursors in high vacuum.^[132,217]

Considering the high refractive index >2.2 of MHP films,^[132,139] various methods to increase the outcoupling efficiency are more effective to increase the EL efficiency in PeLEDs than in OLEDs and QD LEDs. Appropriate selection of device (HTL/ETL/EML) thickness and electrode or transparent metal-free PeLEDs will reduce the dipole–metal interaction and minimize the optical losses at the metal electrode.^[30] Recently, CsPbBr_3 nanocube films,^[253] CsPbBr_3 nanoplatelets,^[254] and CsPbI_3 QDs^[255] were reported to have polarized emission. Inspired by the progress of OLEDs which achieved EQE $> 30\%$ by using heteroleptic iridium complexes with preferred orientation of dipole moments,^[30] we suggest that EL efficiency of PeLEDs can be increased by adopting those polarized emitting MHP crystals. Furthermore, in addition to Au nanoparticles and Ag nanorods dispersed in interlayers,^[241,242] Au nanoparticles^[256] and Ag nanoparticles^[257] that adhere to the surface of MHP NCs can induce surface plasmon resonance and maximize the light extraction from PeLEDs toward the outside. We also expect that the combination of high-index electrode and low-index HIL,^[258] optimization of electrode or interlayer thicknesses,^[259] corrugated device structure,^[260] and light-outcoupling layers^[261] would help to extract the light and

increase the EL efficiency of PeLEDs. Optical simulation may assist to optimize the device structure to maximize the outcoupling efficiency, as it did in OLEDs.^[30]

In addition to the unprecedentedly fast growth of EL efficiency in PeLEDs, many research groups have tried to increase their operating stability and reduce their environmental effects. Considering their efforts and multidisciplinary collaborations of researchers, we believe that commercialization of PeLEDs will be achieved much faster than that of OLEDs. By analogy with inorganic QD LEDs, we anticipate that color conversion–type LEDs in which perovskite EMLs or films are placed in front of the backlight unit in displays will be industrialized before self-emissive PeLEDs. We hope that this review will help readers to grasp the progress of research on PeLEDs, to appreciate the remaining problems, and to concentrate on development and industrialization of highly efficient PeLEDs.

Acknowledgements

This work was supported by the National Research Foundation of Korea (NRF) grant funded by the Korea government (MSIT; Grant No. NRF-2016R1A3B1908431). This research was also supported by Creative Materials Discovery Program through the National Research Foundation of Korea (NRF) funded by Ministry of Science and ICT (2018M3D1A1058536).

Conflict of Interest

The authors declare no conflict of interest.

Keywords

electroluminescence efficiency, light-emitting diodes, metal-halide perovskite, next-generation emitters, photoluminescence quantum efficiency

Received: July 17, 2018

Revised: September 17, 2018

Published online: December 17, 2018

- [1] Y.-H. Kim, H. Cho, T.-W. Lee, *Proc. Natl. Acad. Sci. USA* **2016**, *113*, 11694.
- [2] Z.-K. Tan, R. S. Moghaddam, M. L. Lai, P. Docampo, R. Higler, F. Deschler, M. Price, A. Sadhanala, L. M. Pazos, D. Credgington, F. Hanusch, T. Bein, H. J. Snaith, R. H. Friend, *Nat. Nanotechnol.* **2014**, *9*, 687.
- [3] Y.-H. Kim, H. Cho, J. H. Heo, T.-S. Kim, N. Myoung, C.-L. Lee, S. H. Im, T.-W. Lee, *Adv. Mater.* **2015**, *27*, 1248.
- [4] H. Cho, S.-H. Jeong, M.-H. Park, Y.-H. Kim, C. Wolf, C.-L. Lee, J. H. Heo, A. Sadhanala, N. Myoung, S. Yoo, S. H. Im, R. H. Friend, T.-W. Lee, *Science* **2015**, *350*, 1222.
- [5] L. Protesescu, S. Yakunin, M. I. Bodnarchuk, F. Krieg, R. Caputo, C. H. Hendon, R. X. Yang, A. Walsh, M. V. Kovalenko, *Nano Lett.* **2015**, *15*, 3692.
- [6] S. Kumar, J. Jagielski, N. Kallikounis, Y.-H. Kim, C. Wolf, F. Jenny, T. Tian, C. J. Hofer, Y.-C. Chiu, W. J. Stark, T.-W. Lee, C.-J. Shih, *Nano Lett.* **2017**, *17*, 5277.
- [7] C. W. Tang, S. A. Vanslyke, C. H. Chen, *J. Appl. Phys.* **1989**, *65*, 3610.

- [8] J.-H. Jou, S. Kumar, A. Agrawal, T.-H. Li, S. Sahoo, *J. Mater. Chem. C* **2015**, *3*, 2974.
- [9] Y.-H. Kim, C. Wolf, H. Cho, S.-H. Jeong, T.-W. Lee, *Adv. Mater.* **2016**, *28*, 734.
- [10] H. Uoyama, K. Goushi, K. Shizu, H. Nomura, C. Adachi, *Nature* **2012**, *492*, 234.
- [11] V. L. Colvin, M. C. Schlamp, A. P. Alivisatos, *Nature* **1994**, *370*, 354.
- [12] B. O. Dabbousi, M. G. Bawendi, O. Onitsuka, M. F. Rubner, *Appl. Phys. Lett.* **1995**, *66*, 1316.
- [13] S. Coe, W.-K. Woo, M. Bawendi, V. Bulović, *Nature* **2002**, *420*, 800.
- [14] Y. Yang, Y. Zheng, W. Cao, A. Titov, J. Hyvonen, J. R. Manders, J. Xue, P. H. Holloway, L. Qian, *Nat. Photonics* **2015**, *9*, 259.
- [15] F. Zhang, S. Wang, L. Wang, Q. Lin, H. Shen, W. Cao, C. Yang, H. Wang, L. Yu, Z. Du, J. Xue, L. S. Li, *Nanoscale* **2016**, *8*, 12182.
- [16] J. Kim, S.-H. Lee, J. H. Lee, K.-H. Hong, *J. Phys. Chem. Lett.* **2014**, *5*, 1312.
- [17] T. Umebayashi, K. Asai, T. Umebayashi, K. Asai, T. Kondo, T. Kondo, A. Nakao, *Phys. Rev. B* **2003**, *67*, 155405.
- [18] J. Kim, S.-C. Lee, S.-H. Lee, K.-H. Hong, *J. Phys. Chem. C* **2015**, *119*, 4627.
- [19] A. Amat, E. Mosconi, E. Ronca, C. Quarti, P. Umari, M. K. Nazeeruddin, M. Grätzel, F. De Angelis, *Nano Lett.* **2014**, *14*, 3608.
- [20] C. Motta, F. El-Mellouhi, S. Kais, N. Tabet, F. Alharbi, S. Sanvito, *Nat. Commun.* **2014**, *6*, 7026.
- [21] Y.-H. Kim, C. Wolf, Y.-T. Kim, H. Cho, W. Kwon, S. Do, A. Sadhanala, C. G. Park, S.-W. Rhee, S. H. Im, R. H. Friend, T.-W. Lee, *ACS Nano* **2017**, *11*, 6586.
- [22] Y.-H. Kim, G.-H. Lee, Y.-T. Kim, C. Wolf, H. J. Yun, W. Kwon, C. G. Park, T.-W. Lee, *Nano Energy* **2017**, *38*, 51.
- [23] C. C. Stoumpos, C. D. Malliakas, J. A. Peters, Z. Liu, M. Sebastian, J. Im, T. C. Chasapis, A. C. Wibowo, D. Y. Chung, A. J. Freeman, B. W. Wessels, M. G. Kanatzidis, *Cryst. Growth Des.* **2013**, *13*, 2722.
- [24] P. Schulz, E. Edri, S. Kirmayer, G. Hodes, D. Cahen, A. Kahn, *Energy Environ. Sci.* **2014**, *7*, 1377.
- [25] T. Hattori, T. Taira, M. Era, T. Tsutsui, S. Saito, *Chem. Phys. Lett.* **1996**, *254*, 103.
- [26] I. Koutselas, P. Bampoulis, E. Maratou, T. Evagelinou, G. Pagona, G. C. Papavassiliou, *J. Phys. Chem. C* **2011**, *115*, 8475.
- [27] K. Chondroudis, D. B. Mitzi, *Chem. Mater.* **1999**, *11*, 3028.
- [28] N. J. Jeon, J. H. Noh, Y. C. Kim, W. S. Yang, S. Ryu, S. Il Seok, *Nat. Mater.* **2014**, *13*, 897.
- [29] W. S. Yang, J. H. Noh, N. J. Jeon, Y. C. Kim, S. Ryu, J. Seo, S. I. Seok, *Science* **2015**, *348*, 1234.
- [30] K.-H. Kim, S. Lee, C.-K. Moon, S.-Y. Kim, Y.-S. Park, J.-H. Lee, J. W. Lee, J. Huh, Y. You, J.-J. Kim, *Nat. Commun.* **2014**, *5*, 4769.
- [31] X. Dai, Z. Zhang, Y. Jin, Y. Niu, H. Cao, X. Liang, L. Chen, J. Wang, X. Peng, *Nature* **2014**, *515*, 96.
- [32] B. S. Mashford, M. Stevenson, Z. Popovic, C. Hamilton, Z. Zhou, C. Breen, J. Steckel, V. Bulovic, M. Bawendi, S. Coe-Sullivan, P. T. Kazlas, *Nat. Photonics* **2013**, *7*, 407.
- [33] A. Kojima, M. Ikegami, K. Teshima, T. Miyasaka, *Chem. Lett.* **2012**, *41*, 397.
- [34] L. C. Schmidt, A. Pertegás, S. González-Carrero, O. Malinkiewicz, S. Agouram, G. M. Espallargas, H. J. Bolink, R. E. Galian, J. Pérez-Prieto, *J. Am. Chem. Soc.* **2014**, *136*, 850.
- [35] M. F. Aygüler, M. D. Weber, B. M. D. Puscher, D. D. Medina, P. Docampo, R. D. Costa, *J. Phys. Chem. C* **2015**, *119*, 12047.
- [36] M.-H. Park, S.-H. Jeong, H.-K. Seo, C. Wolf, Y.-H. Kim, H. Kim, J. Byun, J. S. Kim, H. Cho, T.-W. Lee, *Nano Energy* **2017**, *42*, 157.
- [37] X. Yang, X. Zhang, J. Deng, Z. Chu, Q. Jiang, J. Meng, P. Wang, L. Zhang, Z. Yin, J. You, *Nat. Commun.* **2018**, *9*, 570.
- [38] N. Wang, L. Cheng, R. Ge, S. Zhang, Y. Miao, W. Zou, C. Yi, Y. Sun, Y. Cao, R. Yang, Y. Wei, Q. Guo, Y. Ke, M. Yu, Y. Jin, Y. Liu, Q. Ding, D. Di, L. Yang, G. Xing, H. Tian, C. Jin, F. Gao, R. H. Friend, J. Wang, W. Huang, *Nat. Photonics* **2016**, *10*, 699.
- [39] X. Y. Chin, A. Perumal, A. Bruno, N. Yantara, S. A. Veldhuis, L. Martínez-Sarti, B. Chandran, V. Chirvony, A. S.-Z. Lo, J. So, C. Soci, M. Grätzel, H. J. Bolink, N. Mathews, S. G. Mhaisalkar, *Energy Environ. Sci.* **2018**, *11*, 1770.
- [40] X. Zhang, C. Sun, Y. Zhang, H. Wu, C. Ji, Y. Chuai, P. Wang, S. Wen, C. Zhang, W. W. Yu, *J. Phys. Chem. Lett.* **2016**, *7*, 4602.
- [41] X. Hu, H. Zhou, Z. Jiang, X. Wang, S. Yuan, J. Lan, Y. Fu, X. Zhang, W. Zheng, X. Wang, X. Zhu, L. Liao, G. Xu, S. Jin, A. Pan, *ACS Nano* **2017**, *11*, 9869.
- [42] S. Kumar, J. Jagielski, S. Yakunin, P. Rice, Y.-C. Chiu, M. Wang, G. Nedelcu, Y. Kim, S. Lin, E. J. G. Santos, M. V. Kovalenko, C.-J. Shih, *ACS Nano* **2016**, *10*, 9720.
- [43] J. Pan, L. N. Quan, Y. Zhao, W. Peng, B. Murali, S. P. Sarmah, M. Yuan, L. Sinatra, N. M. Alyami, J. Liu, E. Yassitepe, Z. Yang, O. Voznyy, R. Comin, M. N. Hedhili, O. F. Mohammed, Z. H. Lu, D. H. Kim, E. H. Sargent, O. M. Bakr, *Adv. Mater.* **2016**, *28*, 8718.
- [44] G. Li, F. W. R. Rivarola, N. J. L. K. Davis, S. Bai, T. C. Jellicoe, F. De La Peña, S. Hou, C. Ducati, F. Gao, R. H. Friend, N. C. Greenham, Z.-K. Tan, *Adv. Mater.* **2016**, *28*, 3528.
- [45] D. Liang, Y. Peng, Y. Fu, M. J. Shearer, J. Zhang, J. Zhai, Y. Zhang, R. J. Hamers, T. L. Andrew, S. Jin, *ACS Nano* **2016**, *10*, 6897.
- [46] S. D. Stranks, S. D. Stranks, G. E. Eperon, G. Grancini, C. Menelaou, M. J. P. Alcocer, T. Leijtens, L. M. Herz, A. Petrozza, H. J. Snaith, *Science* **2014**, *342*, 341.
- [47] R. Comin, G. Walters, E. S. Thibau, O. Voznyy, Z. H. Lu, E. H. Sargent, *J. Mater. Chem. C* **2015**, *3*, 8839.
- [48] S. Adjokatse, H.-H. Fang, M. A. Loi, *Mater. Today* **2017**, *20*, 413.
- [49] K. Tanaka, T. Takahashi, T. Ban, T. Kondo, K. Uchida, N. Miura, *Solid State Commun.* **2003**, *127*, 619.
- [50] I. B. Koutselas, L. Ducasse, G. C. Papavassiliou, *J. Phys. Condens. Matter* **1996**, *8*, 1217.
- [51] K. Galkowski, A. Mitioglu, A. Miyata, P. Plochocka, O. Portugall, G. E. Eperon, J. T.-W. Wang, T. Stergiopoulos, S. D. Stranks, H. J. Snaith, R. J. Nicholas, *Energy Environ. Sci.* **2016**, *9*, 962.
- [52] N. Sestu, M. Cadelano, V. Sarritzu, F. Chen, D. Marongiu, R. Piras, M. Mainas, F. Quochi, M. Saba, A. Mura, G. Bongiovanni, *J. Phys. Chem. Lett.* **2015**, *6*, 4566.
- [53] K. Wu, A. Bera, C. Ma, Y. Du, Y. Yang, L. Li, T. Wu, *Phys. Chem. Chem. Phys.* **2014**, *16*, 22476.
- [54] V. D'Innocenzo, G. Grancini, M. J. P. Alcocer, A. R. S. Kandada, S. D. Stranks, M. M. Lee, G. Lanzani, H. J. Snaith, A. Petrozza, *Nat. Commun.* **2014**, *5*, 3586.
- [55] G. Xing, B. Wu, X. Wu, M. Li, B. Du, Q. Wei, J. Guo, E. K. L. Yeow, T. C. Sum, W. Huang, *Nat. Commun.* **2017**, *8*, 14558.
- [56] Y. Yang, M. Yang, Z. Li, R. Crisp, K. Zhu, M. C. Beard, *J. Phys. Chem. Lett.* **2015**, *6*, 4688.
- [57] F. Zheng, L. Z. Tan, S. Liu, A. M. Rappe, *Nano Lett.* **2015**, *15*, 7794.
- [58] Y. Zhai, S. Baniya, C. Zhang, J. Li, P. Haney, C.-X. Sheng, E. Ehrenfreund, Z. V. Vardeny, *Sci. Adv.* **2017**, *3*, e1700704.
- [59] I. P. Swinson, C. Stock, S. F. Parker, L. Van Eijck, M. Russina, J. W. Taylor, *Phys. Rev. B* **2015**, *92*, 100303.
- [60] M. Li, L. Li, R. Mukherjee, K. Wang, Q. Liu, Q. Zou, H. Xu, J. Tisdale, Z. Gai, I. N. Ivanov, D. Mandrus, B. Hu, *Adv. Mater.* **2017**, *29*, 1603667.
- [61] H. Zhu, K. Miyata, Y. Fu, J. Wang, P. P. Joshi, D. Niesner, K. W. Williams, S. Jin, X.-Y. Zhu, *Science* **2016**, *353*, 1409.
- [62] X. Y. Zhu, V. Podzorov, *J. Phys. Chem. Lett.* **2015**, *6*, 4758.
- [63] K. Miyata, T. L. Atallah, X.-Y. Zhu, *Sci. Adv.* **2017**, *3*, e1701469.
- [64] J. M. Frost, A. Walsh, *Acc. Chem. Res.* **2016**, *49*, 528.
- [65] K. Miyata, D. Meggiolaro, M. T. Trinh, P. P. Joshi, E. Mosconi, S. C. Jones, F. De Angelis, X.-Y. Zhu, *Sci. Adv.* **2017**, *3*, e1701217.
- [66] H. Zhu, M. T. Trinh, J. Wang, Y. Fu, P. P. Joshi, K. Miyata, S. Jin, X.-Y. Zhu, *Adv. Mater.* **2017**, *29*, 1603072.

- [67] Y. Rosenwaks, M. C. Hanna, D. H. Levi, D. M. Szmyd, R. K. Ahrenkiel, A. J. Nozik, *Phys. Rev. B* **1993**, *48*, 14675.
- [68] M. B. Price, J. Butkus, T. C. Jellicoe, A. Sadhanala, A. Briane, J. E. Halpert, K. Broch, J. M. Hodgkiss, R. H. Friend, F. Deschler, *Nat. Commun.* **2015**, *6*, 8420.
- [69] Y. Yang, D. P. Ostrowski, R. M. France, K. Zhu, J. Van De Lagemaat, J. M. Luther, M. C. Beard, *Nat. Photonics* **2016**, *10*, 53.
- [70] A. D. Wright, C. Verdi, R. L. Milot, G. E. Eperon, M. A. Pérez-Osorio, H. J. Snaith, F. Giustino, M. B. Johnston, L. M. Herz, *Nat. Commun.* **2016**, *7*, 11755.
- [71] D. W. de Quilettes, S. M. Vorpahl, S. D. Stranks, H. Nagaoka, G. E. Eperon, M. E. Ziffer, H. J. Snaith, D. S. Ginger, *Science* **2015**, *348*, 683.
- [72] F. Zhang, H. Zhong, C. Chen, X. Wu, X. Hu, H. Huang, J. Han, B. Zou, Y. Dong, *ACS Nano* **2015**, *9*, 4533.
- [73] G. Xing, N. Mathews, S. S. Lim, N. Yantara, X. Liu, D. Sabba, M. Grätzel, S. Mhaisalkar, T. C. Sum, *Nat. Mater.* **2014**, *13*, 476.
- [74] H. Yuan, E. Debroye, G. Caliendo, K. P. F. Janssen, J. van Loon, C. E. A. Kirschhock, J. A. Martens, J. Hofkens, M. B. J. Roeffaers, *ACS Omega* **2016**, *1*, 148.
- [75] L. Wang, C. McCleese, A. Kovalsky, Y. Zhao, C. Burda, *J. Am. Chem. Soc.* **2014**, *136*, 12205.
- [76] Y. Yuan, J. Huang, *Acc. Chem. Res.* **2016**, *49*, 286.
- [77] M. L. Agiorgousis, Y. Y. Sun, H. Zeng, S. Zhang, *J. Am. Chem. Soc.* **2014**, *136*, 14570.
- [78] W.-J. Yin, T. Shi, Y. Yan, *Appl. Phys. Lett.* **2014**, *104*, 63903.
- [79] R. A. Kerner, L. Zhao, Z. Xiao, B. P. Rand, *J. Mater. Chem. A* **2016**, *4*, 8308.
- [80] M. Long, T. Zhang, Y. Chai, C. F. Ng, T. C. W. Mak, J. Xu, K. Yan, *Nat. Commun.* **2016**, *7*, 13503.
- [81] F. Hao, C. C. Stoumpos, Z. Liu, R. P. H. Chang, M. G. Kanatzidis, *J. Am. Chem. Soc.* **2014**, *136*, 16411.
- [82] Y. Cheng, H.-W. Li, J. Zhang, Q.-D. Yang, T. Liu, Z. Guan, J. Qing, C.-S. Lee, S.-W. Tsang, *J. Mater. Chem. A* **2016**, *4*, 561.
- [83] H. Hu, D. Wang, Y. Zhou, J. Zhang, S. Lv, S. Pang, X. Chen, Z. Liu, N. P. Padture, G. Cui, *RSC Adv.* **2014**, *4*, 28964.
- [84] M. R. Leyden, L. Meng, Y. Jiang, L. K. Ono, L. Qiu, E. J. Juarez-Perez, C. Qin, C. Adachi, Y. Qi, *J. Phys. Chem. Lett.* **2017**, *8*, 3193.
- [85] H. Ji, Z. Shi, X. Sun, Y. Li, S. Li, L. Lei, D. Wu, T. Xu, X. Li, G. Du, *ACS Appl. Mater. Interfaces* **2017**, *9*, 42893.
- [86] A. Walsh, D. O. Scanlon, S. Chen, X. G. Gong, S.-H. Wei, *Angew. Chem., Int. Ed.* **2015**, *54*, 1791.
- [87] N. A. Manshor, Q. Wali, K. K. Wong, S. K. Muzakir, A. Fakharuddin, L. Schmidt-Mende, R. Jose, *Phys. Chem. Chem. Phys.* **2016**, *18*, 21629.
- [88] S. D. Stranks, V. M. Burlakov, T. Leijtens, J. M. Ball, A. Goriely, H. J. Snaith, *Phys. Rev. Appl.* **2014**, *2*, 34007.
- [89] D. W. DeQuilettes, W. Zhang, V. M. Burlakov, D. J. Graham, T. Leijtens, A. Osherov, V. Bulović, H. J. Snaith, D. S. Ginger, S. D. Stranks, *Nat. Commun.* **2016**, *7*, 11683.
- [90] L. A. Frolova, N. N. Dremova, P. A. Troshin, *Chem. Commun.* **2015**, *51*, 14917.
- [91] S. Huang, Z. Li, B. Wang, N. Zhu, C. Zhang, L. Kong, Q. Zhang, A. Shan, L. Li, *ACS Appl. Mater. Interfaces* **2017**, *9*, 7249.
- [92] S. Ito, S. Tanaka, K. Manabe, H. Nishino, *J. Phys. Chem. C* **2014**, *118*, 16995.
- [93] G. Niu, X. Guo, L. Wang, *J. Mater. Chem. A* **2015**, *3*, 8970.
- [94] S. Wang, Y. Jiang, E. J. Juarez-Perez, L. K. Ono, Y. Qi, *Nat. Energy* **2016**, *2*, 16195.
- [95] O. Hentz, Z. Zhao, S. Gradečak, *Nano Lett.* **2016**, *16*, 1485.
- [96] R. Gottesman, L. Gouda, B. S. Kalanoor, E. Haltzi, S. Tirosh, E. Rosh-Hodesh, Y. Tischler, A. Zaban, C. Quarti, E. Mosconi, F. De Angelis, *J. Phys. Chem. Lett.* **2015**, *6*, 2332.
- [97] W. Nie, J.-C. Blancon, A. J. Neukirch, K. Appavoo, H. Tsai, M. Chhowalla, M. A. Alam, M. Y. Sfeir, C. Katan, J. Even, S. Tretiak, J. J. Crochet, G. Gupta, A. D. Mohite, *Nat. Commun.* **2016**, *7*, 11574.
- [98] S. Chen, X. Wen, R. Sheng, S. Huang, X. Deng, M. A. Green, A. Ho-Baillie, *ACS Appl. Mater. Interfaces* **2016**, *8*, 5351.
- [99] J. F. Galisteo-López, M. Anaya, M. E. Calvo, H. Míguez, *J. Phys. Chem. Lett.* **2015**, *6*, 2200.
- [100] N. K. Noel, A. Abate, S. D. Stranks, E. S. Parrott, V. M. Burlakov, A. Goriely, H. J. Snaith, *ACS Nano* **2014**, *8*, 9815.
- [101] F. Liu, Q. Dong, M. K. Wong, A. B. Djurišić, A. Ng, Z. Ren, Q. Shen, C. Surya, W. K. Chan, J. Wang, A. M. C. Ng, C. Liao, H. Li, K. Shih, C. Wei, H. Su, J. Dai, *Adv. Energy Mater.* **2016**, *6*, 1502206.
- [102] N. Aristidou, I. Sanchez-Molina, T. Chotchuangchutchaval, M. Brown, L. Martinez, T. Rath, S. A. Haque, *Angew. Chem., Int. Ed.* **2015**, *54*, 8208.
- [103] J. A. Christians, P. A. Miranda Herrera, P. V. Kamat, *J. Am. Chem. Soc.* **2015**, *137*, 1530.
- [104] B. R. Vincent, K. N. Robertson, T. S. Cameron, O. Knop, *Can. J. Chem.* **1987**, *65*, 1042.
- [105] Z. Liu, Y. Bekenstein, X. Ye, S. C. Nguyen, J. Swabeck, D. Zhang, S. T. Lee, P. Yang, W. Ma, A. P. Alivisatos, *J. Am. Chem. Soc.* **2017**, *139*, 5309.
- [106] Y. Zhang, M. I. Saidaminov, I. Dursun, H. Yang, B. Murali, E. Alarousu, E. Yengel, B. A. Alshankiti, O. M. Bakr, O. F. Mohammed, *J. Phys. Chem. Lett.* **2017**, *8*, 961.
- [107] H. Cho, Y.-H. Kim, C. Wolf, H.-D. Lee, T.-W. Lee, *Adv. Mater.* **2018**, *30*, 1704587.
- [108] J. H. Noh, S. H. Im, J. H. Heo, T. N. Mandal, S. Il Seok, *Nano Lett.* **2013**, *13*, 1764.
- [109] F. Ma, N. Li, J. Li, Z. Jia, J. Xue, L. Wang, J. Qiao, *J. Mater. Chem. C* **2017**, *5*, 11121.
- [110] Y.-H. Kim, H. Cho, J. H. Heo, S. H. Im, T.-W. Lee, *Curr. Appl. Phys.* **2016**, *16*, 1069.
- [111] Y. Tidhar, E. Edri, H. Weissman, D. Zohar, G. Hodes, D. Cahen, B. Rybtchinski, S. Kirmayer, *J. Am. Chem. Soc.* **2014**, *136*, 13249.
- [112] P. Tyagi, L. Indu Giri, S. Tuli, R. Srivastava, *J. Appl. Phys.* **2014**, *115*, 34518.
- [113] Y. Zhao, K. Zhu, *J. Am. Chem. Soc.* **2014**, *136*, 12241.
- [114] Z. Song, S. C. Waththage, A. B. Phillips, B. L. Tompkins, R. J. Ellingson, M. J. Heben, *Chem. Mater.* **2015**, *27*, 4612.
- [115] M. Kulbak, S. Gupta, N. Kedem, I. Levine, T. Bendikov, G. Hodes, D. Cahen, *J. Phys. Chem. Lett.* **2016**, *7*, 167.
- [116] Q. Chen, H. Zhou, T.-B. Song, S. Luo, Z. Hong, H.-S. Duan, L. Dou, Y. Liu, Y. Yang, *Nano Lett.* **2014**, *14*, 4158.
- [117] A. Dualeh, N. Tétreault, T. Moehl, P. Gao, M. K. Nazeeruddin, M. Grätzel, *Adv. Funct. Mater.* **2014**, *24*, 3250.
- [118] R. K. Misra, S. Aharon, B. Li, D. Mogilyansky, I. Visoly-Fisher, L. Etgar, E. A. Katz, *J. Phys. Chem. Lett.* **2015**, *6*, 326.
- [119] B. Conings, J. Drijkoningen, N. Gauquelin, A. Babayigit, J. D'Haen, L. D'Olieslaeger, A. Ethirajan, J. Verbeeck, J. Manca, E. Mosconi, F. De Angelis, H.-G. Boyen, *Adv. Energy Mater.* **2015**, *5*, 1500477.
- [120] H. Gao, C. Bao, F. Li, T. Yu, J. Yang, W. Zhu, X. Zhou, G. Fu, Z. Zou, *ACS Appl. Mater. Interfaces* **2015**, *7*, 9110.
- [121] K. Saxena, V. K. Jain, D. S. Mehta, *Opt. Mater.* **2009**, *32*, 221.
- [122] J. H. Heo, D. H. Song, S. H. Im, *Adv. Mater.* **2014**, *26*, 8179.
- [123] K. Yan, M. Long, T. Zhang, Z. Wei, H. Chen, S. Yang, J. Xu, *J. Am. Chem. Soc.* **2015**, *137*, 4460.
- [124] C.-W. Chen, H.-W. Kang, S.-Y. Hsiao, P.-F. Yang, K.-M. Chiang, H.-W. Lin, *Adv. Mater.* **2014**, *26*, 6647.
- [125] W. Deng, X. Xu, X. Zhang, Y. Zhang, X. Jin, L. Wang, S.-T. Lee, J. Jie, *Adv. Funct. Mater.* **2016**, *26*, 4797.
- [126] T. Chiba, K. Hoshi, Y.-J. Pu, Y. Takeda, Y. Hayashi, S. Ohisa, S. Kawata, J. Kido, *ACS Appl. Mater. Interfaces* **2017**, *9*, 18054.
- [127] J. C. Yu, A.-Y. Lee, D. Bin Kim, E. D. Jung, D. W. Kim, M. H. Song, *Adv. Mater. Technol.* **2017**, *2*, 1700003.

- [128] Y. Ling, Z. Yuan, Y. Tian, X. Wang, J. C. Wang, Y. Xin, K. Hanson, B. Ma, H. Gao, *Adv. Mater.* **2016**, *28*, 305.
- [129] L. Protesescu, S. Yakunin, M. I. Bodnarchuk, F. Bertolotti, N. Masciocchi, A. Guagliardi, M. V. Kovalenko, *J. Am. Chem. Soc.* **2016**, *138*, 14202.
- [130] J. Li, L. Xu, T. Wang, J. Song, J. Chen, J. Xue, Y. Dong, B. Cai, Q. Shan, B. Han, H. Zeng, *Adv. Mater.* **2017**, *29*, 1603885.
- [131] Q. Van Le, J. B. Kim, S. Y. Kim, B. Lee, D. R. Lee, *J. Phys. Chem. Lett.* **2017**, *8*, 4140.
- [132] K.-M. Chiang, B.-W. Hsu, Y.-A. Chang, L. Yang, W.-L. Tsai, H.-W. Lin, *ACS Appl. Mater. Interfaces* **2017**, *9*, 40516.
- [133] M. Saliba, S. M. Wood, J. B. Patel, P. K. Nayak, J. Huang, J. A. Alexander-Webber, B. Wenger, S. D. Stranks, M. T. Hörantner, J. T. W. Wang, R. J. Nicholas, L. M. Herz, M. B. Johnston, S. M. Morris, H. J. Snaith, M. K. Riede, *Adv. Mater.* **2016**, *28*, 923.
- [134] Y.-K. Chih, J.-C. Wang, R.-T. Yang, C.-C. Liu, Y.-C. Chang, Y.-S. Fu, W.-C. Lai, P. Chen, T.-C. Wen, Y.-C. Huang, C.-S. Tsao, T.-F. Guo, *Adv. Mater.* **2016**, *28*, 8687.
- [135] L. Meng, E.-P. Yao, Z. Hong, H. Chen, P. Sun, Z. Yang, G. Li, Y. Yang, *Adv. Mater.* **2017**, *29*, 1603826.
- [136] M. G. Helander, M. T. Greiner, Z. B. Wang, W. M. Tang, Z. H. Lu, *J. Vac. Sci. Technol., A* **2011**, *29*, 11019.
- [137] H.-J. Kim, K.-W. Seo, Y.-J. Noh, S.-I. Na, A. Sohn, D.-W. Kim, H.-K. Kim, *Sol. Energy Mater. Sol. Cells* **2015**, *141*, 194.
- [138] J. Wang, N. Wang, Y. Jin, J. Si, Z.-K. Tan, H. Du, L. Cheng, X. Dai, S. Bai, H. He, Z. Ye, M. L. Lai, R. H. Friend, W. Huang, *Adv. Mater.* **2015**, *27*, 2311.
- [139] A. M. A. Leguy, P. Azarhoosh, M. I. Alonso, M. Campoy-Quiles, O. J. Weber, J. Yao, D. Bryant, M. T. Weller, J. Nelson, A. Walsh, M. van Schilfgaarde, P. R. F. Barnes, *Nanoscale* **2016**, *8*, 6317.
- [140] F. Zhao, D. Ma, *Mater. Chem. Front.* **2017**, *1*, 1933.
- [141] G. C. Xing, N. Mathews, S. Y. Sun, S. S. Lim, Y. M. Lam, M. Gratzel, S. Mhaisalkar, T. C. Sum, *Science* **2013**, *342*, 344.
- [142] Y.-H. Kim, T.-H. Han, H. Cho, S.-Y. Min, C.-L. Lee, T.-W. Lee, *Adv. Funct. Mater.* **2014**, *24*, 3808.
- [143] L. Zhang, X. Yang, Q. Jiang, P. Wang, Z. Yin, X. Zhang, H. Tan, Y. M. Yang, M. Wei, B. R. Sutherland, E. H. Sargent, J. You, *Nat. Commun.* **2017**, *8*, 15640.
- [144] K. Domanski, J. P. Correa-Baena, N. Mine, M. K. Nazeeruddin, A. Abate, M. Saliba, W. Tress, A. Hagfeldt, M. Grätzel, *ACS Nano* **2016**, *10*, 6306.
- [145] H.-K. Seo, H. Kim, J. Lee, M.-H. Park, S.-H. Jeong, Y.-H. Kim, S.-J. Kwon, T.-H. Han, S. Yoo, T.-W. Lee, *Adv. Mater.* **2017**, *29*, 1605587.
- [146] S. S. Mammana, A. Greatti, F. H. Luiz, F. I. Da Costa, A. P. Mammana, G. A. Calligaris, L. P. Cardoso, C. I. Z. Mammana, D. Den Engelsens, *Thin Solid Films* **2014**, *567*, 20.
- [147] M. P. de Jong, L. J. van IJzendoorn, M. J. A. de Voigt, *Appl. Phys. Lett.* **2000**, *77*, 2255.
- [148] S. D. Yambem, K.-S. Liao, N. J. Alley, S. A. Curran, *J. Mater. Chem.* **2012**, *22*, 6894.
- [149] L. Zhao, R. A. Kerner, Z. Xiao, Y. L. Lin, K. M. Lee, J. Schwartz, B. P. Rand, *ACS Energy Lett.* **2016**, *1*, 595.
- [150] Y. Kato, L. K. Ono, M. V. Lee, S. Wang, S. R. Raga, Y. Qi, *Adv. Mater. Interfaces* **2015**, *2*, 1500195.
- [151] L. Zhao, J. Gao, Y. L. Lin, Y.-W. Yeh, K. M. Lee, N. Yao, Y.-L. Loo, B. P. Rand, *Adv. Mater.* **2017**, *29*, 1605317.
- [152] J. M. Azpiroz, E. Mosconi, J. Bisquert, F. De Angelis, *Energy Environ. Sci.* **2015**, *8*, 2118.
- [153] Y. Yuan, Q. Wang, Y. Shao, H. Lu, T. Li, A. Gruverman, J. Huang, *Adv. Energy Mater.* **2016**, *6*, 1501803.
- [154] J. Haruyama, K. Sodeyama, L. Han, Y. Tateyama, *J. Am. Chem. Soc.* **2015**, *137*, 10048.
- [155] J. Mizusaki, K. Arai, K. Fueki, *Solid State Ionics* **1983**, *11*, 203.
- [156] H. Cho, C. Wolf, J. S. Kim, H. J. Yun, J. S. Bae, H. Kim, J.-M. Heo, S. Ahn, T.-W. Lee, *Adv. Mater.* **2017**, *29*, 1700579.
- [157] Y. Yuan, J. Chae, Y. Shao, Q. Wang, Z. Xiao, A. Centrone, J. Huang, *Adv. Energy Mater.* **2015**, *5*, 1500615.
- [158] Y. Shao, Y. Fang, T. Li, Q. Wang, Q. Dong, Y. Deng, Y. Yuan, H. Wei, M. Wang, A. Gruverman, J. Shield, J. Huang, *Energy Environ. Sci.* **2016**, *9*, 1752.
- [159] J. Li, X. Shan, S. G. R. Bade, T. Geske, Q. Jiang, X. Yang, Z. Yu, *J. Phys. Chem. Lett.* **2016**, *7*, 4059.
- [160] T.-H. Han, Y.-H. Kim, M. H. Kim, W. Song, T.-W. Lee, *ACS Appl. Mater. Interfaces* **2016**, *8*, 6152.
- [161] H. Zhang, H. Lin, C. Liang, H. Liu, J. Liang, Y. Zhao, W. Zhang, M. Sun, W. Xiao, H. Li, S. Polizzi, D. Li, F. Zhang, Z. He, W. C. H. Choy, *Adv. Funct. Mater.* **2015**, *25*, 7226.
- [162] P. Vashishtha, J. E. Halpert, *Chem. Mater.* **2017**, *29*, 5965.
- [163] C. G. Bischak, C. L. Hetherington, H. Wu, S. Aloni, D. F. Ogletree, D. T. Limmer, N. S. Ginsberg, *Nano Lett.* **2017**, *17*, 1028.
- [164] J. C. Yu, D. Bin Kim, E. D. Jung, B. R. Lee, M. H. Song, *Nanoscale* **2016**, *8*, 7036.
- [165] J. Li, S. G. R. Bade, X. Shan, Z. Yu, *Adv. Mater.* **2015**, *27*, 5196.
- [166] J. Yan, B. Zhang, Y. Chen, A. Zhang, X. Ke, *ACS Appl. Mater. Interfaces* **2016**, *8*, 12756.
- [167] J. Byun, H. Cho, C. Wolf, M. Jang, A. Sadhanala, R. H. Friend, H. Yang, T.-W. Lee, *Adv. Mater.* **2016**, *28*, 7515.
- [168] M. Yuan, L. N. Quan, R. Comin, G. Walters, R. Sabatini, O. Voznyy, S. Hoogland, Y. Zhao, E. M. Bearegard, P. Kanjanaboos, Z. Lu, D. H. Kim, E. H. Sargent, *Nat. Nanotechnol.* **2016**, *11*, 872.
- [169] J. Song, J. Li, X. Li, L. Xu, Y. Dong, H. Zeng, *Adv. Mater.* **2015**, *27*, 7162.
- [170] S. Lee, J. H. Park, B. R. Lee, E. D. Jung, J. C. Yu, D. Di Nuzzo, R. H. Friend, M. H. Song, *J. Phys. Chem. Lett.* **2017**, *8*, 1784.
- [171] A. Abate, M. Saliba, D. J. Hollman, S. D. Stranks, K. Wojciechowski, R. Avolio, G. Grancini, A. Petrozza, H. J. Snaith, *Nano Lett.* **2014**, *14*, 3247.
- [172] J. C. Yu, D. W. Kim, D. Bin Kim, E. D. Jung, K.-S. Lee, S. Lee, D. Di Nuzzo, J.-S. Kim, M. H. Song, *Nanoscale* **2017**, *9*, 2088.
- [173] M. Xiao, F. Huang, W. Huang, Y. Dkhissi, Y. Zhu, J. Etheridge, A. Gray-Weale, U. Bach, Y.-B. Cheng, L. Spiccia, *Angew. Chem.* **2014**, *126*, 10056.
- [174] L. Zhao, Y.-W. Yeh, N. L. Tran, F. Wu, Z. Xiao, R. A. Kerner, Y. L. Lin, G. D. Scholes, N. Yao, B. P. Rand, *ACS Nano* **2017**, *11*, 3957.
- [175] N. Kawano, M. Koshimizu, Y. Sun, N. Yahaba, Y. Fujimoto, T. Yanagida, K. Asai, *J. Phys. Chem. C* **2014**, *118*, 9101.
- [176] L. N. Quan, Y. Zhao, F. P. García De Arquer, R. Sabatini, G. Walters, O. Voznyy, R. Comin, Y. Li, J. Z. Fan, H. Tan, J. Pan, M. Yuan, O. M. Bakr, Z. Lu, D. H. Kim, E. H. Sargent, *Nano Lett.* **2017**, *17*, 3701.
- [177] Z. Chen, C. Zhang, X.-F. Jiang, M. Liu, R. Xia, T. Shi, D. Chen, Q. Xue, Y.-J. Zhao, S. Su, H.-L. Yip, Y. Cao, *Adv. Mater.* **2017**, *29*, 1603157.
- [178] Z. Xiao, R. A. Kerner, L. Zhao, N. L. Tran, K. M. Lee, T.-W. Koh, G. D. Scholes, B. P. Rand, *Nat. Photonics* **2017**, *11*, 108.
- [179] J. Si, Y. Liu, Z. He, H. Du, K. Du, D. Chen, J. Li, M. Xu, H. Tian, H. He, D. Di, C. Lin, Y. Cheng, J. Wang, Y. Jin, *ACS Nano* **2017**, *11*, 11100.
- [180] J.-W. Lee, D.-H. Kim, H.-S. Kim, S.-W. Seo, S. M. Cho, N.-G. Park, *Adv. Energy Mater.* **2015**, *5*, 1501310.
- [181] Z. Li, M. Yang, J.-S. Park, S.-H. Wei, J. J. Berry, K. Zhu, *Chem. Mater.* **2016**, *28*, 284.
- [182] C. Yi, J. Luo, S. Meloni, A. Boziki, N. Ashari-Astani, C. Grätzel, S. M. Zakeeruddin, U. Röthlisberger, M. Grätzel, *Energy Environ. Sci.* **2016**, *9*, 656.
- [183] H. Cho, J. S. Kim, C. Wolf, Y.-H. Kim, H. J. Yun, S.-H. Jeong, A. Sadhanala, V. Venugopalan, J. W. Choi, C.-L. Lee, R. H. Friend, T.-W. Lee, *ACS Nano* **2018**, *12*, 2883.

- [184] Z. Xiao, L. Zhao, N. L. Tran, Y. L. Lin, S. H. Silver, R. A. Kerner, N. Yao, A. Kahn, G. D. Scholes, B. P. Rand, *Nano Lett.* **2017**, *17*, 6863.
- [185] A. Pan, B. He, X. Fan, Z. Liu, J. J. Urban, A. P. Alivisatos, L. He, Y. Liu, *ACS Nano* **2016**, *10*, 7943.
- [186] S. Sun, D. Yuan, Y. Xu, A. Wang, Z. Deng, *ACS Nano* **2016**, *10*, 3648.
- [187] S. N. Raja, Y. Bekenstein, M. A. Koc, S. Fischer, D. Zhang, L. Lin, R. O. Ritchie, P. Yang, A. P. Alivisatos, *ACS Appl. Mater. Interfaces* **2016**, *8*, 35523.
- [188] J. Shamsi, P. Rastogi, V. Caligiuri, A. L. Abdelhady, D. Spirito, L. Manna, R. Krahne, *ACS Nano* **2017**, *11*, 10206.
- [189] Z. Dang, J. Shamsi, F. Palazon, M. Imran, Q. A. Akkerman, S. Park, G. Bertoni, M. Prato, R. Brescia, L. Manna, *ACS Nano* **2017**, *11*, 2124.
- [190] Z. Long, H. Ren, J. Sun, J. Ouyang, N. Na, *Chem. Commun.* **2017**, 53, 9914.
- [191] Y. Tong, E. Bladt, M. F. Aygüler, A. Manzi, K. Z. Milowska, V. A. Hintermayr, P. Docampo, S. Bals, A. S. Urban, L. Polavarapu, J. Feldmann, *Angew. Chem., Int. Ed.* **2016**, *55*, 13887.
- [192] X. Chen, L. Peng, K. Huang, Z. Shi, R. Xie, W. Yang, *Nano Res.* **2016**, *9*, 1994.
- [193] D. M. Jang, K. Park, D. H. Kim, J. Park, F. Shojaei, H. S. Kang, J.-P. Ahn, J. W. Lee, J. K. Song, *Nano Lett.* **2015**, *15*, 5191.
- [194] G. E. Eperon, S. D. Stranks, C. Menelaou, M. B. Johnston, L. M. Herz, H. J. Snaith, *Energy Environ. Sci.* **2014**, *7*, 982.
- [195] P.-W. Liang, C.-Y. Liao, C.-C. Chueh, F. Zuo, S. T. Williams, X.-K. Xin, J. Lin, A. K.-Y. Jen, *Adv. Mater.* **2014**, *26*, 3748.
- [196] Y.-J. Jeon, S. Lee, R. Kang, J.-E. Kim, J.-S. Yeo, S.-H. Lee, S.-S. Kim, J.-M. Yun, D.-Y. Kim, *Sci. Rep.* **2015**, *4*, 6953.
- [197] Y. Chen, Y. Zhao, Z. Liang, *Chem. Mater.* **2015**, *27*, 1448.
- [198] F. F. Chausov, *Theor. Found. Chem. Eng.* **2008**, *42*, 179.
- [199] Y. Ling, Y. Tian, X. Wang, J. C. Wang, J. M. Knox, F. Perez-Orive, Y. Du, L. Tan, K. Hanson, B. Ma, H. Gao, *Adv. Mater.* **2016**, *28*, 8983.
- [200] C. Wu, Y. Zou, T. Wu, M. Ban, V. Pecunia, Y. Han, Q. Liu, T. Song, S. Duhm, B. Sun, *Adv. Funct. Mater.* **2017**, *27*, 1700338.
- [201] F. Meng, C. Zhang, D. Chen, W. Zhu, H.-L. Yip, S.-J. Su, *J. Mater. Chem. C* **2017**, *5*, 6169.
- [202] G. Li, Z.-K. Tan, D. Di, M. L. Lai, L. Jiang, J. H.-W. Lim, R. H. Friend, N. C. Greenham, *Nano Lett.* **2015**, *15*, 2640.
- [203] L. Song, X. Guo, Y. Hu, Y. Lv, J. Lin, Z. Liu, Y. Fan, X. Liu, *J. Phys. Chem. Lett.* **2017**, *8*, 4148.
- [204] P. Chen, Z. Xiong, X. Wu, M. Shao, X. Ma, Z. H. Xiong, C. Gao, *J. Phys. Chem. Lett.* **2017**, *8*, 1810.
- [205] Z. Wei, A. Perumal, R. Su, S. Sushant, J. Xing, Q. Zhang, S. T. Tan, H. V. Demir, Q. Xiong, *Nanoscale* **2016**, *8*, 18021.
- [206] X. Zhao, B. Zhang, R. Zhao, B. Yao, X. Liu, J. Liu, Z. Xie, *J. Phys. Chem. Lett.* **2016**, *7*, 4259.
- [207] M. K. Kim, T. Jeon, H. Il Park, J. M. Lee, S. A. Nam, S. O. Kim, *CrystEngComm* **2016**, *18*, 6090.
- [208] T. Salim, S. Sun, Y. Abe, A. Krishna, A. C. Grimsdale, Y. M. Lam, *J. Mater. Chem. A* **2015**, *3*, 8943.
- [209] L. Zuo, Z. Gu, T. Ye, W. Fu, G. Wu, H. Li, H. Chen, *J. Am. Chem. Soc.* **2015**, *137*, 2674.
- [210] N. Ahn, S. M. Kang, J.-W. Lee, M. Choi, N.-G. Park, *J. Mater. Chem. A* **2015**, *3*, 19901.
- [211] H. Ko, D. H. Sin, M. Kim, K. Cho, *Chem. Mater.* **2017**, *29*, 1165.
- [212] N. K. Kumawat, N. Jain, A. Dey, K. L. Narasimhan, D. Kabra, *Adv. Funct. Mater.* **2017**, *27*, 1603219.
- [213] Y. Wu, A. Islam, X. Yang, C. Qin, J. Liu, K. Zhang, W. Peng, L. Han, *Energy Environ. Sci.* **2014**, *7*, 2934.
- [214] J. Wu, X. Xu, Y. Zhao, J. Shi, Y. Xu, Y. Luo, D. Li, H. Wu, Q. Meng, *ACS Appl. Mater. Interfaces* **2017**, *9*, 26937.
- [215] K. Qasim, B. Wang, Y. Zhang, P. Li, Y. Wang, S. Li, S.-T. Lee, L.-S. Liao, W. Lei, Q. Bao, *Adv. Funct. Mater.* **2017**, *27*, 1606874.
- [216] S. G. R. Bade, J. Li, X. Shan, Y. Ling, Y. Tian, T. Dilbeck, T. Besara, T. Geske, H. Gao, B. Ma, K. Hanson, T. Siegrist, C. Xu, Z. Yu, *ACS Nano* **2016**, *10*, 1795.
- [217] L. Gil-Escrig, A. Miquel-Sempere, M. Sessolo, H. J. Bolink, *J. Phys. Chem. Lett.* **2015**, *6*, 3743.
- [218] H. Sun, Z. Yang, M. Wei, W. Sun, X. Li, S. Ye, Y. Zhao, H. Tan, E. L. Kynaston, T. B. Schon, H. Yan, Z.-H. Lu, G. A. Ozin, E. H. Sargent, D. S. Seferos, *Adv. Mater.* **2017**, *29*, 1701153.
- [219] F. Palazon, Q. A. Akkerman, M. Prato, L. Manna, *ACS Nano* **2016**, *10*, 1224.
- [220] Y. Liu, F. Li, Z. Xu, C. Zheng, T. Guo, X. Xie, L. Qian, D. Fu, X. Yan, *ACS Appl. Mater. Interfaces* **2017**, *9*, 25506.
- [221] C. Qin, T. Matsushima, A. S. D. Sandanayaka, Y. Tsuchiya, C. Adachi, *J. Phys. Chem. Lett.* **2017**, *8*, 5415.
- [222] J.-W. Lee, Y. J. Choi, J.-M. Yang, S. Ham, S. K. Jeon, J. Y. Lee, Y.-H. Song, E. K. Ji, D.-H. Yoon, S. Seo, H. Shin, G. S. Han, H. S. Jung, D. Kim, N.-G. Park, *ACS Nano* **2017**, *11*, 3311.
- [223] X. Zhang, H. Liu, W. Wang, J. Zhang, B. Xu, K. L. Karen, Y. Zheng, S. Liu, S. Chen, K. Wang, X. W. Sun, *Adv. Mater.* **2017**, *29*, 1606405.
- [224] B. Xu, W. Wang, X. Zhang, W. Cao, D. Wu, S. Liu, H. Dai, S. Chen, K. Wang, X. Sun, *J. Mater. Chem. C* **2017**, *5*, 6123.
- [225] X. Zhang, B. Xu, J. Zhang, Y. Gao, Y. Zheng, K. Wang, X. W. Sun, *Adv. Funct. Mater.* **2016**, *26*, 4595.
- [226] S. Zou, Y. Liu, J. Li, C. Liu, R. Feng, F. Jiang, Y. Li, J. Song, H. Zeng, M. Hong, X. Chen, *J. Am. Chem. Soc.* **2017**, *139*, 11443.
- [227] H. Huang, H. Lin, S. V. Kershaw, A. S. Susa, W. C. H. Choy, A. L. Rogach, *J. Phys. Chem. Lett.* **2016**, *7*, 4398.
- [228] Y. Tan, Y. Zou, L. Wu, Q. Huang, D. Yang, M. Chen, M. Ban, C. Wu, T. Wu, S. Bai, T. Song, Q. Zhang, B. Sun, *ACS Appl. Mater. Interfaces* **2018**, *10*, 3784.
- [229] P. Liu, W. Chen, W. Wang, B. Xu, D. Wu, J. Hao, W. Cao, F. Fang, Y. Li, Y. Zeng, R. Pan, S. Chen, W. Cao, X. W. Sun, K. Wang, *Chem. Mater.* **2017**, *29*, 5168.
- [230] J. C. Yu, D. W. Kim, D. Bin Kim, E. D. Jung, J. H. Park, A.-Y. Lee, B. R. Lee, D. Di Nuzzo, R. H. Friend, M. H. Song, *Adv. Mater.* **2016**, *28*, 6906.
- [231] H.-H. Fang, F. Wang, S. Adjokatse, N. Zhao, M. A. Loi, *Adv. Funct. Mater.* **2016**, *26*, 4653.
- [232] X. Zhang, W. Wang, B. Xu, S. Liu, H. Dai, D. Bian, S. Chen, K. Wang, X. W. Sun, *Nano Energy* **2017**, *37*, 40.
- [233] Y. Deng, Z. Xiao, J. Huang, *Adv. Energy Mater.* **2015**, *5*, 1500721.
- [234] P. Docampo, F. C. Hanusch, N. Giesbrecht, P. Angloher, A. Ivanova, T. Bein, *APL Mater.* **2014**, *2*, 81508.
- [235] K. K. Bass, R. E. McAnally, S. Zhou, P. I. Djurovich, M. E. Thompson, B. C. Melot, *Chem. Commun.* **2014**, *50*, 15819.
- [236] J. You, Y. (Michael) Yang, Z. Hong, T.-B. Song, L. Meng, Y. Liu, C. Jiang, H. Zhou, W.-H. Chang, G. Li, Y. Yang, *Appl. Phys. Lett.* **2014**, *105*, 183902.
- [237] X. Zhang, H. Lin, H. Huang, C. Reckmeier, Y. Zhang, W. C. H. Choy, A. L. Rogach, *Nano Lett.* **2016**, *16*, 1415.
- [238] R. L. Z. Hoyer, M. R. Chua, K. P. Musselman, G. Li, M.-L. Lai, Z.-K. Tan, N. C. Greenham, J. L. MacManus-Driscoll, R. H. Friend, D. Credginton, *Adv. Mater.* **2015**, *27*, 1414.
- [239] J. C. Yu, D. Bin Kim, G. Baek, B. R. Lee, E. D. Jung, S. Lee, J. H. Chu, D.-K. Lee, K. J. Choi, S. Cho, M. H. Song, *Adv. Mater.* **2015**, *27*, 3492.
- [240] T.-H. Han, M.-R. Choi, C.-W. Jeon, Y.-H. Kim, S.-K. Kwon, T.-W. Lee, *Sci. Adv.* **2016**, *2*, e1601428.
- [241] P. Chen, Z. Xiong, X. Wu, M. Shao, Y. Meng, Z.-H. Xiong, C. Gao, *J. Phys. Chem. Lett.* **2017**, *8*, 3961.
- [242] X. Zhang, B. Xu, W. Wang, S. Liu, Y. Zheng, S. Chen, K. Wang, X. W. Sun, *ACS Appl. Mater. Interfaces* **2017**, *9*, 4926.

- [243] S. G. R. Bade, X. Shan, P. T. Hoang, J. Li, T. Geske, L. Cai, Q. Pei, C. Wang, Z. Yu, *Adv. Mater.* **2017**, *29*, 1607053.
- [244] Y. Zhou, Z.-J. Yong, K.-C. Zhang, B.-M. Liu, Z.-W. Wang, J.-S. Hou, Y.-Z. Fang, Y. Zhou, H.-T. Sun, B. Song, *J. Phys. Chem. Lett.* **2016**, *7*, 2735.
- [245] R. Begum, M. R. Parida, A. L. Abdelhady, B. Murali, N. M. Alyami, G. H. Ahmed, M. N. Hedhili, O. M. Bakr, O. F. Mohammed, *J. Am. Chem. Soc.* **2017**, *139*, 731.
- [246] C. C. Stoumpos, C. D. Malliakas, M. G. Kanatzidis, *Inorg. Chem.* **2013**, *52*, 9019.
- [247] J. De Roo, M. Ibáñez, P. Geiregat, G. Nedelcu, W. Walravens, J. Maes, J. C. Martins, I. Van Driessche, M. V. Kovalenko, Z. Hens, *ACS Nano* **2016**, *10*, 2071.
- [248] E. Yassitepe, Z. Yang, O. Voznyy, Y. Kim, G. Walters, J. A. Castañeda, P. Kanjanaboos, M. Yuan, X. Gong, F. Fan, J. Pan, S. Hoogland, R. Comin, O. M. Bakr, L. A. Padilha, A. F. Nogueira, E. H. Sargent, *Adv. Funct. Mater.* **2016**, *26*, 8757.
- [249] F. Krieg, S. T. Ochsenbein, S. Yakunin, S. ten Brinck, P. Aellen, A. Süess, B. Clerc, D. Guggisberg, O. Nazarenko, Y. Shynkarenko, S. Kumar, C.-J. Shih, I. Infante, M. V. Kovalenko, *ACS Energy Lett.* **2018**, *3*, 641.
- [250] Y. Xin, H. Zhao, J. Zhang, *ACS Appl. Mater. Interfaces* **2018**, *10*, 4971.
- [251] W. Chen, J. Hao, W. Hu, Z. Zang, X. Tang, L. Fang, T. Niu, M. Zhou, *Small* **2017**, *13*, 1604085.
- [252] Z.-J. Li, E. Hofman, J. Li, A. H. Davis, C.-H. Tung, L.-Z. Wu, W. Zheng, *Adv. Funct. Mater.* **2018**, *28*, 1704288.
- [253] M. J. Jurow, T. Lampe, E. Penzo, J. Kang, M. A. Koc, T. Zechel, Z. Nett, M. Brady, L. W. Wang, A. P. Alivisatos, S. Cabrini, W. Brütting, Y. Liu, *Nano Lett.* **2017**, *17*, 4534.
- [254] L. Liu, S. Huang, L. Pan, L.-J. Shi, B. Zou, L. Deng, H. Zhong, *Angew. Chem., Int. Ed.* **2017**, *56*, 1780.
- [255] D. Wang, D. Wu, D. Dong, W. Chen, J. Hao, J. Qin, B. Xu, K. Wang, X. Sun, *Nanoscale* **2016**, *8*, 11565.
- [256] S. K. Balakrishnan, P. V. Kamat, *ACS Energy Lett.* **2017**, *2*, 88.
- [257] S. Ye, M. Yu, W. Yan, J. Song, J. Qu, *J. Mater. Chem. C* **2017**, *5*, 8187.
- [258] J. Lee, T.-H. Han, M.-H. Park, D. Y. Jung, J. Seo, H.-K. Seo, H. Cho, E. Kim, J. Chung, S.-Y. Choi, T.-S. Kim, T.-W. Lee, S. Yoo, *Nat. Commun.* **2016**, *7*, 11791.
- [259] S.-Y. Kim, J.-J. Kim, *Org. Electron.* **2010**, *11*, 1010.
- [260] B. R. Lee, E. D. Jung, J. S. Park, Y. S. Nam, S. H. Min, B.-S. Kim, K.-M. Lee, J.-R. Jeong, R. H. Friend, J.-S. Kim, S. O. Kim, M. H. Song, *Nat. Commun.* **2014**, *5*, 4840.
- [261] C.-Y. Cheng, C.-W. Wang, J.-R. Cheng, H.-F. Chen, Y.-S. Yeh, H.-C. Su, C.-H. Chang, K.-T. Wong, *J. Mater. Chem. C* **2015**, *3*, 5665.